AN ABSTRACT OF THE THESIS OF

DAVID LOUIS CUTCHIN   for the   DOCTOR OF PHILOSOPHY
        (Name)   (Degree)

in   OCEANOGRAPHY   presented on   July 14, 1971
        (Major)   (Date)

Title: LOW FREQUENCY VARIATIONS IN THE SEA LEVEL AND

CURRENTS OVER THE OREGON CONTINENTAL SHELF

Abstract approved: Redacted for Privacy

Redacted for Privacy

Sea level and current observations made over the Oregon continental shelf exhibit wavelike characteristics in a frequency band from approximately 0.15 to 0.45 cpd. In a narrow band around 0.22 cpd the current-sea level relationship is consistent with the predicted values for the first mode of Robinson's continental shelf waves. In addition, an interesting relationship exists between the form of the sea level-current coherency spectra and the arrangement of the maximum frequencies for the first three shelf wave modes.

The currents were measured in 100 m of water about seven nautical miles off Depoe Bay, Oregon. Current meters were placed at 25, 50 and 75 m depth. The duration of the experiment was from 18 April 1968 until 11 September 1968. Due to some instrument failures a complete current data set for this period was not obtained.

Simultaneous and continuous measurements of surface elevation and atmospheric pressure were also obtained at Newport, Oregon, a nearby coastal station.

Shelf wave dispersion curves and eigenfunctions for the Oregon coastal profile are computed using a new numerical technique. These are compared with a low frequency (about 0.03 cpd to 0.75 cpd) spectral analysis of the current, sea level and atmospheric pressure records.

The relative vertical uniformity of the currents, as a function of frequency, is examined. The longshore component of the current appears to be substantially more barotropic than the onshore-offshore component.

Low Frequency Variations in the Sea Level and Currents
Over the Oregon Continental Shelf

by

David Louis Cutchin

A THESIS

submitted to

Oregon State University

in partial fulfillment of
the requirements for the
degree of

Doctor of Philosophy

June 1972

APPROVED:

Redacted for Privacy

Assistant Professor of Oceanography

in charge of major

Redacted for Privacy

Associate Professor of Oceanography

in charge of major

Redacted for Privacy

Chairman of Department of Oceanography

Redacted for Privacy

Dean of Graduate School

Date thesis is presented _____ July 14, 1971 _____

Typed by Clover Redfern for _____ David Louis Cutchin _____

Figures drafted by William E. Gilbert and Ronald Hill

This thesis is dedicated to my wife, Mary. Her
concern, good humor, encouragement and support
have played a very important part in this effort.
This was particularly true during the last difficult
months while I was involved in the agonizing task
of putting things down in words.

worst ones are my own. Mr. Steve Sullivan is responsible for the production of the unusual three dimensional plot of a shelf wave.

TABLE OF CONTENTS

LIST OF FIGURES

LOW FREQUENCY VARIATIONS IN THE SEA LEVEL AND CURRENTS OVER THE OREGON CONTINENTAL SHELF

I. INTRODUCTION

The physical, geological, biological and chemical processes active in a coastal sea are influenced strongly by current patterns. These patterns are variable, with time scales ranging from milliseconds to milleniums. Of particular interest, however, are those currents associated with variational periods ranging between tidal periods and periods of a few weeks. Spatial current patterns or distributions of parameters on this time scale are often intense and difficult to observe. These facts cause severe practical difficulties for ocean researchers. The distributions of biota and chemistry cannot be observed synoptically due to the very limited speed of the research vessel. To map even a small coastal region may take several days to several weeks. During that period of time changing currents in unknown patterns may have completely re-ordered the distribution of the organisms and production processes within that region. This causes perplexing difficulties for someone attempting to interpret the results of such a data sampling program.

The waters of the sea are constrained by the laws of motion to 1) respond to impressed forces in a consistent and determinable manner and 2) to organize their internal workings in definite arrangements.

However, which particular realization is chosen out of the ensemble
of allowable fluid motions seems, except for certain seasonal and
tidal components, to be governed by the laws of random processes.
From the history of the water motions their future is predictable only
in the same limited statistical sense as future weather is predictable.
There are, however, at least three things which we can come to know
about the current-sea level system and which would be of practical
value: 1) their elementary statistics, such as means and variances as
a function of geographical position and of depth; 2) the statistics of
the relationship between the currents measured at one or a few points
and the regional current pattern as a whole; 3) the cause and effect
relationship between the currents and more easily observed param-
eters such as the distributions of winds, atmospheric pressure or sea
level at coastal stations. The determination of these factors in a
straightforward and strictly empirical manner, if it were at all pos-
sible, would require a particularly long, difficult and expensive meas-
urement program. The more reasonable alternative is to make
critical observations designed to verify or complement a theoretical
treatment of the problem.

In this thesis I have attempted to advance our knowledge by:
1) making current observations over the Oregon continental shelf to
elucidate the transtidal (0.03 to 0.7 cpd) motions; 2) attempting to
examine the validity of certain theories which predict the existence of

low frequency wavelike motions trapped over the continental shelf;

and 3) determining the uniformity of currents with depth at low fre-

quencies.

The field experiment closely parallels the St. Kilda investiga-

tions (Cartwright, 1969) also done during the summer of 1968.

A. Coastal Bathymetry

Figure 1-1 is a map of the bathymetric features which occur

along the coast of Oregon. The smaller boxes at the right show sev-

eral selected vertical profiles of the depth taken along the correspond-

ing solid lines drawn on the map. The foot of the continental slope

and the beginning of the deep sea abyssal plains is noted by a dashed

line. The depth of the plain slopes down from 2000 m depth at about

46°N to about 3000 m at 43°N, so this line does not correspond to any

particular isobath. A series of contours between 60 m and 200m

depth have been drawn in to show the conformation of the shelf. The

shallow areas bulging out between 44°N and 44°20'N are called

Heceta Bank and the small rise slightly shoreward and to the north is

called Stonewall Bank. Except for Stonewall Bank and a few other

small features, the coast of Oregon and of the entire west coast of

the U. S. is comparatively straight and uniform.[1]

---

[1] The degree to which such irregularly shaped land masses as
this can be called "straight and uniform" can be only appreciated by
examining a chart of the world's oceans.
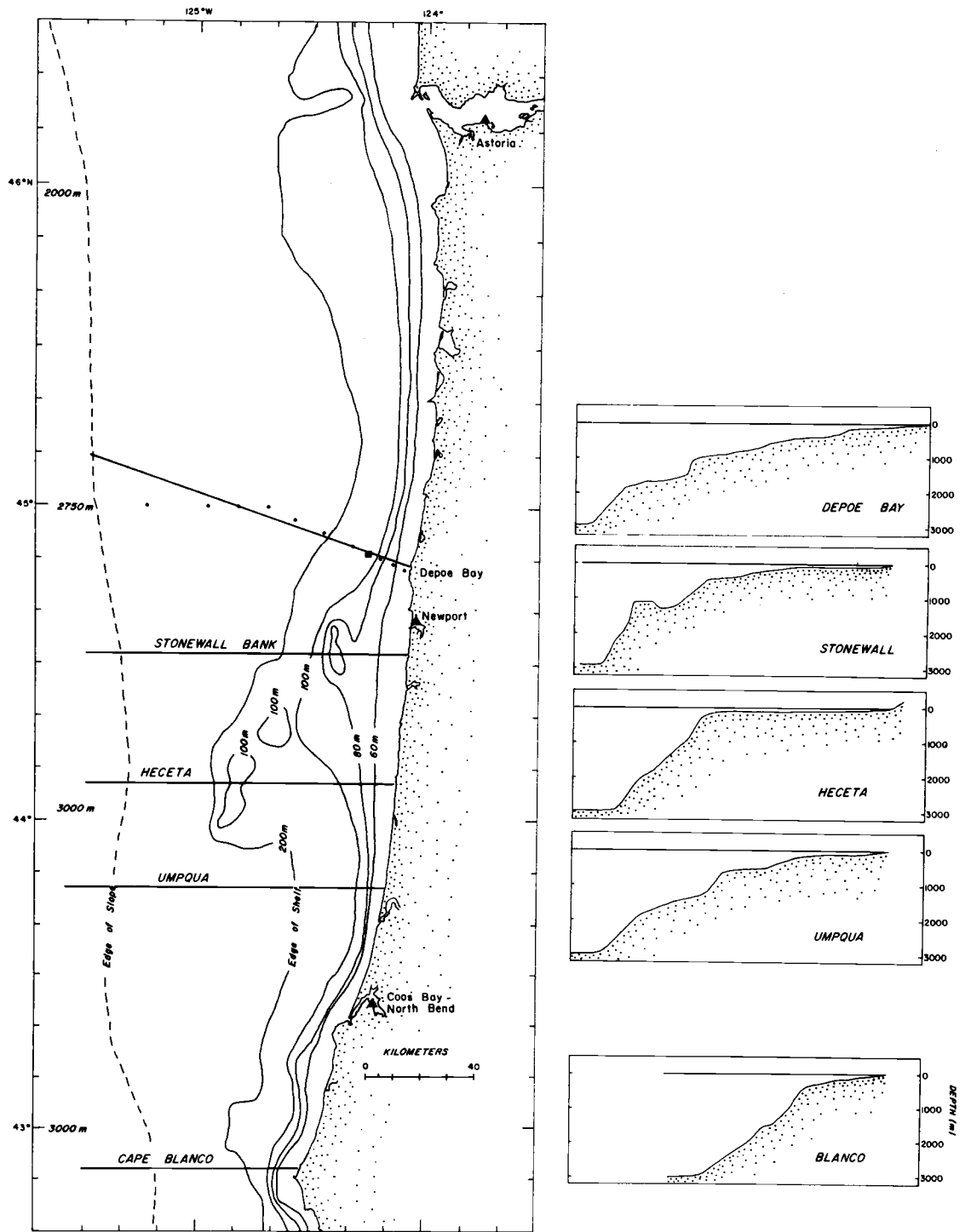
Figure 1-1.   Bathymetry of the Oregon coastal region.

B. Prevalent Currents

The Prevalent current system off the Oregon coast is the south-ward flowing California Current. It is diffuse, shallow and relatively weak. Seasonally varying winds create local current patterns over the continental margin.

In the summer season a semi-permanent high pressure system off the Oregon coast supports northerly and northwesterly winds. These winds produce a generally southward and offshore flow in the upper layers. There is also a northward flowing subsurface counter-current.

In the winter season, predominately southerly winds drive the surface waters north in a pattern known as the Davidson Inshore Current (Burt and Wyatt, 1964).

C. Density Stratification and Coastal Upwelling

A physical phenomena of considerable importance to human activity occurs off Oregon during the summer season. Nutrient rich water from the deep ocean is upwelled into the surface layers near the coastline. When the nutrients reach the sunlit layers they often trigger a phytoplankton bloom which provides the basis of a food chain terminating in commercially important species.

The velocity of upwelling is so slow that it is difficult to measure

directly. Indirect yet convincing evidence for upward flow is provided by the rearrangement of the temperature and salinity structure. In the summer, the salinity and temperature isopleths are dramatically upwarped over the continental shelf. Upwelling of water along the coast is generally considered to occur as a compensating mechanism for Ekman Drift produced by seasonal winds from the north or northwest (Smith, 1964). Deep water, from several hundred meters in the open ocean, flows onshore and upwards to replace the surface waters which are blown out to sea.

The density structure is upwarped along with the salinity and temperature structure. This has several important physical consequences. The sloped pycnocline supports a subsurface counter-current (Collins and Pattullo, 1970) and the vertical shear between the surface and deep currents creates an internal Ekman boundary layer with cross stream transports (Mooers, 1968; Pak, Beardsley and Smith, 1970). The sloped pycnocline also modifies the propagation of internal waves and tides (Mooers, 1970).

The stratification of coastal waters in the summer is intensified by insolation of the surface layers and fresh water runoff from the Columbia River. The decline of upwelling in the fall and vertical mixing due to winter storms destroy the stratification and produce an almost homogeneous condition over the shelf.

D. Time Series Current Observations

Other than those presented here, time series observations of Oregon coastal currents suitable for a limited analysis of low frequency deviations from the mean flow have formed a part of three previous theses (Collins, 1968; Mooers, 1970; Huyer, 1971). Most of their observations were made during the summer upwelling season, as were the observations presented in this thesis. However, all of their current records were considerably shorter. Collins (1968) noted the existence of strong variations in the currents with periods of a few days to a month. He also noted a strong, in-phase correlation between longshore winds and the longshore component of the current at low frequencies. This relationship was confirmed by Huyer (1971). Collins was also able to establish that a strong relationship existed between coastal sea level and longshore flow at low frequencies. From the elevation of sea level at the coast together with the slope of the sea level over the shelf, as determined from the longshore current by geostrophic computations, he predicted the width of the coastal current band to be only 75 km. Mooers (1970) did not exploit the low frequency information contained in his observations but concentrated his attention on the current components associated with the diurnal and semidiurnal tides.

The current measurements described in this thesis are also being investigated by Pillsbury (1972). His principal interest is in variations of the tidal and inertial periods.

II. SOME THEORETICAL CONSIDERATIONS FOR
FLUID MOTION IN A COASTAL SEA

The first section (A) of this chapter reviews a system of equations that are commonly used to treat fluid movements in a coastal sea. It is difficult for a mathematician, physicist, or other physical scientist who has not worked on oceanographic problems to assume, in a short period of time, the viewpoint of those specializing in this field. Therefore, I have also attempted to list and explain some of the special simplifying assumptions which led to this form for the equations.

Section B examines the absence of realistic wavelike solutions to the unforced system of equations in the simplest case of an infinite ocean of constant depth. The lack of free modes is shown to correspond to this ocean's very poor response to oscillating forcing functions.

By way of contrast, Section C reviews the free wave solutions, first discovered by Robinson (1964), which may exist over the strong topographic gradients of a continental shelf. These solutions are called "continental shelf waves." The existence of these free modes corresponds to an interesting resonance between the forcing function, presumably atmospheric pressure, and the motion of the coastal sea. Section C also contains a review of several advances in shelf wave theory.

Section D separately reviews one very recent and as yet unpub-
lished advance in shelf wave theory. This is the development, by
M.S. Longuet-Higgins (Caldwell and Longuet-Higgins, 1971), of a
semi-numerical technique which can solve the unforced system of
equations under more general conditions. This technique is then
applied, by the author, to the Oregon coastal region around Depoe Bay
and the characteristics of free waves are predicted.

The last section of this chapter, Section E, reviews some of the
previous research, both in the real ocean and in rotating model
basins, which has attempted to verify the contental shelf wave theory.
The author was a co-investigator in the model basin studies.

A. The Governing System of Equations

Initial Assumptions

A set of simplifying assumptions which are often applied to the
fundamental system of equations for low frequency, small amplitude
motions of the sea in a coastal region are:

1) The inertial terms are neglected; i.e., advective accelera-
   tion terms are assumed small.

2) The fluid is incompressible.

3) The fluid is uniform or homogeneous with respect to density;
   it is not stratified.

4) The horizontal wavelength of the disturbances is long in comparison to the depth of the water.

5) The horizontal component of the fictitious coriolis force, due to the rotation of the coordinate system fixed to the surface of the earth, is assumed to be a constant over the region of interest (this is called the "f-plane" model).

6) Viscous effects are negligible.

7) Energy and momentum enter and leave the sea only through horizontal pressure gradients; i.e., the wind and bottom stresses are ignored.

These assumptions are repeated below together with appropriate explanations, comments and excuses.

1) The inertial terms are neglected; i.e., the non-linear, advective acceleration terms are assumed small.

Advective accelerations appear in the Eulerian formulation of the equations of fluid motion. They represent the acceleration which a fluid experiences as it flows around a sharp bend, or from a slow region to a fast region of velocity field. The low frequency motions in the sea are assumed to be of small amplitude and fairly uniform over space. Therefore the advective acceleration terms are very small. To be precise, the advective accelerations are neglected because the Rossby number is small. The Rossby number is a measure of the relative strength between the advective acceleration terms and the

coriolis terms.

2) The fluid is incompressible.

This assumption filters out the acoustic wave solutions and considerably simplifies the fluid dynamics. For this reason it is even invoked in problems of gas dynamics where compression effects may be substantial. The relative incompressibility of water, however, makes this assumption the safest assumption in this list.

3) The fluid is uniform, or homogeneous, with respect to

density; it is not stratified.

The real ocean is most certainly stratified and many oceanographic phenomena occur as a result of stratification. However, we might hope that 1) the solution to the homogeneous formulation of the system are perturbed very little by the presence of stratification and that 2) in the real ocean the "barotropic" modes of oscillation, which correspond to the modes of oscillation of an ideal homogeneous ocean, are more strongly excited than the "internal" or "baroclinic" modes, which depend upon the stratification.

This assumption is made principally to simplify the system to the point where it is more easily solvable. The most advanced treatments of the motions of stratified fluids over a continental shelf are perhaps those presented by Orlanski (1968, 1969) and Rhines (1970). Fortunately, the real ocean data presented in Chapter III and analyzed in Chapter IV seems to indicate that a large part of the coastal current

system is concentrated in barotropic modes.

4) The horizontal wavelength of the disturbances is long in comparison to the depth of the water.

If the wavelength is very long, the amplitude small, and the phase velocity some finite value, then vertical accelerations throughout the water column will be very small. This means that the vertical component of the equations of motion becomes approximately the hydrostatic equation. The hydrostatic equation simply states that the pressure at any point in the water column is equal to the still (static) weight of the column of water directly above it (plus the atmospheric pressure exerted on the surface). The hydrostatic equation allows us to specify the horizontal pressure gradients in terms of the slope of the sea surface.

The long wave assumption plus Assumption 3), no stratification, finally lead to the important conclusion that except for possible frictional boundary layers the horizontal currents now must be uniform from top to bottom. In other words they must have the same magnitude and direction over the complete water column.

5) The horizontal component of the fictitious coriolis force, due to the rotation of the coordinate system fixed to the surface of the earth, is assumed to be a constant over the region of interest; the "f-plane" model or assumption.

The spin of a coordinate system fixed with respect to the surface of the earth is, of course, about an axis aligned with the axis of rotation of the earth. This axis is, in general, at some angle between the local horizontal and vertical. Therefore, the fictitious rotational force, the coriolis force, acting on a moving water particle is directed at angles with respect to the local horizontal. However, the vertical component of this force is always inconsequential compared to the force of gravity or the buoyant force due to even a very small amount of density stratification. The vertical component is therefore usually ignored. The horizontal components of the fictitious force, on the other hand, play a very important role in guiding ocean currents. In ocean problems, the rotation of the coordinate system is considered to be effectively equal to the component of the earth's spin vector projected on the local vertical.

The projection of the spin vector on the local vertical varies sinusoidally with latitude. This variation is called the "beta" effect and it can have a substantial effect upon the motions of the currents. Changes in depth, however, influence the currents in a similar manner. In a coastal region the depth gradients are so strong that they overwhelm the beta effect and it need not be considered. A rigorous proof of this was given by Buchwald and Adams (1968).

6) Viscous effects are small.

Although frictional boundary layers do modify the motions of the

sea, they are usually thin in relationship to the great depths. They are, therefore, much less prominent factors in the oceanic momentum budget than they are in the momentum budget for phenomena or smaller, more familiar scales.

      7) Momentum enters and leaves the sea only through horizontal pressure gradients; i.e., the wind and bottom stresses are neglected.

This assumption might be considered to be a necessary consequence of the inviscid assumption, Assumption 6. However, the problem is more complicated than that. Many theoreticians keep the top and bottom surface stresses, the wind stress and the frictional damping stress respectively, in an inviscid model by distributing them over the entire water column. In the treatment of the problem as presented here, this device has not been applied. The only driving forces considered are the pressure gradients resulting from the atmospheric pressure gradients and the slope of the sea surface. No frictional damping is included.

The high correlations observed by Collins (1968) and Huyer (1971) between longshore winds and subsurface currents do not fit easily with the above assumption--but they do not necessarily invalidate that assumption. Wind variations are strongly correlated with atmospheric pressure gradient variations and it is therefore difficult, on the basis of wind and current measurements alone, to sort out the

problem of how much each factor is contributing to the generation of the current systems. Also, these correlations between wind and currents may possibly be due to the intermediate mechanism of a redistribution of the surface water by wind stress and the production of horizontal pressure gradients. Oregon coastal waters in the summer season are usually well enough stratified to seriously inhibit the direct downward transfer of horizontal momentum from the surface layers to the interior layers via turbulence. Molecular viscosity is, of course, much too weak.

Equations of Motion and Continuity

The system of equations incorporating these assumptions are:

Horizontal equations of motion

x component

$$\frac{\partial u}{\partial t} - fv = -g \frac{\partial}{\partial x} (\zeta + P_A) \tag{1}$$

y component

$$\frac{\partial v}{\partial t} + fu = -g \frac{\partial}{\partial y} (\zeta + P_A) \tag{2}$$

Equation of continuity or conservation of mass

$$\frac{\partial (hu)}{\partial x} + \frac{\partial (hv)}{\partial y} + \frac{\partial \zeta}{\partial t} = 0 \tag{3}$$

Where, as in Figure 2-1, x and y are the horizontal coordinates, u(x, y, t) and v(x, y, t) are the horizontal components of velocity along x and y respectively, h(x, y) is the depth measured from the bottom to the equilibrium position of the free surface (mean sea level), $\zeta(x, y, t)$ is the deviation of the free surface, $P_A(x, y, t)$ is the atmospheric pressure expressed as the height of an equivalent column of sea water bearing down on the free surface and g is the acceleration due to gravity. The hydrostatic assumption for the vertical component equation has been implicitly used in relating the pressure gradients to the slope of the sea surface. The vertical momentum balance does not play any further role in the dynamics of long waves. The fluid density, ρ, does not appear. It has been incorporated into the specification of the forcing terms. $f = 2\Omega \sin(\theta)$ is the coriolis parameter, where Ω is the angular velocity of the earth and θ is the latitude of the center of the region under consideration. The accelerations due to the rotation of the coordinate system are thus simply incorporated into the system as a pseudo "coriolis" force. Figure 2-1 also shows a current profile to remind one that the currents are assumed uniform with depth.
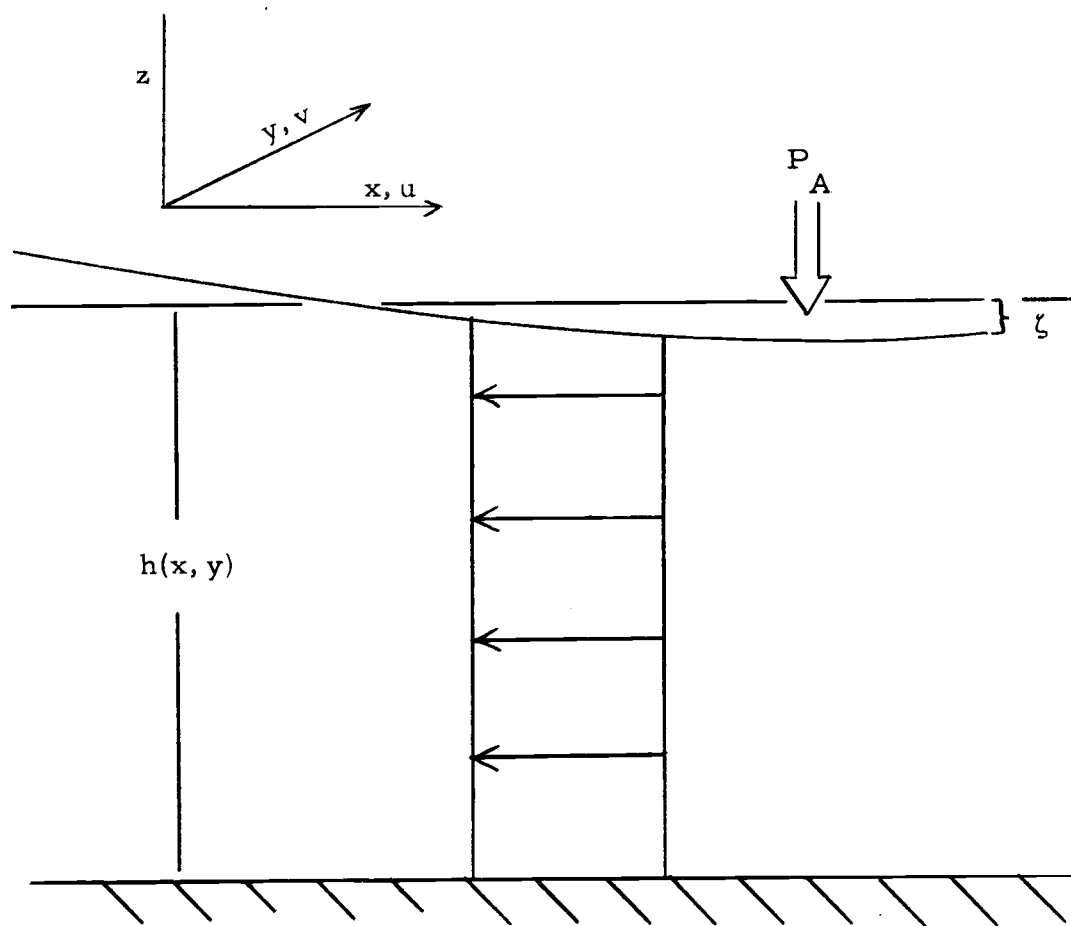
Figure 2-1. Geometry for long waves.

B. Searching for Solutions in the Case of an Infinite Ocean of Uniform Depth

Free Waves

In addition to the seven assumptions already made, also assume that $h(x, y)$, the depth, is a constant and that all ocean boundaries are far away from the region of interest. For the present, also assume that the atmospheric pressure, $P_A(x, y, t)$, is constant in space and time and thus there is no forcing. (1)-(3) then become

$$\frac{\partial u}{\partial t} - fv = -g \frac{\partial \zeta}{\partial x} \tag{4}$$

$$\frac{\partial v}{\partial t} + fu = -g \frac{\partial \zeta}{\partial y} \tag{5}$$

$$\frac{\partial u}{\partial x} + \frac{\partial v}{\partial y} + \frac{1}{h} \frac{\partial \zeta}{\partial t} = 0 \tag{6}$$

Now assume a) that the time variations for u, v, ζ are of the oscillatory form $\exp(+i\sigma t)$, where σ is the angular frequency; and b) the spatial variations are of the wave form $\exp[i(mx+ky)]$, where m and k are the x and y wave numbers respectively. The assumed solution is therefore of the form

$$(u, v, \zeta) = (u_0, v_0, \zeta_0) \exp[i(mx+ky+\sigma t)]$$

where u_0, v_0, ζ_0 are (complex) amplitudes. The substitution of

this wave form into (4)-(6) yields the following relationships between the magnitudes of the dependent variables

$$u_0 = \frac{g}{\sigma^2 - f^2} (-\sigma m + ikf) \zeta_0$$

and

$$v_0 = - \frac{g}{\sigma^2 - f^2} (ifm + \sigma k) \zeta_0$$

plus the following important condition upon the wave numbers

$$\sigma^2 - f^2 = gh(k^2 + m^2).$$

For sub-inertial frequencies,[2] $f^2 > \sigma^2$, the quantity $(k^2 + m^2)$ must be negative. This means that k and/or m must be imaginary and cause a real exponential in the assumed form for u, v, ζ. For example, assume $m = \mp i |m|$. Then

$$(u, v, \zeta) = (u_0, v_0, \zeta_0) \exp(iky + i\sigma t) \exp(\pm |m| x).$$

---

[2] The coriolis parameter has units of frequency (radians/sec). At that frequency a rotating system has a natural resonance or singularity. The modes of possible motion above, at and below that frequency, called the "inertial frequency," may be quite different. At the latitude of Oregon, about 45°N, the inertial frequency corresponds to a period of about 17 hours (1.41 cpd). The term "low frequencies" as it appears in this thesis generally means frequencies below about 0.5 cycles per day (the infra-tidal or sub-tidal range).

Real exponentials cause problems because they blow up at either large

plus or minus values of x or y. It happens that when all of the

assumptions

     1) f = constant,

     2) $f^2 > \sigma^2$,

     3) h = constant, and

     4) no boundaries in x, y plane

are made, (1) through (3) have no allowable solutions which are

physically realizable free waves. An ocean of this type should have

no natural mode of oscillation at frequencies below the inertial. If the

forces due to the variation of f with latitude are included, then this

system does have a set of solutions at sub-inertial frequencies, called

Rossby waves (Longuet-Higgins, 1965).

In the case of $\sigma^2 > f^2$, both k and m may be real and the

equations have a set of physically allowable solutions called Poincare

waves.

However, if one introduces a boundary into this ocean then for

all frequencies certain of the exponentially increasing forms are

physically allowable. For example, if a vertical boundary lies along

the y axis with the sea occupying the positive x plane (Figure

2-2), then an allowable solution which fits the boundary condition of no

transport into the wall is
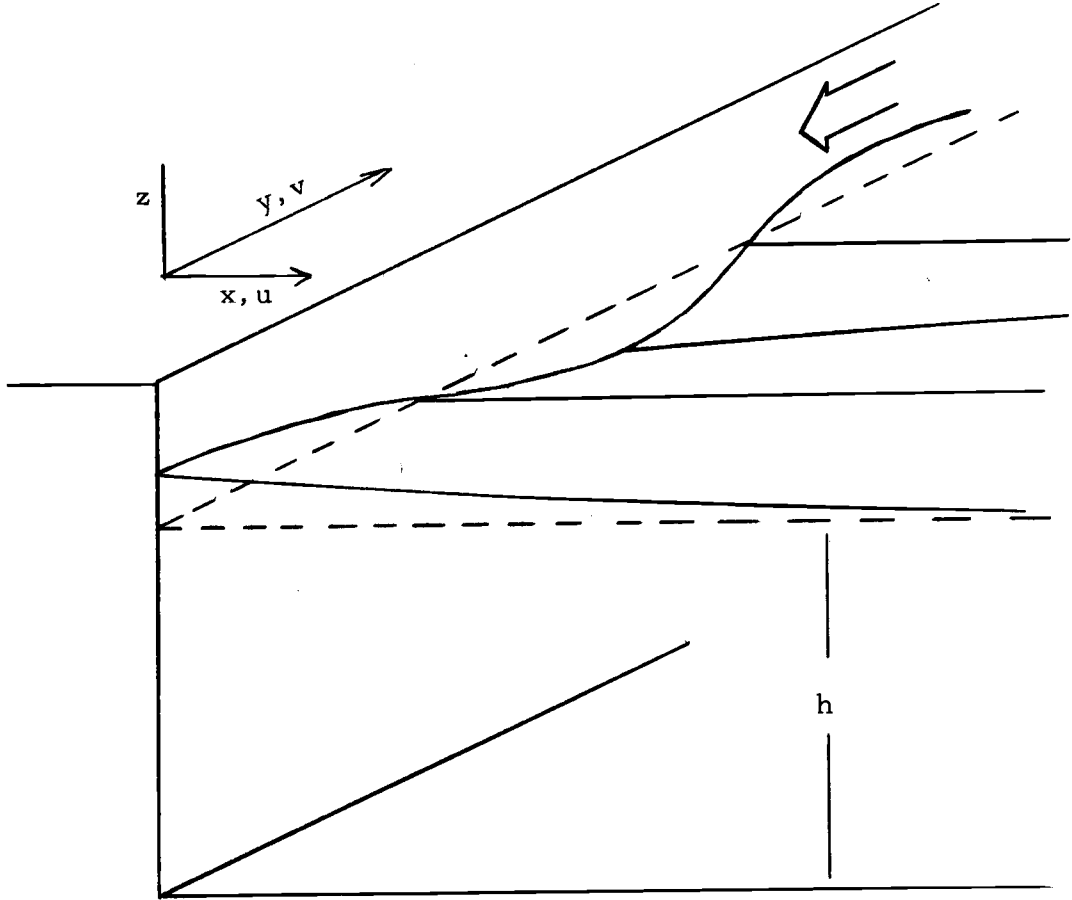
Figure 2-2.   The classical Kelvin wave.

$$\zeta = \zeta_0 \, \exp[i(ky+\sigma t)] \, \exp[-\frac{fx}{\sqrt{gh}}].$$

The wave travels, in the northern hemisphere (f > 0), with its right shoulder against the wall and at a phase speed $C_p = \sqrt{gh}$, the phase speed of a shallow water gravity wave. Its crests are perpendicular to the wall and its amplitude diminishes with distance from the wall. Typical oceanic values of h = 4000 m and $f = 10^{-4}$ rad/sec yield the phase velocity C_p = 200 m/sec and the amplitude 1/e folding distance from the coast of about 2000 km. All of the currents under the wave are aligned parallel to the wall; i.e., u(x, y, t) = 0.

The Effect of a Simple Forcing Function at Low Frequencies

Assume $f^2 > \sigma^2$, h a constant, and no lateral boundaries. Consider a plane wave pressure perturbation moving along the y axis in the -y direction. Assume

$$P_A = \overline{P} + P'$$

where $\overline{P}$ is the mean pressure and P', the fluctuating part, is

$$P' = P'_0 \, \exp[i(ky+\sigma t)]$$

and that the modes excited are of similar form

$$u, v, \zeta = (u_0, v_0, \zeta_0) \, \exp[i(ky+\sigma t)].$$

Note that all parameters are uniform in the x direction, and there-fore $\frac{\partial(\ )}{\partial x} = 0$. At this point allow the convenient substitution

$P' = -\phi$ where ϕ is just the negative of the fluctuating part of the atmospheric pressure. It is also convenient to define $\eta = \zeta - \phi$ which can be thought of as the deviation from the isostatic response to atmospheric pressure fluctuations. If the sea surface depresses 1 cm for an increase in P_A of 1 mb then the response is isostatic and $\eta = 0$.

Using the above assumptions and substitutions, Equations (1) and (2) become

$$-i\sigma u_0 - f v_0 = 0 \tag{7}$$

and

$$-i\sigma v_0 + f u_0 + igk\eta_0 = 0 . \tag{8}$$

Alternately eliminating u and v from the above equations we obtain the expressions

$$u_0 = i \frac{gfk}{f^2 - \sigma^2} \eta_0 \tag{9}$$

and

$$v_0 = - \frac{g\sigma k}{f^2 - \sigma^2} \eta_0 . \tag{10}$$

Substituting these expressions into (3), the equation of continuity, we obtain

$$ihk \frac{g\sigma k}{f^2 - \sigma^2} \eta_0 + i\sigma\eta_0 + i\sigma\phi_0 = 0 \tag{11}$$

which may be reexpressed substituting for $\eta_0 = \zeta_0 - \phi_0$

$$\zeta_0 = \left[1 - \frac{1}{(\frac{hk^2 g}{f^2 - \sigma^2} + 1)} \right] \phi_0 \tag{12}$$

Equation (12) gives the relationship between ϕ_0, the amplitude of the pressure wave, and ζ_0, the amplitude of the generated wave in the ocean. For $h = 4000$ m, $f = 10^{-4}$ rad/sec, and $k = 2\pi \times 10^{-6}$ (corresponding to a wave length of 1000 km) the bracketed expression in (12) is equal to unity (to within 0.5%) over the frequency range $0 < \sigma^2 < f^2$. This means that at low frequencies an unbounded sea acts pretty much as an inverse barometer. Matching troughs in the ocean surface move along obediently beneath high pressure ridges. The response for a pressure system moving with any finite speed is slightly less than perfectly barometric because of inertial effects.

C. Considering the Case of the Sea Over the Continental Shelf

Robinson's Shelf Waves

We now consider the above case allowing h, the depth, to vary with the horizontal coordinates. In particular, consider a boundary

in the form of a continental shelf running along the y axis with the

land occupying the +x half-plane. As before, ζ is the sea level

distortion, and the pressure system passing over the sea is in the

form of a plane wave moving toward the -y direction

$$P_A = \bar{P} + P'$$

where

$$P' = P'_0 \exp[i(ky+\sigma t)]$$

and $\bar{P}$ is the constant mean pressure. P'_0, the magnitude of the

fluctuating part of P_A, is assumed to be constant with respect to x.

We again seek solutions for u, v, ζ that are of the form

$$(u, v, \zeta) = [u_0(x), v_0(x), \zeta_0(x)] \exp[i(ky+\sigma t)].$$

Because of the boundary at x = 0 and the variation in h with x,

we cannot assume here that all solutions are independent of x.

With the substitutions

$$P' = -\phi$$

and

$$\eta = \zeta - \phi$$

(1) and (2) then become

$$i\sigma u_0 - fv_0 = -g\eta'_0 \tag{13}$$

$$i\sigma v_0 + fu_0 = -gik\eta_0 \tag{14}$$

where here primes indicate derivatives with respect to   x.

Alternately eliminating v_0 and u_0 we obtain

$$u_0 = \frac{ig(\sigma\eta_0' + fk\eta_0)}{\sigma^2 - f^2} \qquad (15)$$

and

$$v_0 = -\frac{g(\sigma k\eta_0 + f\eta_0')}{\sigma^2 - f^2} \ . \qquad (16)$$

Substituting these into (3) we obtain

$$\sigma[h(\eta_0'' - k^2\eta_0) + h'\eta_0'] - fh'k\eta_0 + \frac{\sigma(\sigma^2 - f^2)}{g}(\eta_0 + \phi_0) = 0 \ . \qquad (17)$$

Robinson (1964) examined this problem for the case of a linearly sloping shelf terminating in an abrupt drop to a deep sea basin of constant depth (Figure 2-3). His treatment is as follows: Let   L equal the shelf width,   d equal the depth of the shelf edge, and   D equal the uniform depth of the deep ocean basin. Solve (17) in the shelf region and the deep region, each subject to appropriate boundary conditions and require that the solutions match at the shelf edge. The boundary conditions are 1) at the coastline $u_0(0) = 0$,   i.e., no transport of water through the beach, and 2) far out to sea and away from the shelf the amplitude vanishes.

In order to obtain an analytical solution to the equation, Robinson
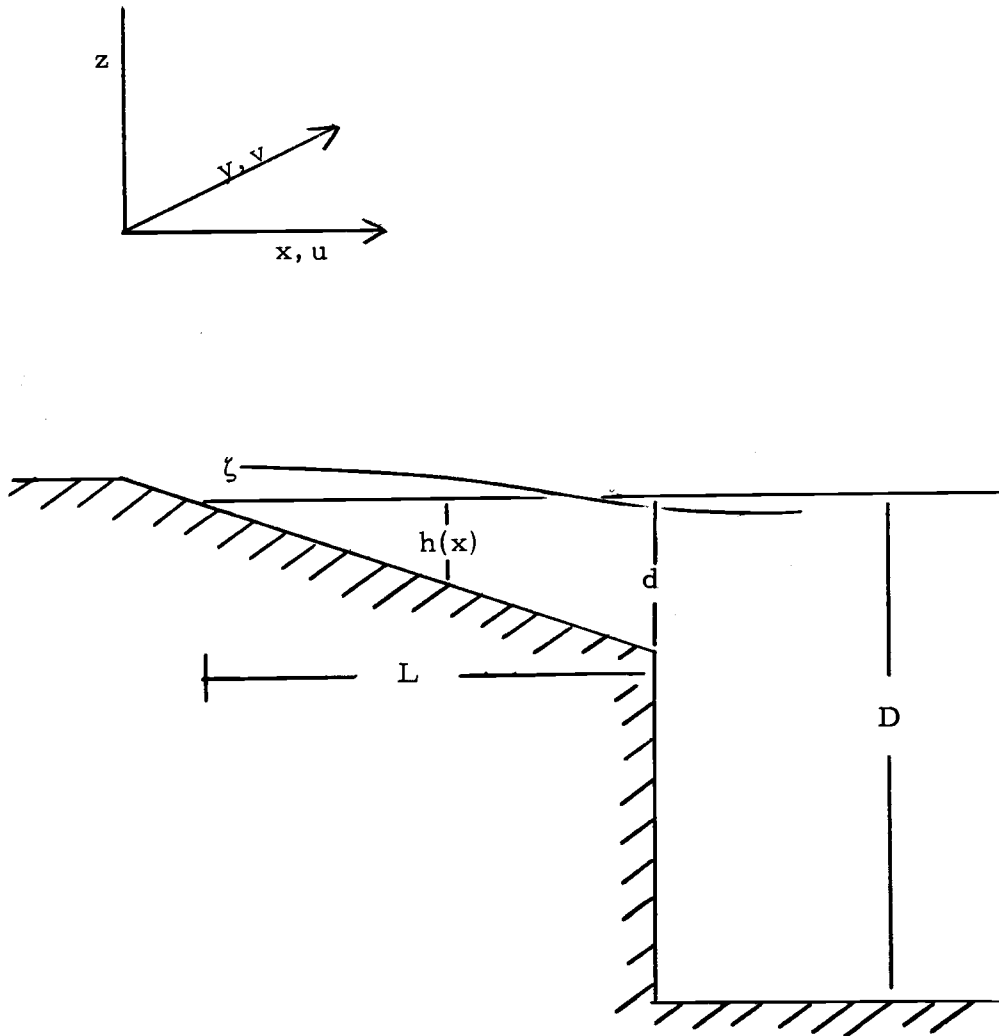
Figure 2-3.   Simple continental shelf model.

then made the simplifying assumption that

$$k^2 L^2 \ll 1$$

(wave length along the shelf much greater than the width of the shelf); and

$$f^2 L^2 \ll gd$$

(divergence effects small, i. e. , the elevation and depression of the free surface is a manifestation of the wave motion rather than an important contributing part of the dynamics).

If we temporarily drop the forcing term and make the substitution $\xi = x/L$, (17) for the shelf region becomes

$$\xi \eta_0'' + \eta_0' + K = 0 \tag{18}$$

where $K = \dfrac{Lkf}{\sigma}$ and primes indicate derivatives with respect to ξ. The appropriate solution is

$$\eta_0(\xi) = J_0(2\sqrt{K\xi})$$

(the Bessel function of zero order). In the deep sea region (17) similarly becomes

$$\eta_0'' - L^2 a^2 \eta + 0 \tag{19}$$

where $a^2 = k^2 + \dfrac{f^2 - \sigma^2}{gD}$. The solution is

$$\exp(-aL\xi).$$

The exponentially decreasing or increasing form is the only one

allowed in the flat bottomed, deep sea region (p. 19).

Combining the conditions for continuity of η and u at the

edge of the shelf, Robinson determined that the eigenvalue relation-

ship (resonance condition) was

$$J_0(2\sqrt{K})(1-\Delta) - (\frac{\Delta}{\sqrt{K}}) J_0'(2\sqrt{K}) = 0 \qquad (20)$$

where $\Delta = \dfrac{d}{D}$. For small Δ the solution of (20) is

$$2\sqrt{K} = 2\sqrt{K_0} + \frac{\Delta}{\sqrt{K_0}} + O(\Delta^2)$$

where K_0 are the zeros or roots of J_0. In the real ocean Δ is

of the order of 10^{-1}. Thus the roots of (20) are, within a few percent,

the roots of $J_0(2\sqrt{K})$. The first zero of J_0 corresponds to a

$K_{01} = 1.44$, i.e., for the "first" mode (the first root of J_0)

$$\frac{kLf}{\sigma} = 1.44.$$

The wave number of the free waves is in a fixed ratio (or actu-

ally a discrete set of ratios) to the frequency of the wave. This allows

for the existence of a whole spectra of such waves, quite differently

from the case of a harmonic oscillator or a violin string which allow

free vibrations at only one or a set of discrete frequencies.

Since L and f are assumed constant the phase velocity $C_p = \sigma/k$ corresponding to a particular mode must also be constant. The waves are non-dispersive.

According to Robinson, a solution to the forced problem evaluated at the coast, $x = \xi = 0$, is

$$\eta(0) = \phi \frac{\sigma f L}{gdk} \left(1 - \frac{1}{J_0 2\sqrt{K}}\right)$$

where again $\Delta \ll 1$. Reexpressed in terms of the sea level elevation at the coast it becomes

$$\zeta(0) = \phi_0 \left[\underbrace{\frac{1}{}}_{\substack{\text{isostatic} \\ \text{response}}} + \frac{fL\sigma}{gdk} \left(\underbrace{\frac{1}{}}_{\substack{\text{has very small} \\ \text{influence on} \\ \text{mag. of} \\ \text{expression}}} - \underbrace{\frac{1}{J_0(2\sqrt{K})}}_{\substack{\text{can have large} \\ \text{influence under} \\ \text{resonance} \\ \text{conditions}} \right) \right] \tag{21}$$

For example at mid latitudes, and for a shelf width L of 70 km, (21) says that the sea resonates, in the first mode, under a pressure wave traveling in the -y direction at a phase speed of about 5 meters/second (σ/k = 5 m/sec). A qualitative plot of the bracketed term in (21), using these assumed values of d and L is shown in Figure 2-4. Since Robinson did not include any frictional damping or any shoreline irregularities in his treatment the
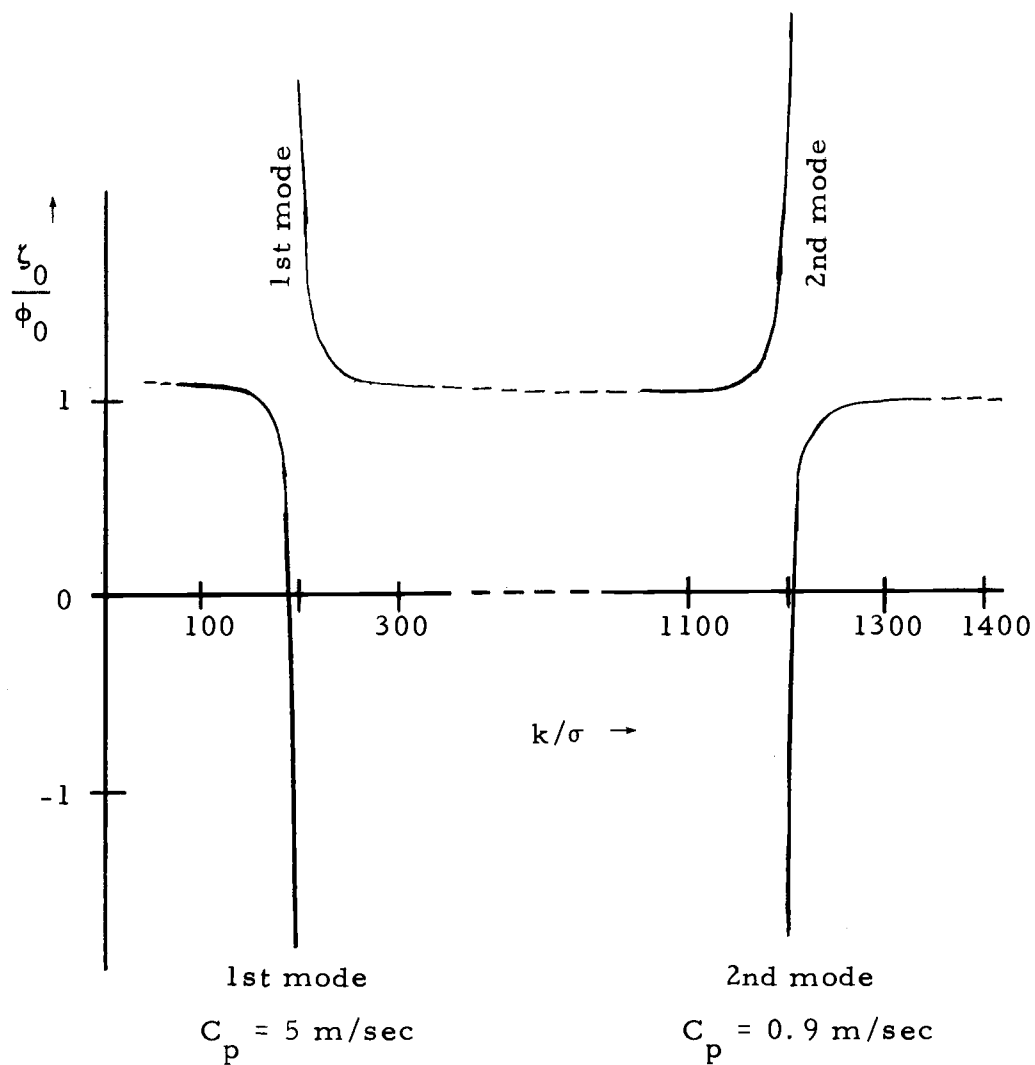
Figure 2-4. Response of sea level to a pressure wave moving along coastline as predicted by Robinson (1964).

resonances are very sharp.

For most values of (k, σ), (21) says that the sea responds like an inverse barometer. One might expect that the real atmospheric pressure wave-number and frequency spectrum is distributed in a big broad lump. This implies that a large fraction of the forcing energy would probably fall at (k, σ) values where the inverse barometer effect prevails. Adjusting an observed sea level by adding the over-pressure, in cm of sea water, would therefore remove the forced motions due to most of the oscillations in the pressure system. This technique has been applied in Chapter IV, "Data Analysis and Interpretation." It does not remove the resonant response. To remove the resonant response would require a detailed knowledge of the time and space dependence of the pressure system.

Advances in Shelf Wave Theory

Mysak (1967a) utilized a Fourier transform technique to solve the problem of the coastal sea forced by a very general pressure sys-tem. The formulation and assumptions were similar to that of Robinson but with the addition of a frictional damping term.

Mysak (1967b) also extended the formulation of the shelf wave problem to include a sloping region between the edge of the shelf and the deep sea floor. He found that this increased the predicted phase speed of the 1st mode free wave by a factor of about two and brought

theory into quantitative agreement with certain features in sea level observations made by Hamon (1962) along the east coast of Australia. In this paper Mysak also treated the problem of shelf wave systems circling the Australian subcontinent, and the effect of deep sea stratification and currents on the propagation of the waves.

Buchwald and Adams (1968) presented an exceptionally compact treatment of the free wave problem for the case where $\sigma^2 < f^2$, the divergence is zero $(\zeta = 0)$, and the continental shelf has an exponential profile. They were thus able to do away with the restrictive assumption that the wave length be long in comparison with the shelf width. They discovered that the waves were dispersive for shorter wave lengths and that the group velocity, at a high frequency cutoff, even went through a reversal in direction.

This assumption of zero divergence is equivalent to considering that the sea is confined beneath a rigid lid located at mean sea level. This prevents the rise and fall of sea level but, with real oceanic dimensions, affects the wave propagation and form of the wave currents very little. Most of the energy is contained in the horizontal currents rather than in the sea level elevation and depression.

Adams and Buchwald (1969) questioned that the waves are generated by moving pressure systems, and presented a case for ascribing wave generation to longshore wind stress. The problems involved in estimating wind stress and its effect upon the water column are,

however, very difficult and mostly unsolved.

D. Application of Theory to Oregon Coastal Region

General Numerical Technique for Solution of the Free Wave
Problem

Caldwell and Longuet-Higgins (1971) have outlined a simple

numerical technique for solving (17) without approximations and with

a considerable amount of freedom in specifying the profile of the shelf,

$h(x)$.

Rewrite (17) as

$$\frac{d}{dx}(h\frac{d\zeta_0}{dx}) = (\frac{f^2(\tau^2-1)}{g\tau^2} + kh + \tau k \frac{dh}{dx}) \zeta_0 \tag{22}$$

where the forcing has been dropped (and therefore $\eta = \zeta$); and

$\tau = f/\sigma$, the period of the motion non-dimensionalized by the inertial

period. This expression is to be solved subject to the following

boundary conditions:

$$u_0, v_0, \zeta_0 \to 0 \quad \text{as} \quad x \to +\infty$$

$$u_0 = 0 \quad \text{for} \quad x = 0.$$

The first condition indicates that we are again seeking modes

with energy trapped against the coastline. The solution to (22) for

$h = a$ constant (deep sea region) which appropriately goes to zero as

$x \to +\infty$ is

$$\zeta_0 \propto \exp[-\left|\sqrt{\frac{f^2(\tau^2-1)}{gh\tau^2}+k^2}\right| x] .$$ (23)

The second condition prescribes zero flow through the coast-line. With (15) this condition imposes the following constraint at $x = 0$:

$$\frac{d\zeta_0}{dx} = -\frac{fk}{\sigma} \zeta_0 .$$ (24)

Equation (22) is prepared for numerical solution by reducing it to a pair of first order equations. Let the range of integration over x be $0 \le x \le I$ where $I > L$ and let

$$\left.\begin{array}{l}\zeta_0(x) = P(x) \\[2em] h(x) \dfrac{d\zeta_0}{dx} = Q(y)\end{array}\right\} \quad \text{for} \quad 0 \le x \le I/2$$

and

$$\left.\begin{array}{l}\zeta_0(x) = R(x) \\[2em] h(x) \dfrac{d\zeta_0}{dx} = S(x)\end{array}\right\} \quad \text{for} \quad I/2 \le x \le I .$$

(22) then becomes

$$\frac{dP}{dx} = -\frac{1}{h}Q$$

$$\frac{dQ}{dx} = -[\frac{f^2(\tau^2-1)}{g\tau^2} + k^2h + \tau k\frac{dh}{dx}]P$$

$\left.\vphantom{\begin{array}{c}a\\a\\a\end{array}}\right\}$ for $0 \le x \le I/2$ (25)

and

$$\frac{dR}{dx} = -\frac{1}{h}S$$

$$\frac{dS}{dx} = -[\frac{f^2(\tau^2-1)}{g\tau^2} + k^2h + \tau k\frac{dh}{dx}]R$$

$\left.\vphantom{\begin{array}{c}a\\a\\a\end{array}}\right\}$ for $I/2 \le x \le I$. (26)

P and Q for $0 \le x \le I/2$ can be obtained by numerically integrating Equations (25) from left to right. They are initialized at $x = 0$ only under the constraint imposed by (24), namely

$$Q = -\tau khP.$$

R and S   for $I/2 \le x \le I$ are obtained by numerically integrating Equations (26) from right to left. They are initialized at $x = I$ under the constraint imposed by (23) namely

$$\frac{d\zeta_0}{dx} = -\sqrt{\frac{f^2(\tau^2-1)}{g\tau^2h} + k^2}\ \zeta_0$$

or in terms of R   and   S

$$S = -\sqrt{\frac{hf^2(\tau^2-1)}{g\tau^2} + hk^2}\ R\ .$$

ζ_0 is required to be smooth and continuous throughout the range

$0 \leq x \leq I$, in particular at $x = I/2$. This condition can be satisfied

if the Wronskian

$$W = [P\frac{S}{h} - R\frac{Q}{h}] = [-\zeta_{0_L}(\frac{d\zeta_0}{dx})_R + \zeta_{0_R}(\frac{d\zeta_0}{dx})_L]$$

vanishes for $x = I/2$. The vanishing of this Wronskian occurs when

the ratio of ζ_0 to $d\zeta_0/dx$, as determined from P and Q just

to the left of $x = I/2$, is identical to the ratio of ζ_0 and $d\zeta_0/dx$

as determined from R and S just to the right of $x = I/2$.

ζ_0 and $d\zeta_0/dx$ could then be made continuous merely by adjusting

the amplitude of P and Q with respect to R and S. That

degree of freedom was left open when the boundary conditions at

$x = 0$ and $x = I$ were specified only so far as the ratio of P to

Q and R to S.

In general, for any pair of the values τ and k, the

Wronskian will not vanish and the functions P, Q, R, S will not

produce a solution to (6) on $0 \leq x \leq I$. A program was designed by

Professor Longuet-Higgins to accept a value of k, the wave number,

and a range of values for τ, the period. The values of the

Wronskian are obtained for the several pairs of k and τ values.

They provide a rough estimate of the Wronskian as a function of τ.

Successive iterations are performed in the vicinity of indicated zero

crossings and the solution pair (k, τ) is found very rapidly.

Solution for Oregon Continental Shelf Near Depoe Bay

The locus of all points (k, σ) which allow a solution of (22) constitute a dispersion diagram for the waves. Figure 2-5 shows the disperson curves computed, by the author using the Longuet-Higgins numerical technique, for the coastal profile occurring off Depoe Bay, Oregon (Figure 1-1). Only the dispersion curves for the first three modes plus the 0th mode, the Kelvin wave, are shown. Along the left ordinate frequency is displayed in cycles/day and along the right ordinate in non-dimensional terms of the inertial frequency (at this latitude about 1.41 cpd). The non-dimensional wave number appears along the top abcissa and the dimensional wavelength along the bottom. The slope of a line drawn between the origin and any point (k, σ) on the curves is proportional to $\sigma / k = C_p$, the phase speed of the wave. Some such lines have been drawn in and their dimensional phase speed indicated.

All points on the Kelvin wave curve have very high phase speeds quite close to the value $\sqrt{gh} = 0.167$ km/second, predicted for a Kelvin wave against a vertical beach. Most of the wave is transmitted along the coast primarily in the deep sea region. In the Kelvin wave case the presence of a continental shelf perturbs the eigenfunctions (Figure 2-6) and the propagation characteristics to only a minor extent.
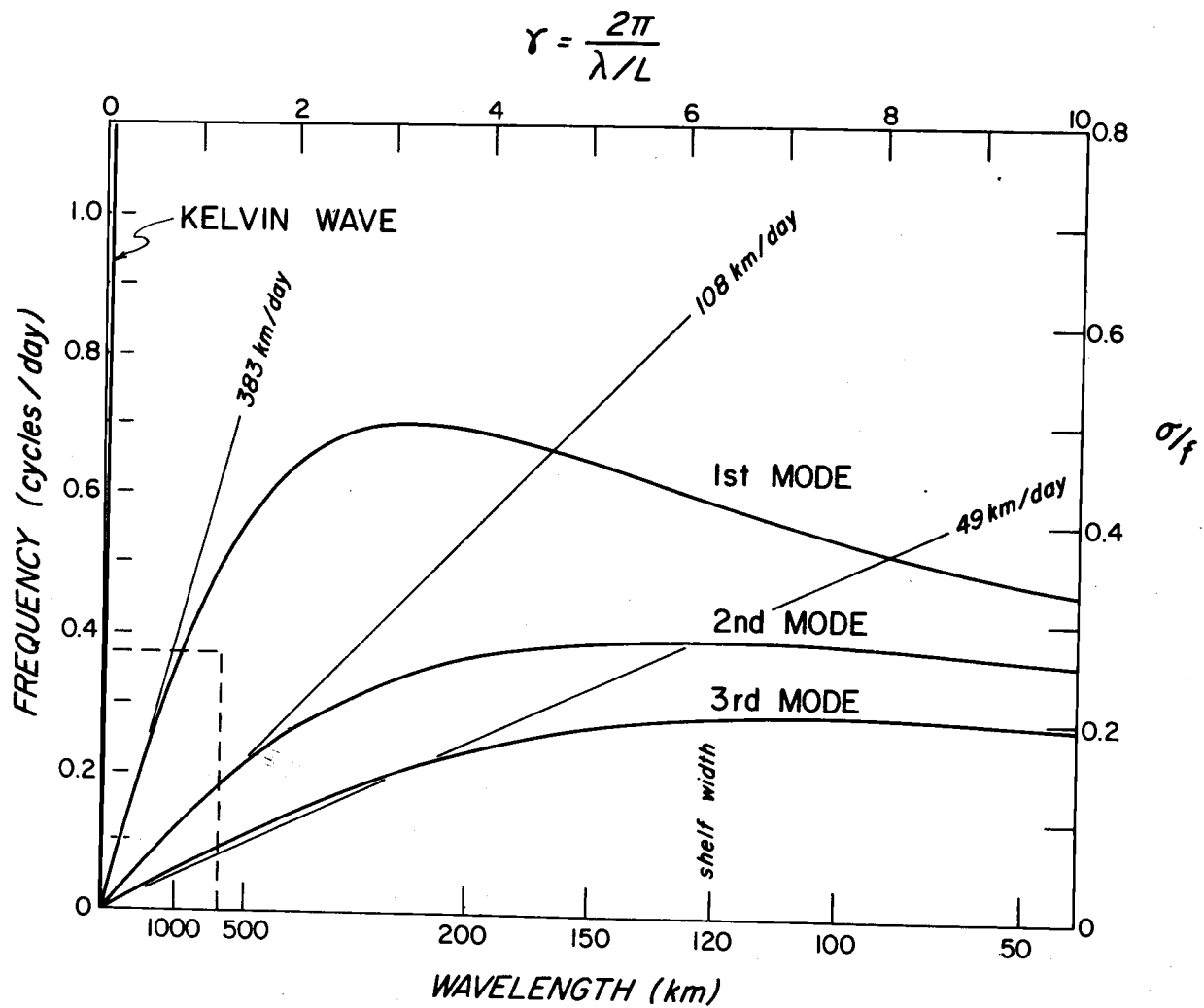
Figure 2-5. Dispersion curves for shelf waves over the Oregon continental shelf (Depoe Bay profile).

The dashed box in the lower left hand corner indicates that region of the (k, σ) plane in which the long wavelength, non-dispersive treatment by Robinson and Mysak is valid.

The slope of the dispersion curve at any point (k, σ) is proportional to $\partial\sigma/\partial k$, the group velocity or energy transport velocity of the wave. Note that the direction of energy transmission for shelf waves reverses at the cutoff frequency for each mode. The direction of the phase velocity, however, remains the same (south to north along the Oregon coast).

Figure 2-6 shows the eigenfunctions for the Kelvin wave mode plus the first three shelf wave modes as computed by the numerical technique. The Depoe Bay shelf profile appears at the top of the figure. DB-7, the location of the current meter station, is indicated. The particular frequency and wavelength at which each eigenfunction was separately computed appears in the figure. These frequencies are slightly different for the different modes because of the computational technique utilized. It would have required some extra effort and expense to obtain the eigenfunctions all at exactly the same frequency. Also this would not have appreciably altered Figure 2-6 because the eigenfunctions change very little with large changes in frequency and wavenumber. Note that for the Kelvin wave the onshore transport (in cm/sec) is very small and the sea level perturbation (in cm) is very large in comparison to the longshore transport (in
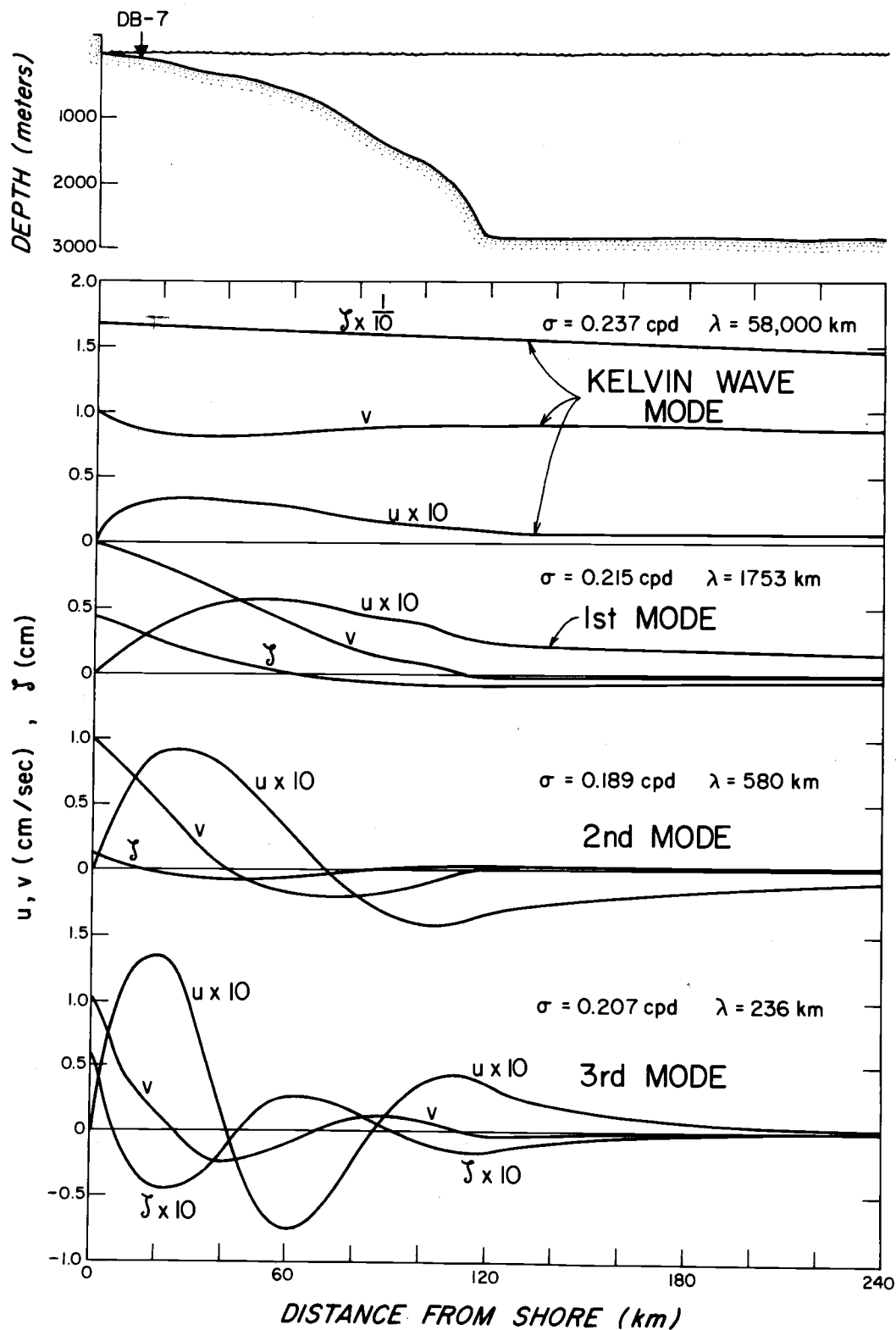
Figure 2-6. Eigenfunctions for the first three shelf wave modes plus the Kelvin wave mode for the Oregon continental shelf (Depoe Bay profile).

cm/sec). Also, the Kelvin wave extends far out to sea, but the shelf waves are very weak beyond the foot of the continental margin. The irregular looking humps and squiggles visible in the eigenfunction curves are reflections of irregularities in the (real) shelf profile. (They are not, as one accustomed to seeing the beautiful plots of analytic functions might surmise, the result of sloppy drafting!)

Figure 2-7 is an artistic rendition of the conformation of the free surface due to the passage of the 1st mode continental shelf wave. The amplitude of the wave and the dimensions of the shelf have been grossly exaggerated. In the cut plane closest to the observer one can see that the sea surface follows the prescription for the first mode eigenfunction as set down in Figure 2-6. It starts high at the coast, drops down beneath mean sea level at about the edge of the shelf, and then approaches MSL asymptotically in the deep sea region. The variations along the coast are sinusoidal and the crests move toward the north if the figure is taken to represent the Oregon coast. The current pattern under the crest line is shown by arrows drawn with lengths proportional to their magnitude. Close to the shore they are oriented in the direction of the advancing wave and are most intense. The magnitude of the current drops off as a function of distance from the beach and goes through a node at a point approximately over the foot of the shelf. Seaward of this node the currents are directed opposite to the phase velocity. Under the trough line this
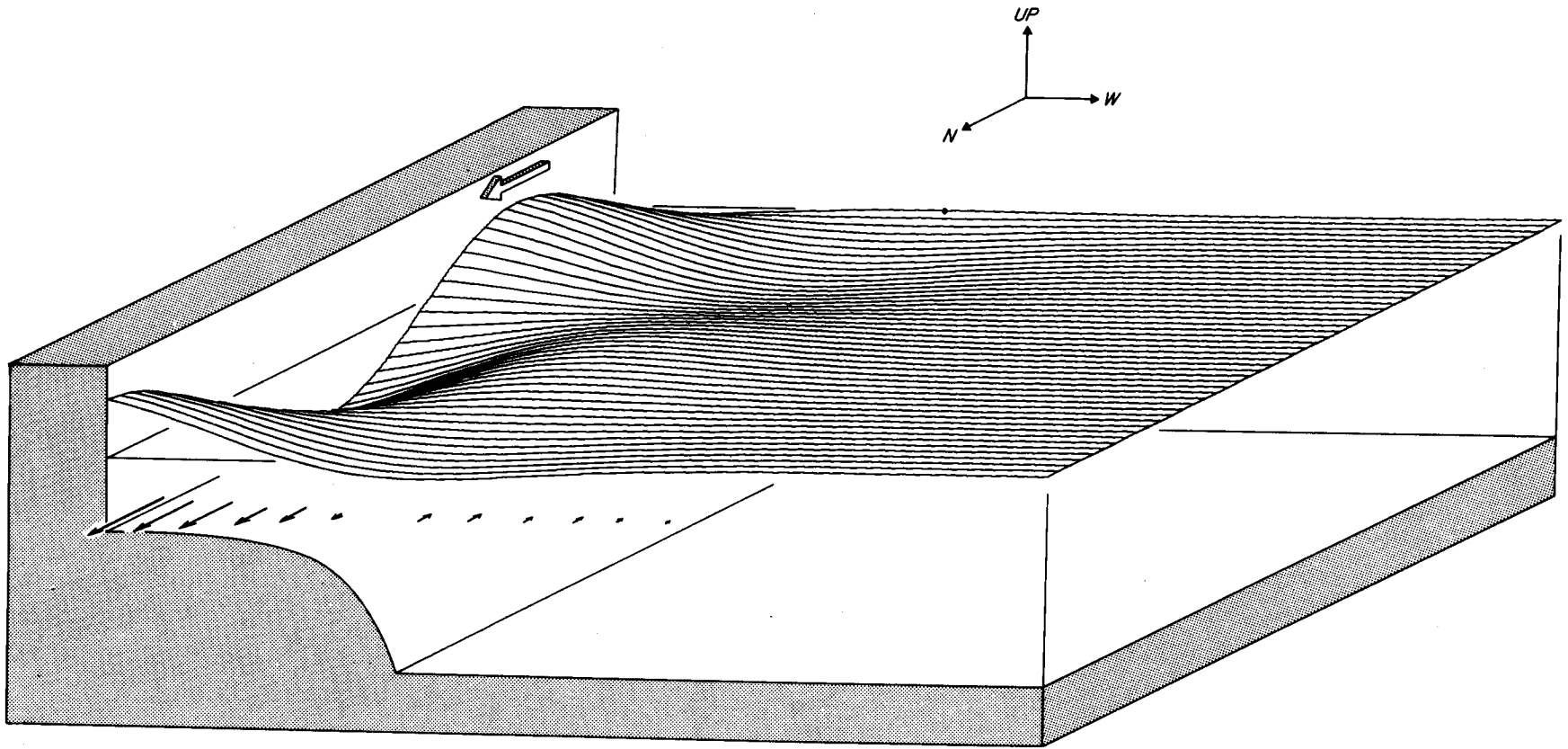
Figure 2-7. First mode continental shelf wave drawn according to the eigenfunction shown in Figure 2-6. Block arrow shows phase velocity (from south to north along the Oregon coast).

current pattern is 180° out of phase. No onshore/offshore currents are present under either the trough or crest lines. Under the "zero crossing" lines, on the other hand, all of the currents are aligned perpendicular to the coastline. At lines intermediate between crest, trough and zero crossing lines, the currents in general have components both perpendicular and parallel to the shoreline.

E. Consideration of Existing Evidence for Low Frequency Waves Trapped Against a Shoreline

Hamon (1962) examined tide gauge and atmospheric pressure records from stations along the coast of Australia and found some strong deviations from the expected isostatic response (1 cm depression for 1 mb overpressure) at frequencies where the sea level and pressure were correlated. His discovery inspired Robinson (1964) to solve the shelf problem theoretically. Later, Hamon (1966) extended this work and noted the apparent existence of sea level disturbances propagated along the coast in the direction predicted by Robinson for shelf waves. By considering stratification in the deep sea region Mysak (1967b) was able to determine a propagation velocity which agreed quantitatively with Hamon's observations.

Mooers and Smith (1968) examined sea level and atmospheric pressure records taken along the coast of Oregon. Their results indicate the existence of a free wave at 0.35 cpd moving from south to

north along the coast. Collins (1968) noted an unusual relationship between Oregon shelf currents and sea level at about the same frequency.

Ma (1969) extended the work by Mooers and Smith to include pressure and sea level records from stations further up and down the coast--Tofino, B.C. and San Francisco, California. His results are similar in form to those presented by Mooers and Smith. However, low coherencies between the Oregon stations and the San Francisco station indicate that there is a low transmission rate of shelf wave energy over this path.

Mysak and Hamon (1969) show additional evidence extracted from sea level and atmospheric pressure records for the existence of free shelf waves propagated from north to south along the coast of North Carolina.

Cartwright (1969) has noted that current and sea level measurements made near the island of St. Kilda off the Hebridies indicate that there the diurnal tidal slot is occupied by a non-divergent oscillation similar to a continental shelf wave. While the vertical tide is almost completely semi-diurnal in character, the currents have a strong diurnal component. At the latitude of St. Kilda, about 58°N, the inertial period is about 14 hrs. This means that the dispersion curves for shelf waves (Figure 2-5) are, for the same general shelf profile,

moved up higher on the frequency scale. Cartwright shows that the high frequency cutoff for the first mode, according to the Buchwald and Adams (1968) theory, coincides with the frequency of the diurnal tide. This would mean that the sea around St. Kilda is tuned to accept or trap energy at this frequency. On the other hand, the dispersion curves for the Oregon continental shelf have a high frequency cutoff which is well below the frequency of the diurnal tide. Therefore the waves over the Oregon shelf must depend upon energy inputs from non-tidal sources such as atmosphere and the deep ocean.

The observations reported by Cartwright (1969) were taken in June and July of 1968. They consisted of current measurements made over a fairly extensive array of stations and tidal measurements made at two points. The duration of the observations was only about one month. From this data it would be possible to observe many features of the shelf wave forms and propagation characteristics. However, Cartwright's 1969 paper contained only a preliminary analysis of the phenomena. Another publication has been promised.

Caldwell, Cutchin and Longuet-Higgins (1971) have found remarkably good quantitative agreement between shelf wave theory and the results of model experiments performed in a rotating tank. Figure 2-8 shows a photograph made by a camera mounted on the tank and looking directly down on the water surface. The tank is rotating counter-clockwise. Currents are made visible through the motions of

aluminum particles sprinkled over the surface. The dashed line indicates the location of the foot of the continental margin. The solid inner curved line shows the location of the beach, here inundated by a shallow layer of water. An oscillating paddle used to generate the waves is located near the black bar in the lower left corner of the photograph. The large swirls seen in Figure 2-8 are shaped like the wave forms predicted by theory for continental shelf waves, and they propagate in a clockwise direction. Also, as first predicted by Buchwald and Adams (1968), for certain frequency ranges the energy is propagated in the opposite (counter-clockwise) direction.

Figure 2-9 shows the data points obtained from the rotating tank experiment against the dispersion curves predicted by the Longuet-Higgins numerical technique. The agreement is quite good.

Figure 2-8. Photo of the first mode continental shelf wave current patterns being generated in a rotating tank. Tank is about four feet in diameter.
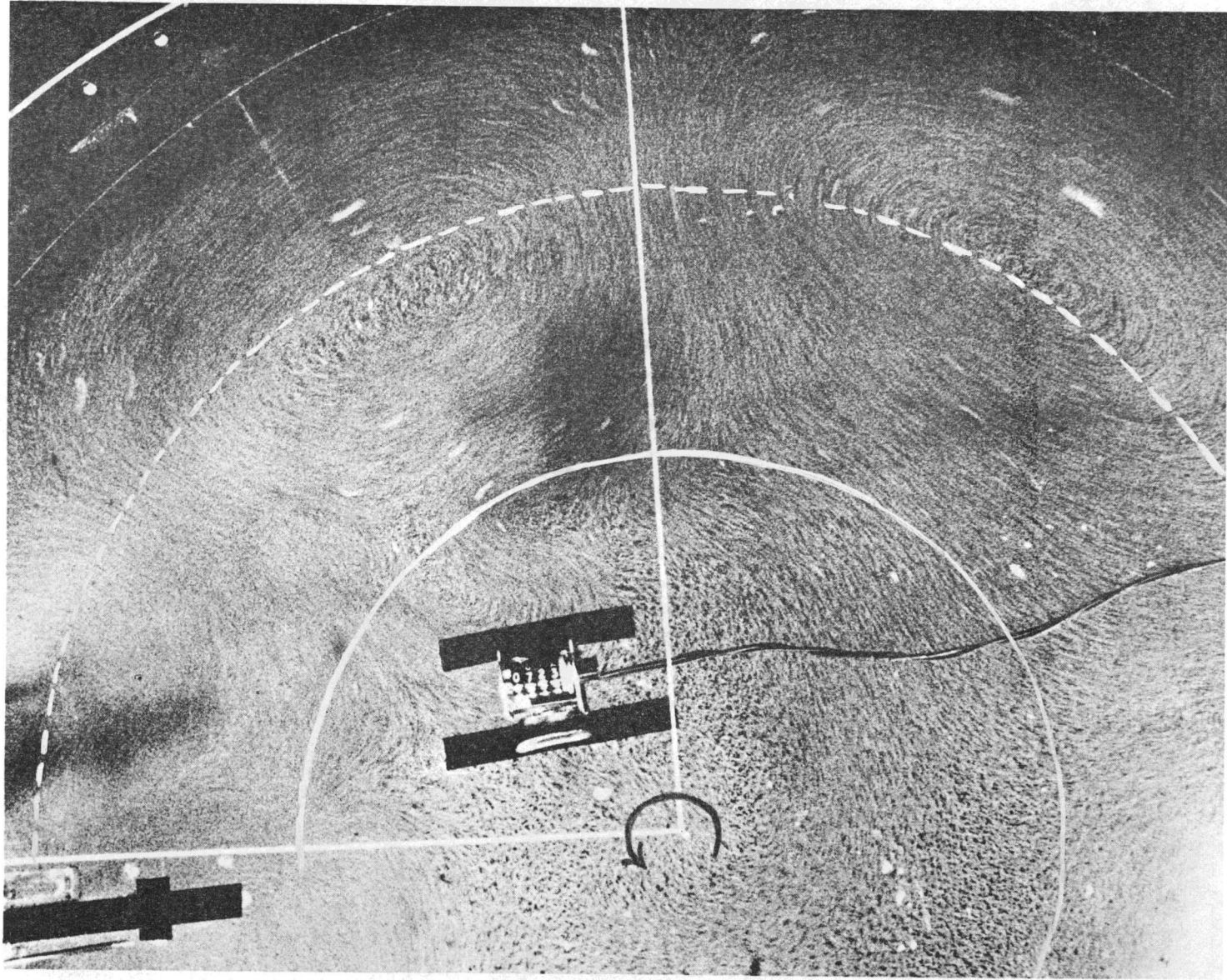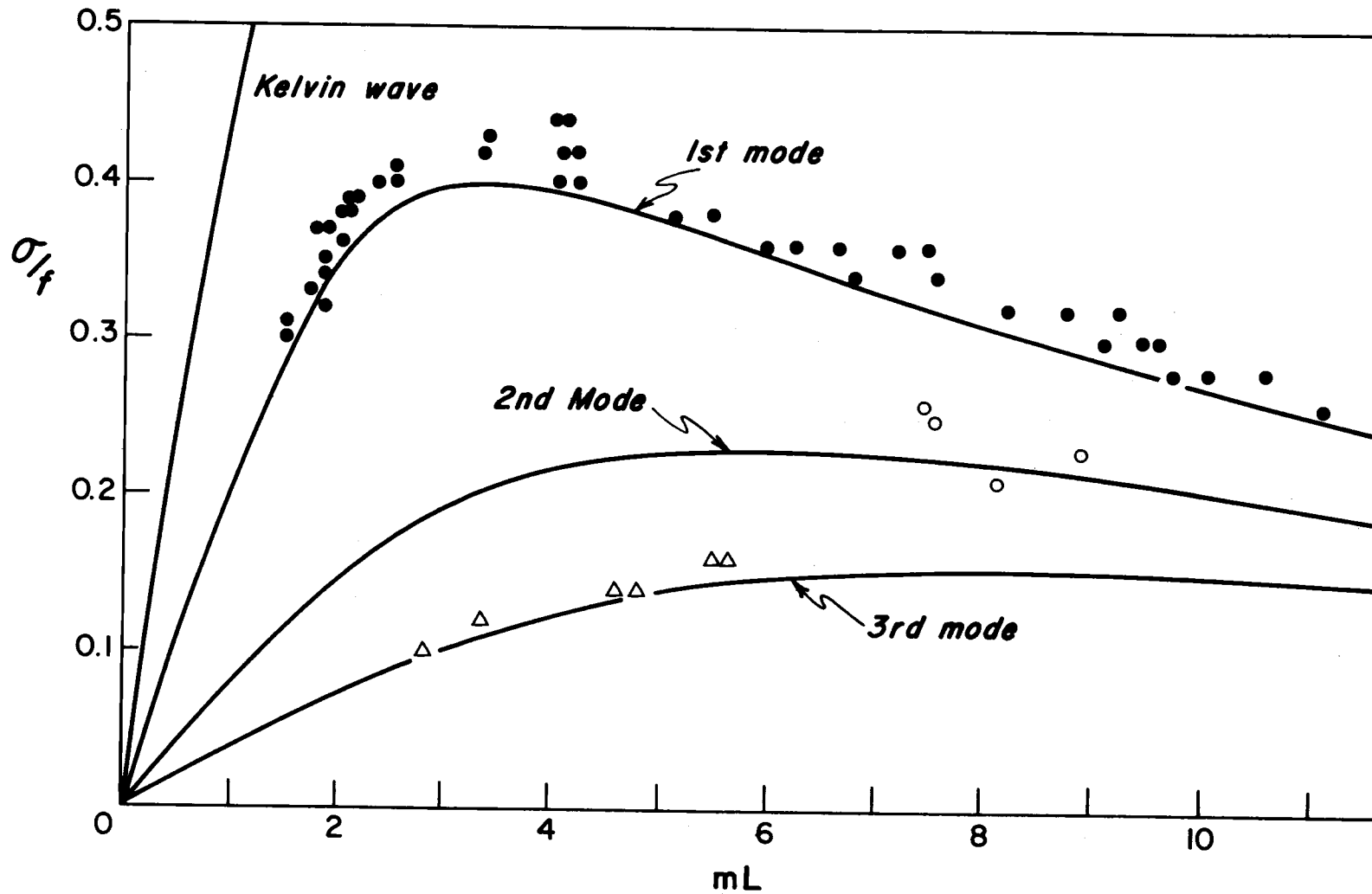
Figure 2-9. Data from rotating tank experiment and continental shelf wave dispersion curves predicted for the tank geometry and rate of rotation. Frequency has been non-dimensionalized by the inertial frequency, 2 radians/sec, and the wave number by the width of the model shelf, L = 6.2 in (Caldwell, Cutchin and Longuet-Higgins, 1971).

III. THE REAL OCEAN EXPERIMENT

A. Experiment Design

Most ocean shelf wave observations have been derived from coastal sea level records. This is largely because of the ready availability of data. However, as Figure 2-6 indicates, the longshore currents associated with a shelf wave are relatively intense. In order to more reliably verify the shelf wave phenomena it is necessary to supplement sea level and other measurements with the information from an array of current sensors.

Only six recording current meters were available at the time of the experiment discussed in this thesis. The operational span of each of the meters was about 30 to 40 days. After this period they required several days of servicing and checkout in the laboratory. In order to obtain continuous observations for 100 days or more, considered necessary to study the low frequency waves, the meters would have to be installed in relays. This means that only three meters would be available at one time.

For the design of the experiment, the two most reasonable options were:

1) to moor the current meters in a horizontal array stretching across and along the shelf; or

2) to place the current meters all at one station in a vertical

array.

If the motions were barotropic, i.e., uniform from top to bottom, the

first arrangement would have facilitated the monitoring of the long-

shore propagation of the waves through the same sort of cross

spectral analysis applied to sea level records in previous research.

Depending upon the spacing of the two meters arranged across the

shelf, it might have been possible to identify the strongest mode pre-

sent in the motions. Figure 2-6 indicates that the amplitude of the

barotropic shelf wave modes vary considerably with distance from

the coast.

It was decided, however, to choose the second option and place

all of the meters at a single station but at different depths. This

decision was largely due to the concern expressed by Mooers and

Smith (1968) that the long period surface waves which they observed

might actually be the surface manifestation of some sort of internal

waves. In addition, the determination of the existence of such internal

waves could be important to the study of time variations in coastal

upwelling. If strong baroclinic waves were present then it would be

necessary to monitor the vertical current profile in order to interpret

the results.

The installation of all three meters at one station also provided

for some redundancy in the system. The current meters had been

used in several previous installations and had earned a very bad reputation for reliability. If one meter in a vertical string of three did fail then the barotropic or baroclinic nature of the current could still be discerned. If the water motion was strongly barotropic then the record from only one operating meter would be representative of the motions of the shole water column at that station.

The current meters were moored at a station in 100 meters of water about seven nautical miles off Depoe Bay, Oregon (Figure 1-1). The station designation is DB-7. The choice of this particular location was based upon several factors:

1) the water depth was sufficiently great to allow for a substantial internal layer between the highly stratified surface layer and the bottom boundary layer;

2) the water depth was shallow enough to allow easy installation and recovery;

3) the location was close to Yaquina Bay, Oregon, the home port of the OSU research vessel and site of a permanently maintained tide gauging station;

4) the shelf contours in this area are relatively smooth and simple; and

5) the location is close to points where several other current measurement programs have been done.

It was decided to maintain the instruments at DB-7 from about mid-April until mid-September 1968. This period would roughly correspond with the summer upwelling season, and the current records would complement other planned research projects in biology and chemistry. The fair weather and calm seas prevalent during this season would facilitate the installation and recovery operations.

Hydrographic sections across the shelf would be obtained at about monthly intervals. The data from these sections would show the extent of density stratification and the baroclinicity of the coastal water due to upwelling.

Four recording thermographs, with approximately the same lifetime and maintenance requirements as the current meters were also available. Two of these instruments were installed with each string of three current meters. It was hoped that one could thus monitor the location of the stratification relative to the current meters, and also detect the vertical oscillations in the density structure that would accompany internal waves.

The tides were being monitored at Yaquina Bay, Oregon. In addition to this measurement it was expected that the Oregon coastal weather stations flanking the installation at Astoria, Newport and Coos Bay/North Bend would be recording atmospheric pressure. Also, the U.S. Coast and Geodetic Survey was maintaining a regular tide gauging station at Astoria within the mouth of the Columbia River.

The experiment design did not include provisions for the direct measurement of surface winds over the ocean at the current meter site. This had been recognized as a serious omission, but the instrumentation was not available at that time.

B. Hydrography

Density Profiles from Hydrographic Sections

During the summer of 1968 several hydrosections were made along the Depoe Bay hydro line (Barstow, Gilbert and Wyatt, 1969). The location of this line is shown by dots in Figure 1-1. Vertical sections along the Depoe Bay line are shown in Figure 3-1. In this sequence of sections one can recognize the progressive intensification of the density stratification through the upwelling season. The sections taken between 23 June and 2 July show a slice across the axis of the plume of extremely light water sweeping down the coast from the mouth of the Columbia River. Figure 3-1 also shows density profiles at DB-7.

The solid squares in the density cross sections indicate the locations of the current meters. One meter was located at each of the three nominal depths, 25 meters, 50 meters and 75 meters. The intention was to place the top current meter above or in the pycnocline yet sufficiently deep to escape the high frequency currents associated

DISTANCE OFFSHORE (nautical miles)

60 50 40 30 20 10 0

23.0

24.0

25.0

17-18 April 1968

25.5

26.0

σ_t
23 25 27

σ_t
23 25 27

17 April
2235 PST

18 April
2320 PST

DEPTH (meters)

DISTANCE OFFSHORE (nautical miles)

60 50 40 30 20 10 0

24.0

25.0

24-26 May 1968

25.5

26.0

σ_t
23 25 27

σ_t
23 25 27

24 May
1915 PST

26 May
1556 PST

DEPTH (meters)
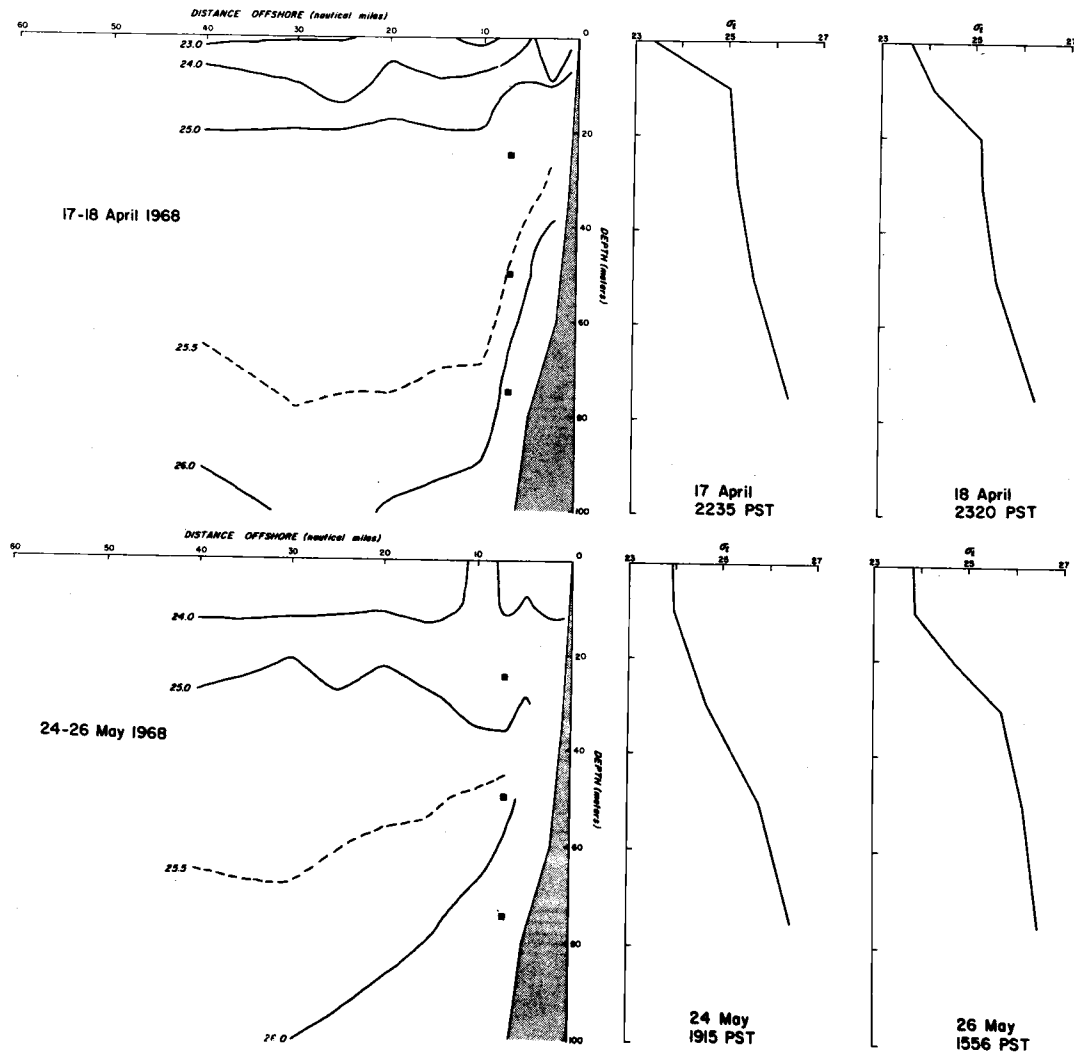
Figure 3-1. Hydrographic sections showing density distributions along
the Depoe Bay hydro line and density profiles at station
DB-7.

55

Figure 3-1. Continued

57
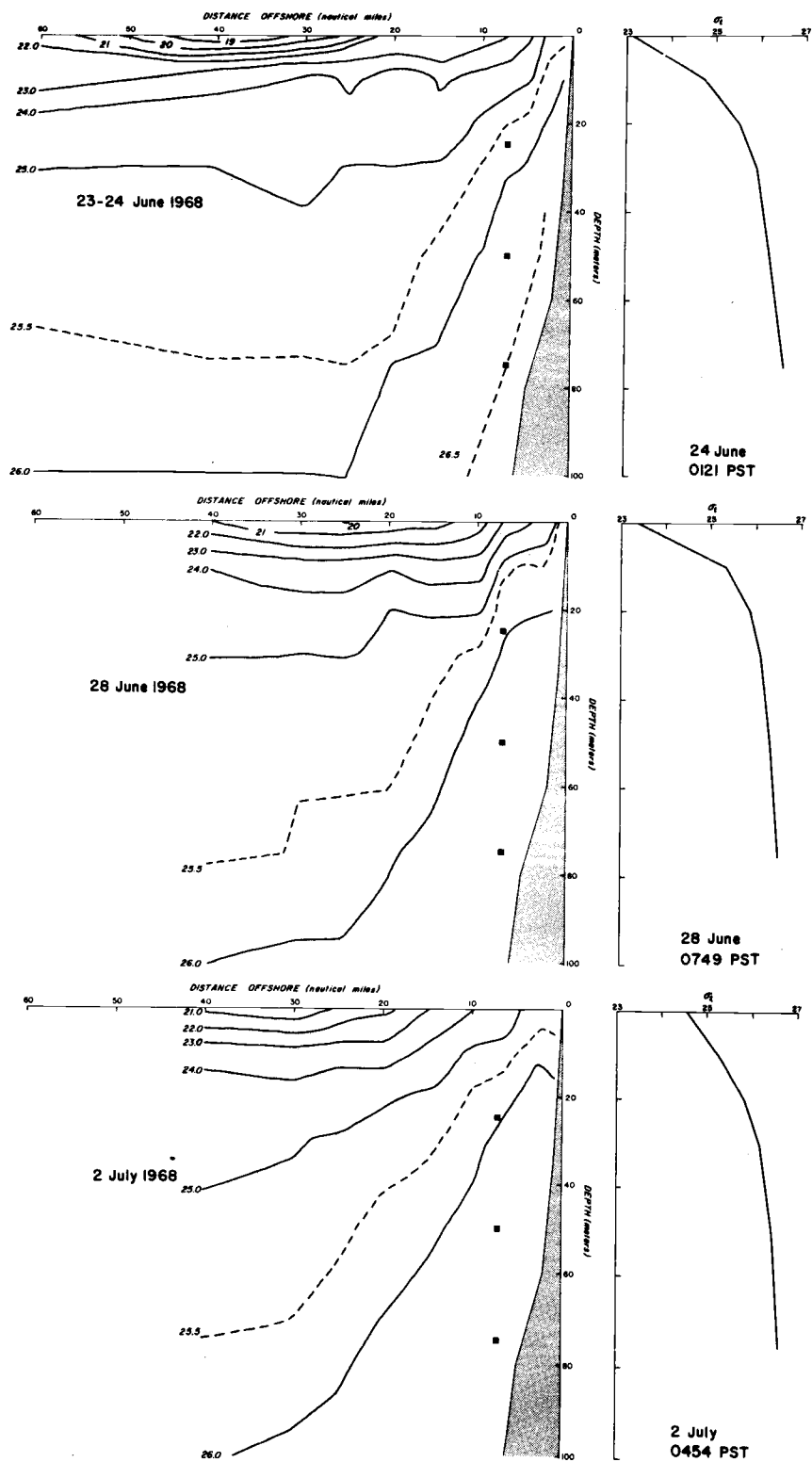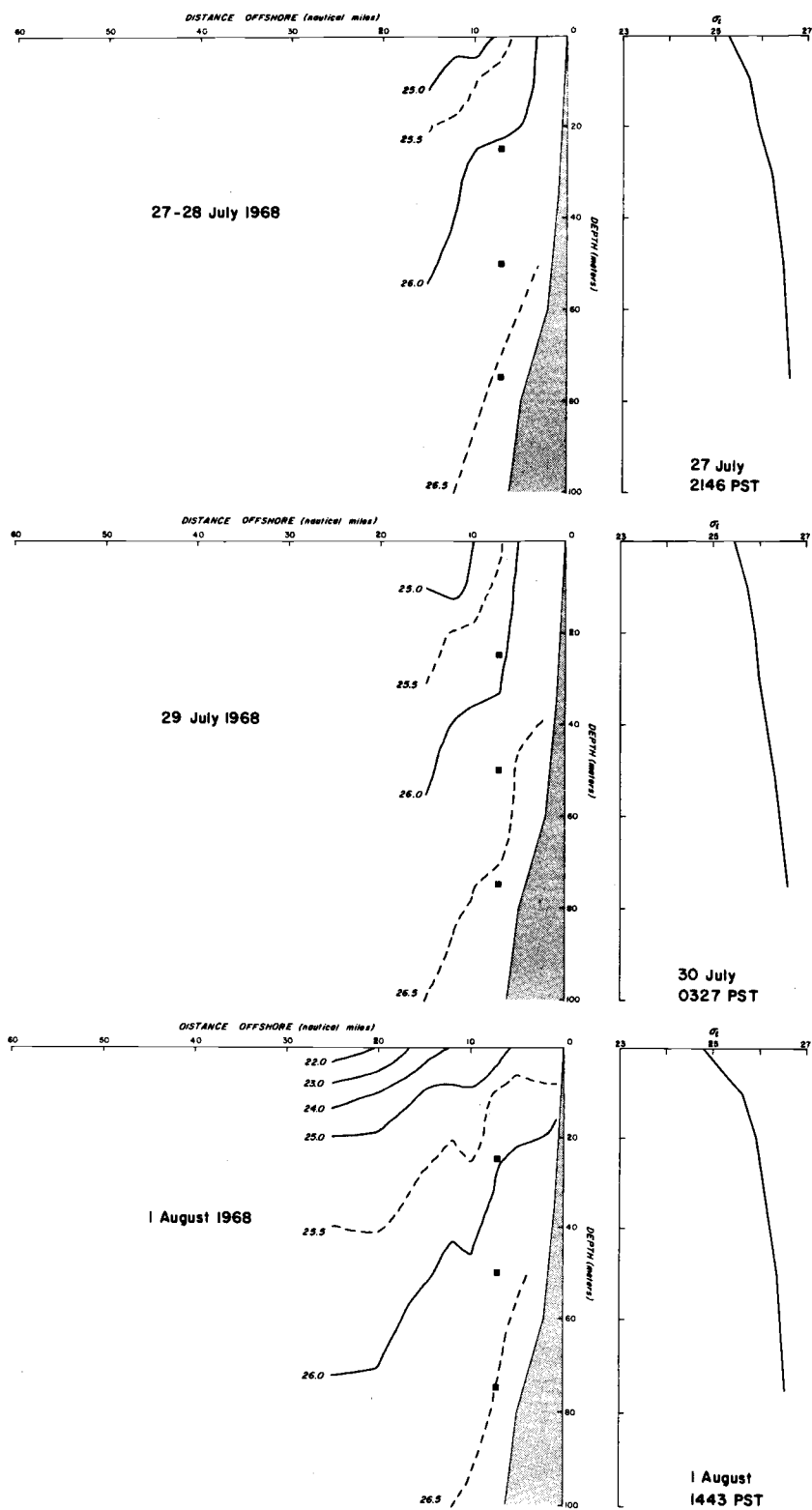
Figure 3-1.   Continued.

with surface wind waves. Unfortunately, the density profiles indicate that the pycnocline was above the 25 m sensor during most of the experiment.

Continuously Recording Thermographs

Some temperature measurements were taken near the 25 and 50 m depths with Braincon type 146 recording thermographs (Fisher, 1969). The instruments did not operate reliably, and only short sections of the desired record were obtained. The records which were gathered showed very few interesting low frequency features. The vertical temperature gradient at 50 m was so small that significant vertical motions of the water could not be detected. The 25 m temperature record is similarly without features except for a single very strong and warm square pulse that occurred between May 22 and May 26. The water temperature rose from about 8.5°C to about 11.0°C and then returned to its original value. This square pulse in the original data series prior to low pass filtering showed a considerable amount of modulation at tidal or possibly inertial frequencies.

C. Current Measurements

Instrumentation

The current meters and thermographs were attached to a vertical

wire which was anchored at the bottom and held taut by subsurface buoys (Pillsbury, Smith and Tipper, 1969).

The current meters used were savonius rotor instruments of the Braincon Type 316. The characteristics of this meter are reviewed by Mooers, Bogert, Smith, and Pattullo (1968). Speed and direction are recorded separately in semi-analogue fashion on 16 mm photographic film. During certain periods the data sampling interval was set at 10 minutes and during others at 20 minutes. The instruments were serviced and replaced in the ocean at about monthly intervals.

Data Reduction

Data was transferred from the film to a digital record by two relatively laborious procedures. Part of the film was converted by visual observation of the projected image on a template. The numbers were read and then recorded by hand on data reduction forms. The rest of the films were digitized with the aid of a digitizing machine. A considerable amount of manual and visual labor was still required, but the process was speeded up and the error count greatly reduced.

The digitized records, containing speed, main direction, direction variability, tilt magnitude and tilt direction, were automatically scanned for possible errors c.f. (Pillsbury, Smith and Pattullo, 1970). The error detection programs were designed to sense

1) impossible or unlikely combinations of numbers pertaining to a single frame and 2) large jumps in the magnitude or direction of the current as determined from a series of successive frames. Flagged frames were individually inspected, and if the digitized record was indeed in error, the correct information was substituted.

The time base on the current records are estimated to be correct to within about ±10 or 20 minutes.

The error corrected records of current speed, in terms of R = average rotor revolutions/sec, were input to the following current meter calibration function

$$S \text{ (cm/sec)} = 1.62 + 36.45 \text{ R (revolutions/sec)}.$$

This expression is a linearized expression of results obtained from test runs by the author in the U.S. Army Corps of Engineers tow basin at Bonneville, Oregon.

The corrected direction records were corrected from magnetic bearing to true bearing. In the vicinity of station DB-7 magnetic north is 20° to the right (east) of true north.

Low Pass Filtering

The calibrated and corrected speed and direction records were converted to velocity components along the E-W and N-S direction. The components were then individually filtered by the symmetrical

low pass filters described in Appendix I. These filters were designed to suppress the tides and all motions of higher frequency. The half power point is about 39 hours. Spectra appearing within the text, except for a small section of Figure 4-2, have not been recolored for the effect of the filter. Recoloring would make only slight differences in the spectra over the range of principal interest, $f = 0$ to $f = 0.5$ cpd.

Since the low pass filter weights spanned a total interval of over four days, when forming filtered values it would ordinarily have been necessary to chop about two days from both ends of the data series. In order to avoid this loss the filters were symmetrically shortened and renormalized when estimating filtered values near the ends of a series. As a filter is thus truncated its response function becomes less sharp, and it admits more high frequency components. Examples of this quality loss in the response functions are also included in Appendix I. The worst possible case would occur when this special filter routine attempted to estimate a filtered value at a time corresponding to the first or last point in the original series. The routine would then return this last point unaltered. In the instances where this difficulty caused obviously unstable data estimates, eyeball estimates were made. A general increase in "wiggliness" at the ends of the low passed series may still be observed in the traces.

The filtering routine formed low passed estimates of the series

at 12 hour intervals. These points were located at 0000 hours and 1200 hours PST. Since only low frequency oscillations were of interest this decimation of the data series considerably eased the storage and analysis operations without limiting its usefulness.

Rotation of the Coordinate System

It was initially determined that most of the oscillating flows were directed along a bearing of 020° which closely coincided with the bearing of the local contours at DB-7. Since the orientation of the contours is one possible natural coordinate system for the currents, it was decided to express the current components in that system. The appropriate transformation from the primed system, with v' positive to the north and u' positive to the east, to the unprimed natural system with v positive along the heading 020° and u positive along 110° is

$$u = u' \cos 20° - v' \sin 20°$$

$$v = v' \cos 20° + u' \sin 20°.$$

This transformation is indicated schematically in Figure 3-2.

D. Surface Tide Measurements

The Yaquina Bay tide gauge was located at the Oregon State University Marine Science Center dock. The data was recorded in
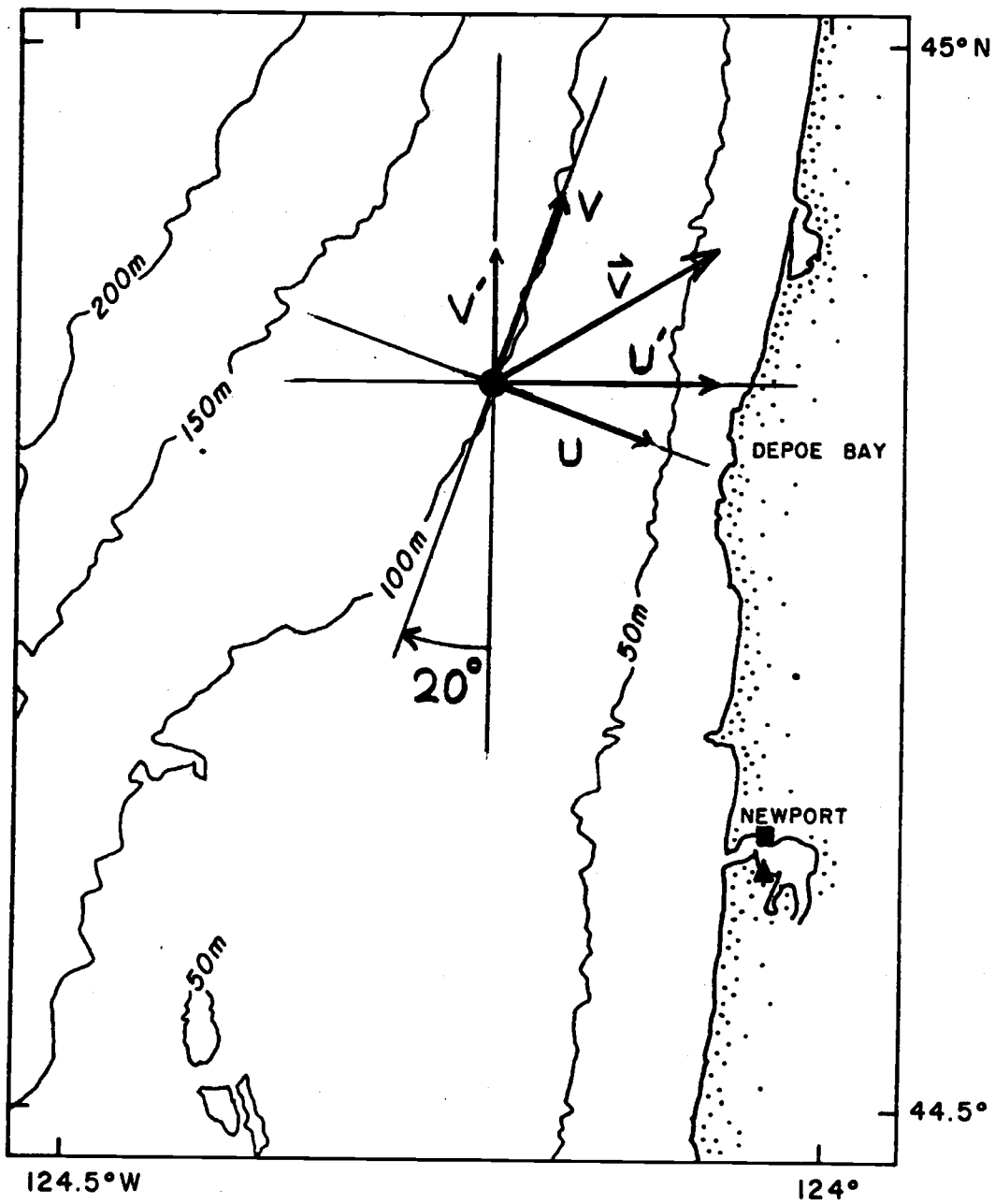
Figure 3-2. Rotation of the coordinates into a system aligned with the local isobaths.

analogue form on a strip chart and in digital form on punched tape.
The rate of digitization was once every six minutes and the precision
is 0.01 ft. Gilbert (1967) noted that during the summer months
analogue traces of sea level in Yaquina Bay were almost free of
oscillations with periods shorter than 12 minutes. Therefore, alias-
ing should not be a problem. The punched tapes were forwarded to
USCGS-ESSA for interpretation and analysis. USCGS-ESSA returned
to OSU both the digitized values of the observed tidal heights and the
predicted tidal heights at hourly intervals based upon their analysis of
a 365 day period beginning 1967-2-1-0 (year, month, day, hour).

The observed values at six minute intervals were filtered with
the low pass filter W3L40 listed in Appendix I. This essentially
eliminated variations with periods of two hours or less and passed
variations with periods of six hours or more.

The USCGS predicted tides were then subtracted from the fil-
tered observed tides to form hourly values of the "residual" tide. It
was noted that the spectrum of the residual still contained peaks at the
diurnal and semi-diurnal periods. The removal of the predicted tide
was intended to reduce the large diurnal and semi-diurnal variations
so that they would pose less of an aliasing problem. This process
also presumably removed the MSf, Mf, Ssa and Sa tides from the
observed sea level record. Since there is no easy way of removing
these long period astronomical effects from the current measurements

this poses a bit of a problem. Fortunately, the amplitudes of these constituents are small.

Also, the USCGS predicted tidal values were only provided to within 0.1 ft. The recomputation of the predicted tides to within 0.01 ft, the precision associated with the observed tides, was not judged to be worth the additional expense. According to Bendat and Piersol (1966) the total quantization noise energy equals the data resolution (0.1 ft or 3.04 cm) squared divided by 12, viz., 0.77 cm^2. If this energy is distributed fairly uniformly over the frequency range it should be insignificant.

The hourly residual sea level values were low pass filtered again (using the filter CL121 in Appendix I), and filtered data values were retained at 12 hour intervals. CL121 has a half power point at about 39 hours when applied to hourly data points.

Preliminary analysis indicated that sea level elevations meas-ured at Astoria, within the mouth of the Columbia River, are related to variations of the open ocean sea level in a complicated fashion. This was undoubtedly recognized by the U.S. Coast and Geodetic Survey in publishing their tide tables for the coast of Oregon and Washington. Although the tables list the tides at Astoria, the only points referenced to those tides are other points within the Columbia River. The tides at Tillamook Bay, just to the south of the mouth of the Columbia, are referenced to Humboldt Bay almost a thousand

kilometers farther south. The tides for coastal points to the north of the mouth of the Columbia are referenced to the predicted tides at Aberdeen, Washington. In addition, variations in the stage of the Columbia River undoubtedly add a considerable amount of low frequency energy to the sea level within the estuary. Further consideration of this problem has been deleted from this thesis.

E. Atmospheric Pressure

Atmospheric pressure data were collected at three hour intervals by the U.S. Weather Bureau observers at Newport and Astoria. The times of recording coincided approximately with 2400, 0300, 0600, . . . , 2100 GMT. The Newport observer is one of a number of observers reporting by telephone to a central station at Salem, Oregon. In order that all of the data from these substations be collected by the prescribed hour of reporting to a national center, the observations must necessarily be made slightly in advance. The observer at Newport makes his observations at approximately 2330, 0230, 0530, . . . , 2030 GMT. The Astoria station reports directly to the central weather bureau via teletype, and the observations are taken only five or ten minutes in advance. The readings at Newport are taken with a precision aneroid barometer which is occasionally checked against a mercury column.

Atmospheric pressure is observed at hourly intervals by the

FAA flight information center at the Coos Bay/North Bend airport.

It is reported via teletype at three hour intervals, coinciding with

2400, 0300,..., 2100 GMT to the central bureau. The observations

are taken five to ten minutes before this report.

The Coos Bay/North Bend and Astoria observations were made

available through the U.S. Weather Records Center, Asheville,

North Carolina. The Newport observations were copied directly from

the log kept by the U.S. Weather Bureau observer at Newport. All

pressures had been corrected to sea level. All pressure records

were passed through an error detection routine which checked for

spikes or discontinuities in the time series.

The three hourly pressure values were low pass filtered with

the symmetrical filter W42L20 (see Appendix I). The half power point

for this filter, as for all of the other filters used here, was about 39

hours. The filtering routine yielded two filtered points per day, one

at 0000 and one at 1200 PST.

The low passed pressure data from Astoria and Coos Bay/North

Bend were surprisingly similar in form and level to the Newport data.

The pressure at Coos Bay was, on the average, only about one milli-

bar above that at Astoria, about 305 kilometers to the north. Plots of

the pressure gradient between these two stations (not shown here)

also showed prominent fluctuations or swings with a period of three to

five days and an amplitude of about three or four millibars.

The current records and the sea level data had been processed so as to yield one point every 12 hours with that point situated at 0000 and 1200 PST. In order the bring the atmospheric data into line with this schedule it was decided to interpolate linearly to obtain values at GMT 2300, 0200, etc., which coincide with PST 1500, 1800, etc. For purposes of simplifying the interpolation, the Newport observations were assumed to have been taken exactly 1/2 hour in advance of the recording time and the Coos Bay/North Bend and Astoria observation exactly at the recording time.

Geostrophic winds for the period of this experiment were computed by Fisher (1969) for the location 45°N, 129°W, on the basis of six hourly surface pressure analyses prepared by the Northwest Regional Forecast Center, U.S. Weather Bureau. Fisher also attempted to correlate the geostrophic winds with the winds observed by the U.S. Coast Guard at Newport and found relatively poor agreement. The wind blowing over the coastal sea is probably considerably different from either of these winds and therefore they were excluded from serious consideration in this thesis.

Bottero and Pillsbury (1971, personal communication) have recently examined winds observed over the Oregon coastal sea (Huyer, 1971) in relation to geostrophic winds predicted for that area by the U.S. Naval Fleet Numerical Weather Facility at Monterey, California. For low frequencies the longshore components seem to agree quite

well. Some further research of this type, involving data from an

array of wind measuring devices, may make is possible to easily

specify the coastal wind field on the basis of large scale pressure

charts. If this were accomplished then it might be possible to unravel

the problem of wind generation versus pressure gradient generation of

shelf waves on the basis of pressure field data alone.

F. Presentation and Discussion of the Complete Data Set

The Data

Figure 3-3 is a composite plot of most of the important data

series actually collected during the experiment. All series have been

low pass filtered to remove variations at tidal frequencies and higher.

The tick marks along the bottom abscissa correspond to 0000 hours

PST on each day. On the first day of each month 0000 hours PST is

marked by a large tick and the date is identified along the top abscissa.

The D's below the traces mark the times of the beginnings of the

Depoe Bay line hydrographic data sampling cruises described in

Section B of this chapter.

The topmost trace in Figure 3-3 is the negative of the atmos-

pheric pressure (in mbs) as measured at Newport. The trace

immediately below is the sea level (in cm) measured at Newport.

The sea level trace is marked as "Sea Level Residual" to indicate that
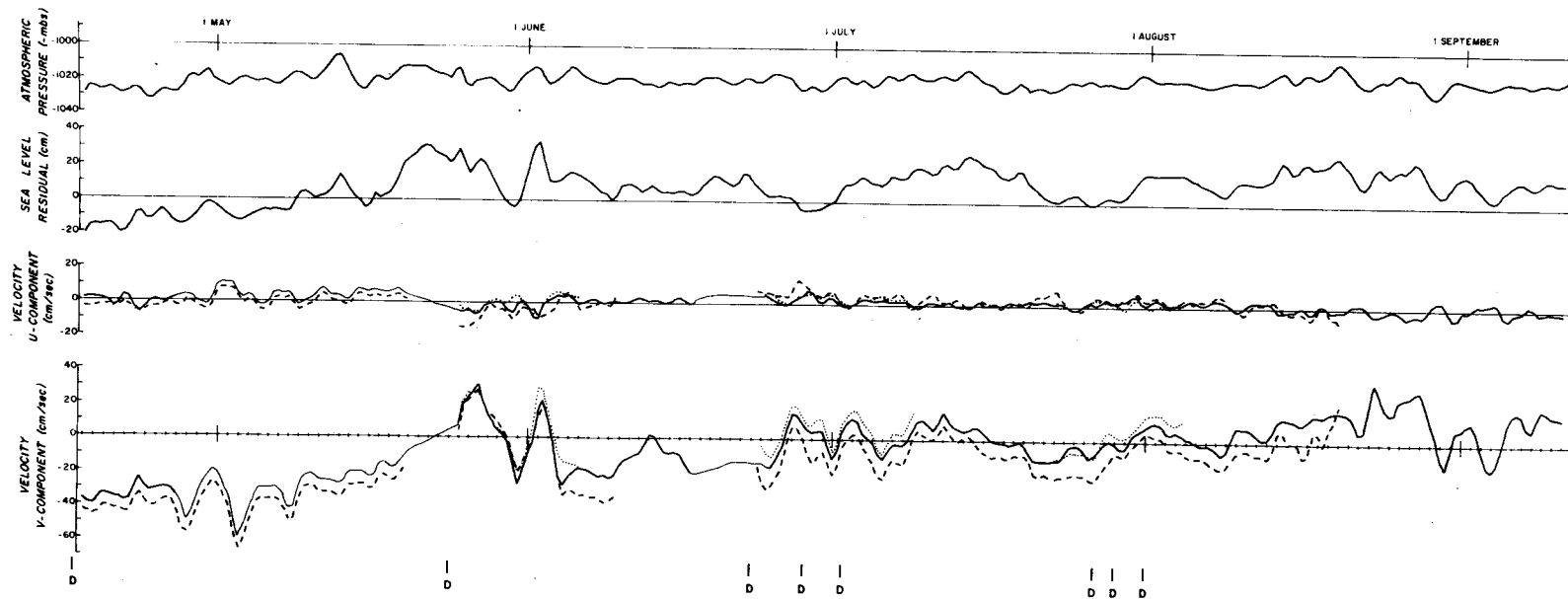
Figure 3-3. Low passed data series from experiment Summer 1968. Dotted lines are currents at 75 m depth. Solid lines are currents at 50 m depth. Dashed lines are currents at 25 m.

predicted tides have been subtracted.

According to the isostatic notion of the sea as an inverse barometer, low pressure troughs should be accompanied by an elevation of the sea surface. The isostatic response to a drop in atmospheric pressure of 1 mb is an elevation in sea level of approximately 1 cm. To facilitate the recognition of this phenomena, the ordinate scales on the sea level and the atmospheric pressure traces are matched so that 1 cm = -1 mb. If the inverse barometer effect holds then the pressure trace and the sea level trace should look almost alike. From an inspection of Figure 3-3 one can see that this effect does not hold in general but that there are definite similarities between the traces.

The current measurements from the three depths are displayed along the same axis. The dotted lines correspond to the currents at 75 m depth, the solid line at 50 m, and the dashed line at 25 m. The "u" component is positive along a heading of 110° true which is approximately onshore at DB-7. The "v" component is positive along a heading of 020° true which is along the local isobaths and roughly alongshore to the north.

There are some substantial gaps in the coverage due to current meter failures. However, there was enough vertical coverage at times to indicate that at low frequencies the longshore component was relatively barotropic. This made the data losses less of a disaster.

As far as the longshore component was concerned one could reason-
ably estimate the motions of much of the water column on the basis of
records from one meter. However at tidal frequencies, which have
been filtered from these series, the onshore and the longshore com-
ponents varied appreciably with depth.

Interpolation of 50 m Current Record

In order to produce a very long current meter record, some
eyeball and smooth line interpolation has been provided for the 50 m
current record. The interpolated sections in Figure 3-3 are indi-
cated by a narrower line. The piece between 1200 hours, 27 April
and 0000 hours, 20 May is simply a tracing of the record obtained at
25 meters depth displaced by +3.0 cm/sec for the u component
and +7.5 cm/sec for the v component. This was done on the
basis of the observed similarities and constant shear between the cur-
rents at different depths for times when simultaneous records were
available. Coherency spectra between the currents at 25 m and 50 m
are presented in Chapter IV. The segment from 0000 hours, 20 May
to 1200 hours, 24 May is a straight line blended into the existing
record. Together these two pieces of contiguous interpolation cover
a period of about 27 days. This is a relatively large patching job and
is probably a bit unreliable. However, for other reasons which will
be discussed later, this entire interpolated section was excluded from

the spectral analysis presented in Chapter IV.

A missing segment between 1200 hours, 17 June and 0000 hours, 24 June was filled with a hand drawn line blended into the surrounding data. This interpolated section constituted about 7% of the 50 m record considered in the spectral analysis. It is therefore not thought to have had any seriously detrimental effect on the statistics.

Discussion

From Figure 3-3 one can readily determine that most of the low frequency current energy is directed alongshore rather than onshore-offshore.

There is a strong, in-phase relationship between variations in the sea level elevation and variations in the longshore current. A northward flowing current near the coast corresponds to an elevation in the sea surface at the coast. A particularly interesting feature is the upward sweep of both the sea level and the longshore component trace from 18 April until about 22 May. This roughly corresponds with the usual beginning of coastal upwelling. The hydrographic coverage during this period was not exceptionally good so one cannot make strong statements about the relationship between upwelling and this current and sea level transition. The hydrographic sections (Figure 3-1) taken from 23 June to 2 July definitely show more upwelling and stratification than the section taken on 18 April. The

section taken on 24 May shows an anomalous feature which probably is not representative of average conditions.

About 19 May, without an appreciable decrease in atmospheric pressure, the sea level went up by about 30 cm. Unfortunately, none of the current meters were operative during this very critical time. Another string of meters installed on 25 May began to record huge oscillations (±30 cm/sec) in the longshore component of the velocity. The hydrographic section taken on 24 May shows the stratification to be weak and the isopycnals to be relatively flat. The current shear between the longshore components at 25 m and 50 m, according to geostrophic flow computations, is almost zero. The current records beginning on 25 May definitely do show vertical uniformity in the long-shore flow. As was mentioned in Section B, thermographs operating during the period of this event recorded a single substantial warm pulse lasting from 22 May until 26 May. The vertical profile of density (Figure 3-1) taken at DB-7 on 24 May shows the presence of an unusual thick layer of light, warm water at the top. The density pro-file taken on 26 May shows that this layer is being replaced by heavy, cold water from below. The strong offshore current at 25 m which was also observed on 26 May is consistent with this interpretation. The generating mechanism for and the physics of this "seiching" motion are not presently understood.

IV. DATA ANALYSIS AND INTERPRETATION

A. Spectral Analysis Procedures

The analysis of the data time series and their interrelationships is based upon the transformation of the information from the time domain to the frequency domain, i.e., the formation of power spectra and their associated statistics. The power spectra were estimated through the intermediate step of computing the lagged correlation and cross correlation functions. In order to reduce the variance of the spectral estimates, the correlation functions were tapered with a Parzen lag window. The tapered correlation functions were then Fourier transformed to give a number of power spectral estimates over the frequency range, 0 to 1 cpd. The standard details of the spectral analysis have been omitted and the reader is referred to Jenkins and Watts (1968) and Blackman and Tukey (1958).

The spectra presented here have not been recolored to compensate for the effect of the low pass filter. (One may note that the spectra fail to rise towards the tidal peak at 1 cpd.) Recoloring would actually effect very little alteration in the spectral shapes over the range of interest, 0 to 1/2 cpd (see Appendix I). In addition the relative statistical indices such as the coherency, gain function and phase shift should be unaltered by the application of identical filters to input data.

The estimated phase relationship between a pair of time series has been plotted only over the frequency range where the squared coherency exceeds 0.20. When the squared coherency is below this value the error bounds on the phase estimates expand so widely as to make the estimate uninterpretable. The phase relationships are plotted on a linear scale. Ninety-five percent confidence intervals have been plotted at selected points.

The coherency spectra have been plotted on a hyperbolic arctangent scale (Jenkins and Watts, 1968). In this system the confidence interval has a constant spread for all estimates. The 95% confidence interval is included in the figures. Squared coherency, perhaps the most commonly used measure of the association between two signals, is the scale indicated.

From Figure 3-3 one may readily ascertain that the current and sea level regime underwent a substantial transition from mid-April until the occurrence of the large storm at the end of May. This indicates that the processes were quite probably not stationary until after that storm. For this reason only the data taken from 0000 hours PST June 5, 1968 until 0000 hours September 11, 1968 were used in the following spectral analysis. The reduction of the available data series by a factor of one-third may be a drastic bit of surgery, but it is by far the most prudent action. If the analysis were extended to cover the entire data series, it would be substantially less interpretable.

Except for the comparisons between currents at 25 meters and 50 meters, the data series subjected to analysis consisted of 197 points spaced at 12 hour intervals. For these series the Parzen window applied to the lagged correlation functions was designed to truncate the function at a maximum of 30 lags. This means that the bandwidth for the estimated spectra is about 0.088 cpd and the equivalent degrees of freedom associated with each spectral estimate is about 24. The spectral estimates were formed at 39 equally spaced frequencies from 0 to 1 cpd.

The comparison between currents at 25 m and 50 m is only possible for the 116 points beginning at 1200 hours PST June 23, 1968 and extending through 0000 hours PST August 20, 1968. In order to maintain a reasonable number of degrees of freedom for the spectral estimates the Parzen window was designed in this case to truncate the correlation functions at a maximum lag of 15. For the Parzen window this means that the equivalent degrees of freedom associated with each spectral estimate is about 28 and the bandwidth is about 0.178 cpd. For the shear series the spectra have been estimated at 20 equally spaced frequencies from 0 to 1 cpd.

Prior to spectral analysis a linear trend was removed from all data series.

B.   Autospectra of Basic Series

Figure 4-1 contains the spectrum of the observed sea level

variations at Newport, Oregon. A characteristic of many geophysical

spectra is this steep rise at very low frequencies. If the diurnal tide

were still present the spectrum would also sweep way up at the other

end at 1 cpd.

Figure 4-2 shows the spectrum of the observed atmospheric

pressure at Newport   The dashed line indicates a portion of the

spectrum recolored for the effect of the low pass filter.

Figure 4-3 shows the spectrum of both the longshore   (v)

component and the onshore   (u)   component measured at a depth of

50 meters. The components were taken with respect to the coordinate

system with   +v   at a bearing of 020° true as explained in Chapter

III. This coordinate system is roughly aligned with the local isobaths.

C. Cross Spectra Between Basic Series

Current Components and Principal Axis Transformation

Figure 4-4 shows the squared coherency spectrum and the phase

spectrum for   u   at 50m vs.   v   at 50 m in the topographic (020°

true) coordinate system. The strong peak in the squared coherency

around 0.22 cpd is evidence for the action of some sort of an organiz-

ing principle in the fluid motion at that frequency. Wave motion is one
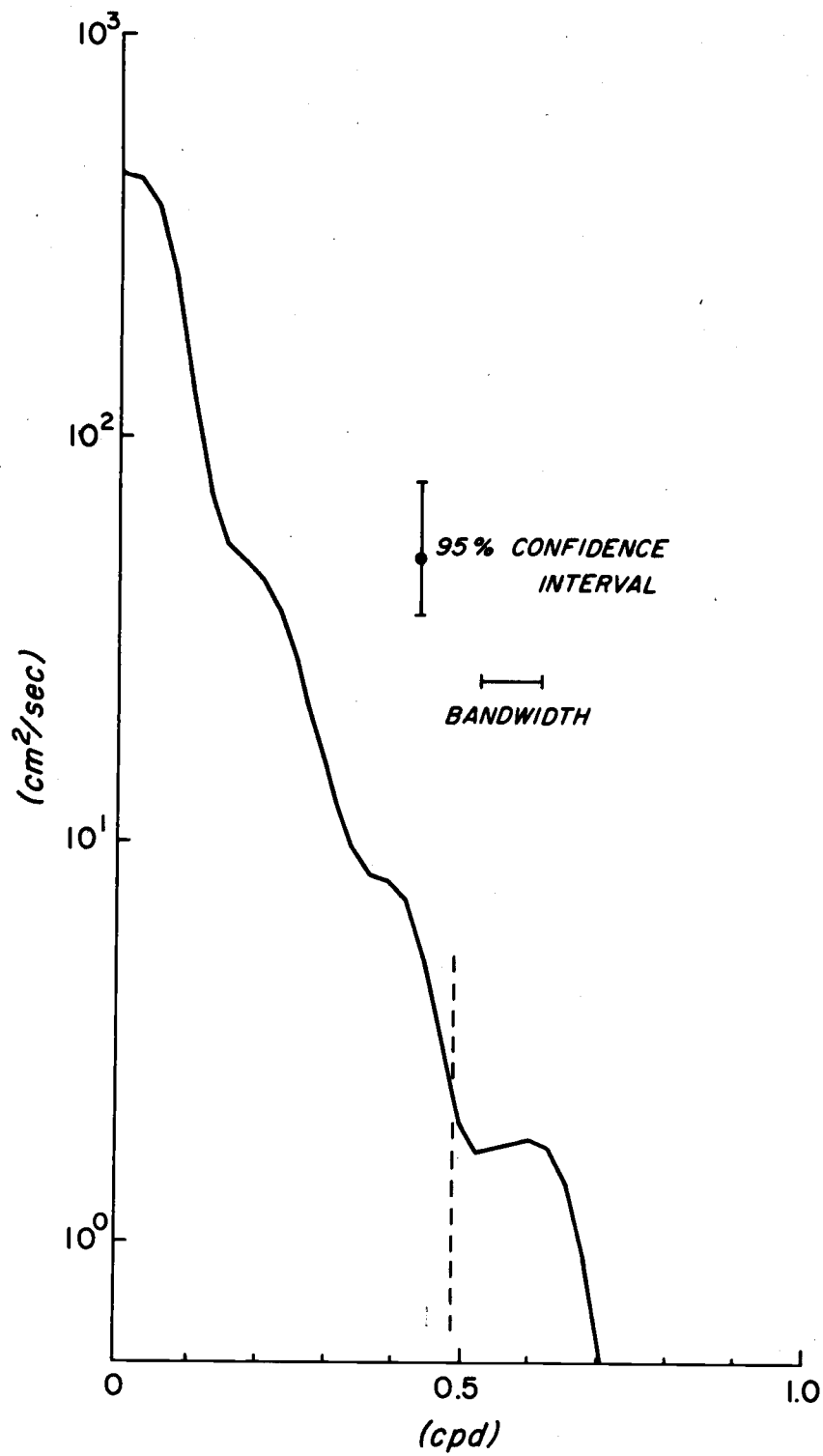
Figure 4-1. Power spectrum of residual Newport sea level.
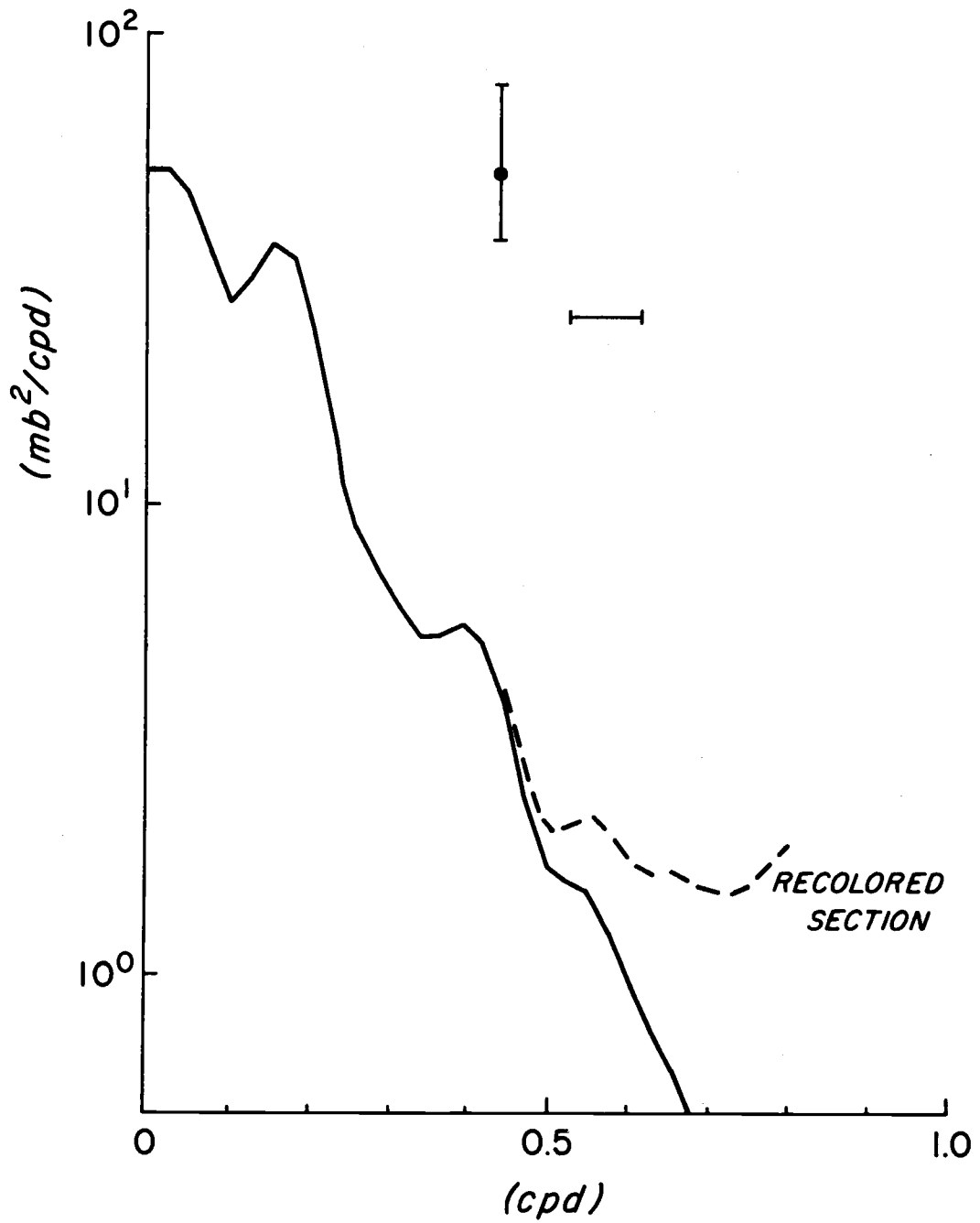
Figure 4-2. Power spectrum of observed atmospheric pressure at Newport. Small recolored section shows effect of low pass filter.
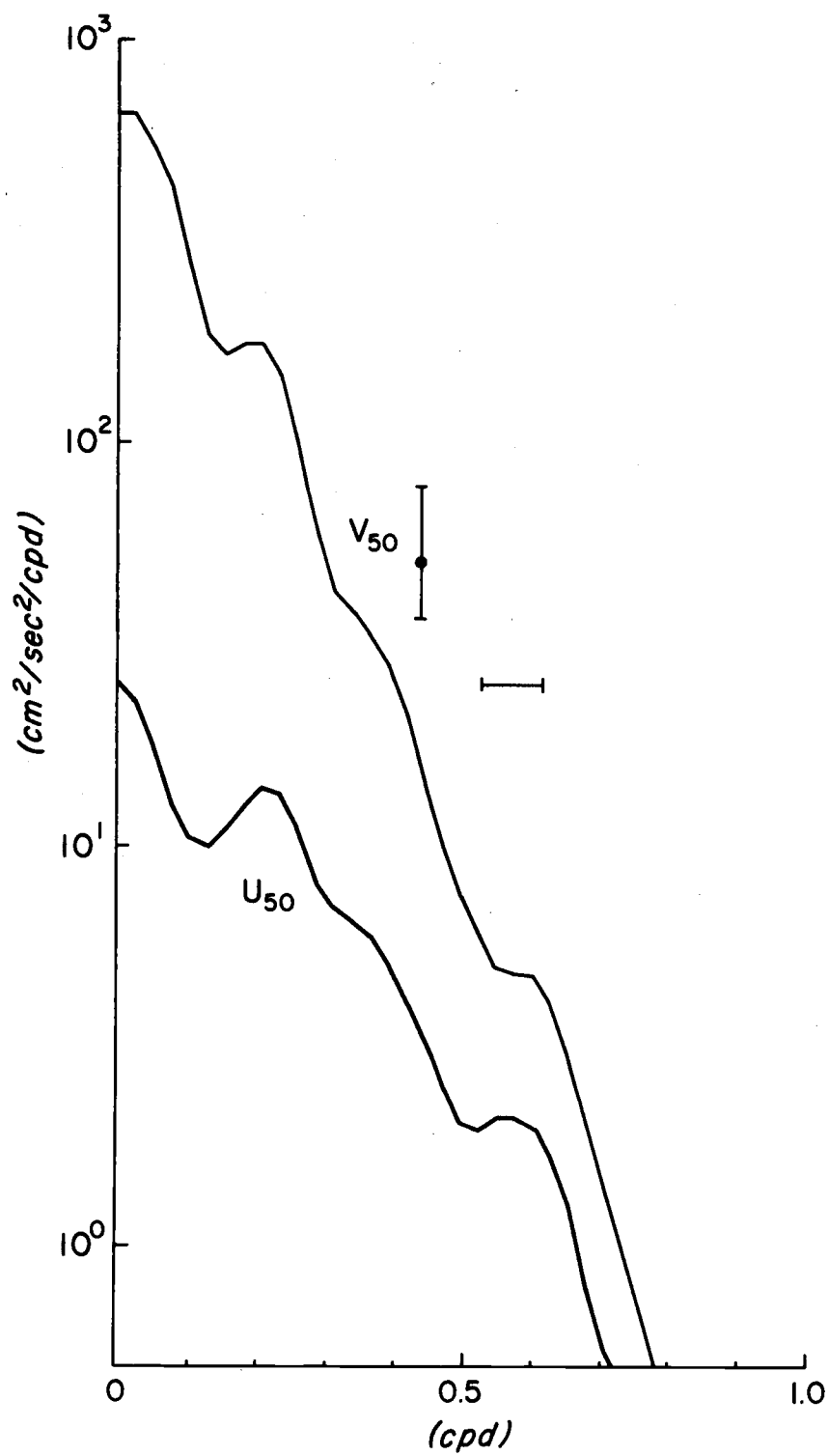
Figure 4-3. Power spectra of u and v components measured at 50 m depth.
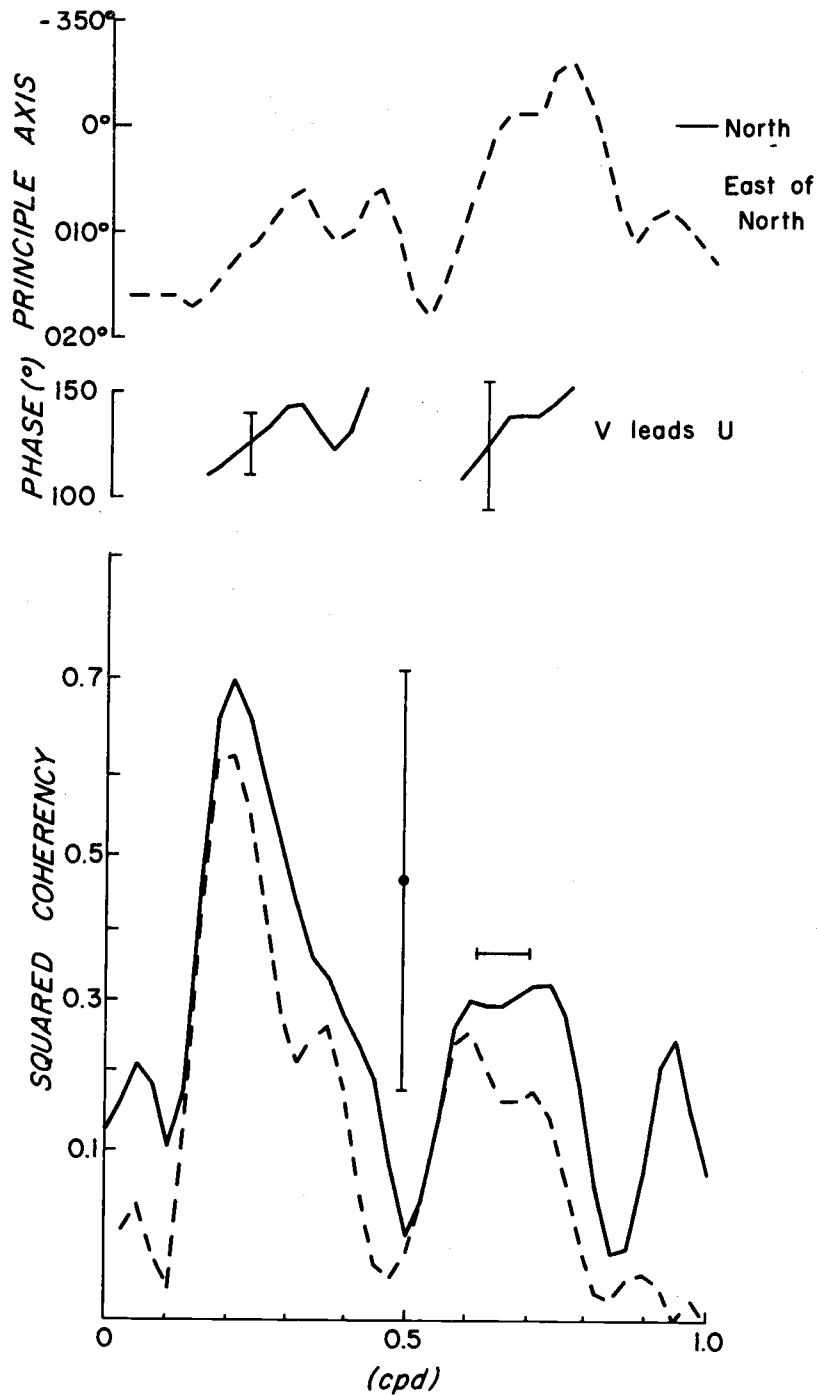
Figure 4-4. Coherency spectra of u_{50} vs. v_{50} in both topographic (solid line) and principal axis (dashed line) coordinate systems; phase spectrum between currents in topographic system; orientation of principal axis system.

possible organizing principle. At a point within a wave field the
current precesses regularly about the points of the compass. The
coherency between the current vectors would be quite high. However,
a high coherency is only necessary and not sufficient evidence for the
presence of wave motion. A very simple phenomena can generate
high coherencies between the components of the fluid motions in a
fully turbulent and disordered field. The proximity of a boundary
tends to flatten out turbulent eddies (and also to modify shelf wave
currents) so that most of their motion is strung out along an axis
parallel to the boundary. If the coordinate system in which the
velocity components are measured is rotated from this axis of elonga-
tion, in some cases even slightly, then the estimated coherency
between the components is spuriously high.

In order to resolve this quandary the "principal axis" transfor-
mation was applied to the measured currents. The principal axis, or
hodograph coordinate system, can be defined as that system in which
the cospectrum is reduced to zero (Mooers, 1970). There is a par-
ticular principal axis transformation for each frequency. The true
heading of the $+v$ axis of the principal axis system for the v_{50}
data record is shown by the dashed curve at the bottom of Figure 4-4.
The principal axis systems are mostly aligned at headings between
the general alignment of the coast and shelf, and the local bathymetry.

Since the quadrature spectrum (Q_{uv}) is invariant with respect

to rotation and since the coherency squared is defined as

$$\gamma^2(\omega) = \frac{Q_{uv}^2(\omega) + P_{uv}^2(\omega)}{P_{uu}(\omega)\, P_{vv}(\omega)}$$

the reduction of the cospectrum P_{uv} to zero by a rotation to the

principal axis system minimizes the coherency. The residual

coherency based upon the quadrature spectra is the type of coherency

expected between the components of the motion of a fluid disturbed by

wave motion. Expressions 2-15 and 2-16 predict that the u and v

components should be in quadrature, i.e., out of phase by 90°.

If the orientation of the shelf were purely evident, such as in the

case of a shelf with perfect longshore uniformity, then it would be a

straightforward matter to rotate the coordinate system to the shelf

orientation and then to test for the phase and coherency between the

u and v vectors. In the case of wave motion one would expect to

find a strong coherence between u and v and the phase shift

should be 90°. In the case of real shelf topography, however, one has

an opportunity to select from a range of shelf orientations reasonably

lying between that of the local topography and that of the general

topography. Under these indefinite circumstances one may reverse

this and initially require that u and v be out of phase by 90°

($P_{uv} = 0$). One thus uniquely determines the orientation of the coordi-

nate system which satisfies this condition. If the system thereby

determined is a reasonable system this is is some evidence for the existence of wave motion. If in addition the coherency between u and v remains strong even in the principal axis system, this is much stronger evidence for wave motion. The confused motions due to turbulence do not exhibit this characteristic.

In order to examine more closely the interesting phenomenon which occurs at a frequency of about 0.22 cpd the coordinate system was again rotated so that the $+y$ axis was oriented along a heading of 012° true. This heading corresponds to the principal axis orientation given in Figure 4-4 for 0.22 cpd. The effect of this rotation is to tune the standard spectral analysis techniques to the phenomena occurring at this frequency. The orientation of the coordinate system for $\vec{v}$ is a natural (or principal axis) for the phenomenon.

The autospectra for u and v in the natural (012° true) system are only very slightly different from the autospectra in the topographic (020° true) system as shown in Figure 4-3. For this reason they are not presented here.

The squared coherency and phase between u and v in the natural system are presented in Figure 4-5. At 0.22 cpd the v component leads the $\dot{u}$ component by about 90°. Since the measurement station was inshore on the predicted nodal line for u and v (Figure 2-6) this is the proper phase relationship for the currents within a continental shelf wave.
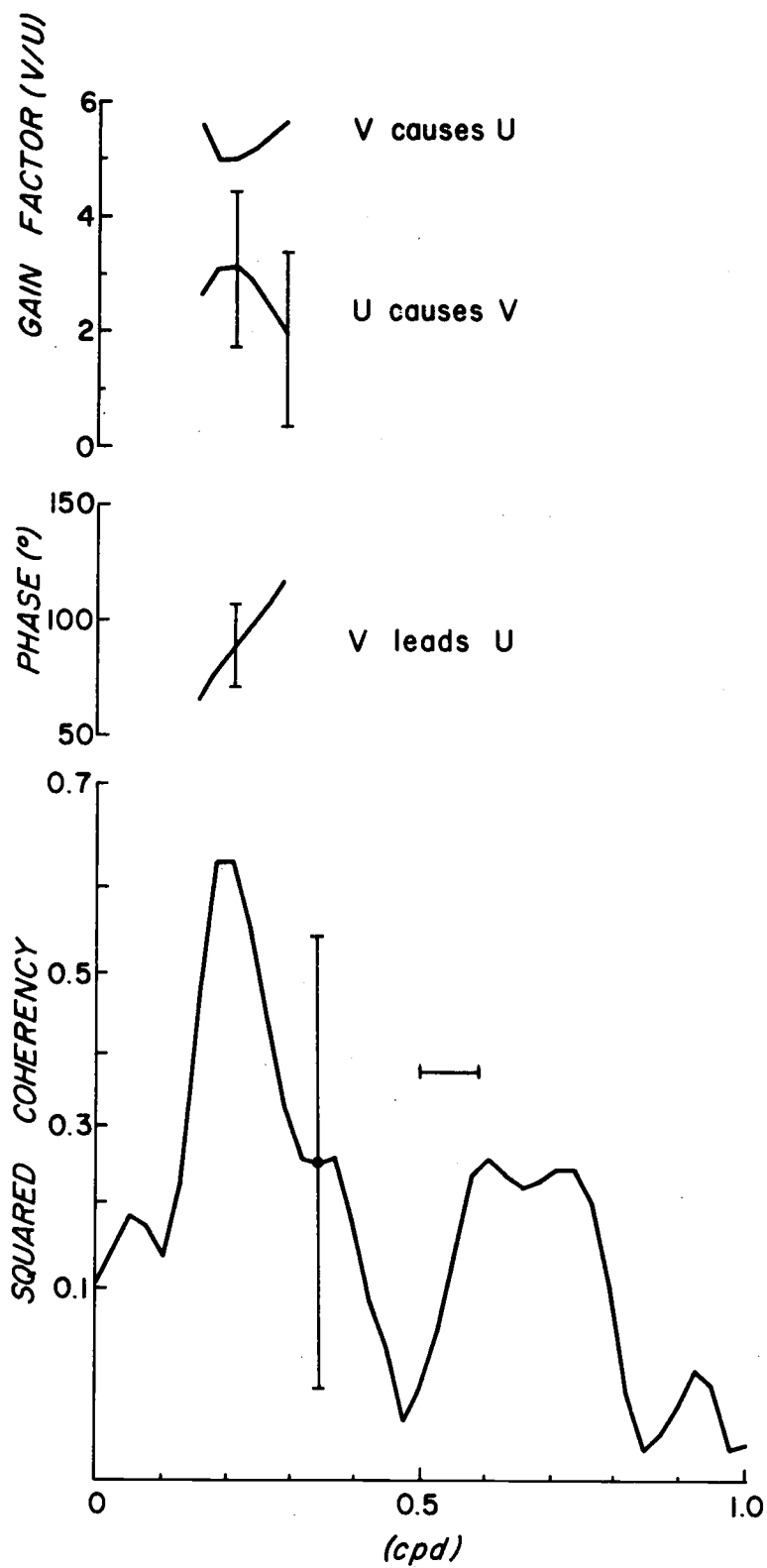
Figure 4-5. Cross spectral indices for u_{50} vs. v_{50} in the natural (012°) coordinate system.

Transfer and Gain Functions

Shelf wave theory predicts not only the phase relationship but also the amplitude ratio between the oscillations in the u and v components of the velocity. These amplitude ratios, as a function of distance from the beach are specified by the eigenfunctions $u_0(x)$ and $v_0(x)$ in Figure 2-6. In order to simplify the presentation of the discussion which follows let us symbolize the predicted amplitude ratios as

$$R_{u/v}(x,\omega) = \frac{u_0(x,\omega)}{v_0(x,\omega)}$$

and

$$R_{v/u}(x,\omega) = \frac{v_0(x,\omega)}{u_0(x,\omega)}$$

where ω is the frequency. From the real ocean current measurements we might attempt to estimate the amplitude ratio between variations in the observed u component and the observed v component, as a function of frequency and then compare this with the predicted ratio. Let us denote the estimated ratios by $\widehat{R}_{u/v}$ and $\widehat{R}_{v/u}$. Since currents were measured at only one station we can estimate the ratios and check them against predictions only for $x = 13$ km from the beach.

Under certain circumstances the analysis procedures for estimating the amplitude ratio between the variations in two series are

quite straightforward. These certain circumstances usually involve the assumption that the two series involved are related as cause and effect. For example take $x(t)$ as an input to a linear system and $y(t)$ as the output. Noise enters only within the system or in the measurement of the output. We may then estimate the (complex) transfer function of the system by

$$H_{xy}(\omega) = \frac{P_{xy}(\omega)}{P_{xx}(\omega)}$$

where $P_{xy}(\omega)$ is the (complex) estimated cross spectrum between $x(t)$ and $y(t)$, and $P_{xx}(\omega)$ is the estimate autospectrum of $x(t)$. $H_{xy}(\omega)$ can also be expressed in the polar form

$$H_{xy}(\omega) = \left| H_{xy}(\omega) \right| e^{-i\phi(\omega)}$$

where

$$\left| H_{xy}(\omega) \right| = \frac{(C^2_{xy}(\omega) + Q^2_{xy}(\omega))^{1/2}}{P_{xx}(\omega)}$$

and

$$\phi_{xy}(\omega) = \tan^{-1}[Q_{xy}(\omega) / C_{xy}(\omega)]$$

are the estimated "gain function" between $x(t)$ and $y(t)$ and the estimated "phase function" between $x(t)$ and $y(t)$. $C_{xy}(\omega)$ and $Q_{xy}(\omega)$ are the co- and quadrature spectral estimates, respectively, between $x(t)$ and $y(t)$.

There are serious difficulties involved in the use of the gain function estimators $H_{uv}(\omega)$ and $H_{vu}(\omega)$ to represent $\widehat{R}_{v/u}(\omega)$ and $\widehat{R}_{u/v}(\omega)$ respectively in the estimated gain functions between the u and v series with the predictions of wave theory. These difficulties stem from the fact that there is no clearly defined cause and effect relationship. u(t) and v(t) arise on the same footing. If we form the estimates $\widehat{R}_{u/v}(\omega)$ and $\widehat{R}_{v/u}(\omega)$ we naturally expect from this symmetry that

$$\widehat{R}_{u/v}(\omega) = 1/\widehat{R}_{v/u}(\omega)$$

or

$$\widehat{R}_{u/v}(\omega)\widehat{R}_{v/u}(\omega) = 1$$

should hold. However,

$$\left|H_{vu}(\omega)\right|\left|H_{uv}(\omega)\right| = \frac{[C^2_{uv}(\omega)+Q^2_{vu}(\omega)]^{1/2}[C^2_{uv}(\omega)+Q^2_{uv}(\omega)]^{1/2}}{P_{uu}(\omega)P_{vv}(\omega)}$$

$$= \gamma^2(\omega)$$

which is, in general, less than one. In the case of two series arising on the same footing, the gain functions are therefore biased by the arbitrary assignment of some cause and effect relationship. The magnitude of this bias depends upon the noise level. If the two series are perfectly coherent then the difficulty completely disappears. However, if the series were completely coherent then the problem

would become degenerate and we could simply form the estimate

$$R_{u/v}(\omega) = \sqrt{\frac{P_{uu}(\omega)}{P_{vv}(\omega)}} \quad .$$

Besides the "cause and effect plus noise" statistical model there are two other simple models for a pair of related time series which fit the current vector problem more closely. One of these is the "feedback" model (Granger and Hatanaka, 1964). The current components under a shelf wave might be locked in a feedback loop because at a point the longshore current does precipitate the offshore current and the offshore current the reversal of the longshore current in turn. The other statistical model is of the two series as co-effects of a third unknown, causal series. The causal series in the case of a coastal sea would be something like the atmospheric pressure or wind stress. Unfortunately, it is impossible to estimate amplitude ratios for these models unless something is known of the partition of noise between the two series. The essential simplifying feature of the cause and effect model is that all of the noise is assumed to be in the effect or output.

Let us proceed with an intuitive formulation for the estimated amplitude ratios. Although they are biased the estimated gain functions quite possibly bracket the desired estimate; i.e., perhaps

$$\left|H_{uv}(\omega)\right| \lessgtr \widehat{R}_{v/u}(\omega) = \frac{1}{\widehat{R}_{u/v}(\omega)} \gtrless \frac{1}{\left|H_{vu}(\omega)\right|}$$

In Figure 4-5 $\left|H_{uv}(\omega)\right|$, the gain function for u causing v, is plotted as the lower curve in the "gain factor" diagram. Some 95% confidence intervals have been included. $1/\left|H_{vu}(\omega)\right|$, the reciprocal of the gain function for v causing u, is plotted as the upper curve. These curves are taken as brackets for the proper estimate $\widehat{R}_{v/u}(\omega)$. Note that the interval between the curves narrows down in that region where the coherency is highest and that in the limit as $\gamma^2(\omega) \rightarrow 1$,

$$\left|H_{uv}(\omega)\right| = \frac{1}{\left|H_{vu}(\omega)\right|} = \sqrt{\frac{P_{vv}(\omega)}{P_{uu}(\omega)}} \ .$$

Table 4-1 lists the gain factor brackets for the estimated amplitude ratio between variations in v and u at a frequency of about 0.22 cpd. It also contains $\sqrt{\dfrac{P_{vv}(\omega)}{P_{uu}(\omega)}}$ for 0.22 cpd. These are compared against the first mode predicted $R_{v/u}$ for $\omega = 0.215$ cpd and $x = 13$ km from the beach (Figure 2-6).

Sea Level and Current Variations

Since the theory for free shelf waves predicts that sea level variations should accompany current variations it is reasonable to search for this connection. It is first necessary, however, to attempt to remove that part of the sea level variance that is due to local

Table 4-1. A comparison of predicted shelf wave eigenfunctions with parameters estimated from current and sea level observations.

	Estimated From Measurements ($\omega = 0.22$ cpd, x = 13 km)		Predicted		
			R(ω, x = 13 km)	ω (cpd)	Mode
v vs. u	$\widehat{R}_{v/u} = \begin{cases} 3.1 \\ 5.0 \end{cases}$ ($\gamma^2 = 0.63$)		37 34 9.9 $\longrightarrow$ 3.3	0.242 0.215 .28 .225	1 1 2 3
	$\sqrt{P_{vv}/P_{uu}} = 3.9$				
Sea Level vs. u	$\widehat{R}_{sl/v} = \begin{cases} 1.1 \\ 2.3 \end{cases}$ ($\gamma^2 = 0.51$)		12 19 $\longrightarrow$ 1.8 0.48	0.242 0.215 .23 .225	1 1 2 3
	$\sqrt{P_{ss}/P_{uu}} = 1.6$				
Sea Level vs. v	$\widehat{R}_{sl/v} = \begin{cases} 0.37 \\ 0.45 \end{cases}$ ($\gamma^2 = 0.82$)		$\longrightarrow$ 0.36 $\longrightarrow$ 0.50 0.18 0.145	0.215 0.242 .23 .225	1 1 2 3
	$\sqrt{P_{ss}/P_{uu}} = 0.41$				

forcing by atmospheric pressure.

Equation 21 predicts that the coastal sea should respond to atmospheric pressure as an inverse barometer except when the pressure systems contain energy of the proper longshore wave number and frequency to cause resonance. Since, from general considerations, one would expect to find only a minor fraction of the variance of atmospheric pressure lying in or near the resonance wave number-frequency pair, it seems reasonable to attempt to remove the forced part of the observed sea level variations by adding the atmospheric pressure (expressed in cm of salt water) to the observed sea level (in cm). This is, of course, not a valid adjustment for the small part of the pressure variations which satisfy the resonance condition. The autospectra for the adjusted sea level at Newport is shown in Figure 4-6. The autospectra for the observed sea level at Newport, as shown in Figure 4-1, has been included for comparison.

Figure 4-7 shows the coherency, phase and gain factor spectra for atmospheric pressure vs. sea level at Newport. In this situation atmospheric pressure and sea level are more clearly related as cause and effect respectively and the gain function is less ambiguous.

Figure 3-8 shows the cross spectral indices between sea level adjusted for atmospheric pressure and the u (onshore) component of the current. The dotted lines are for the unadjusted sea level vs. u. They are included to show the effects of the pressure adjustment.
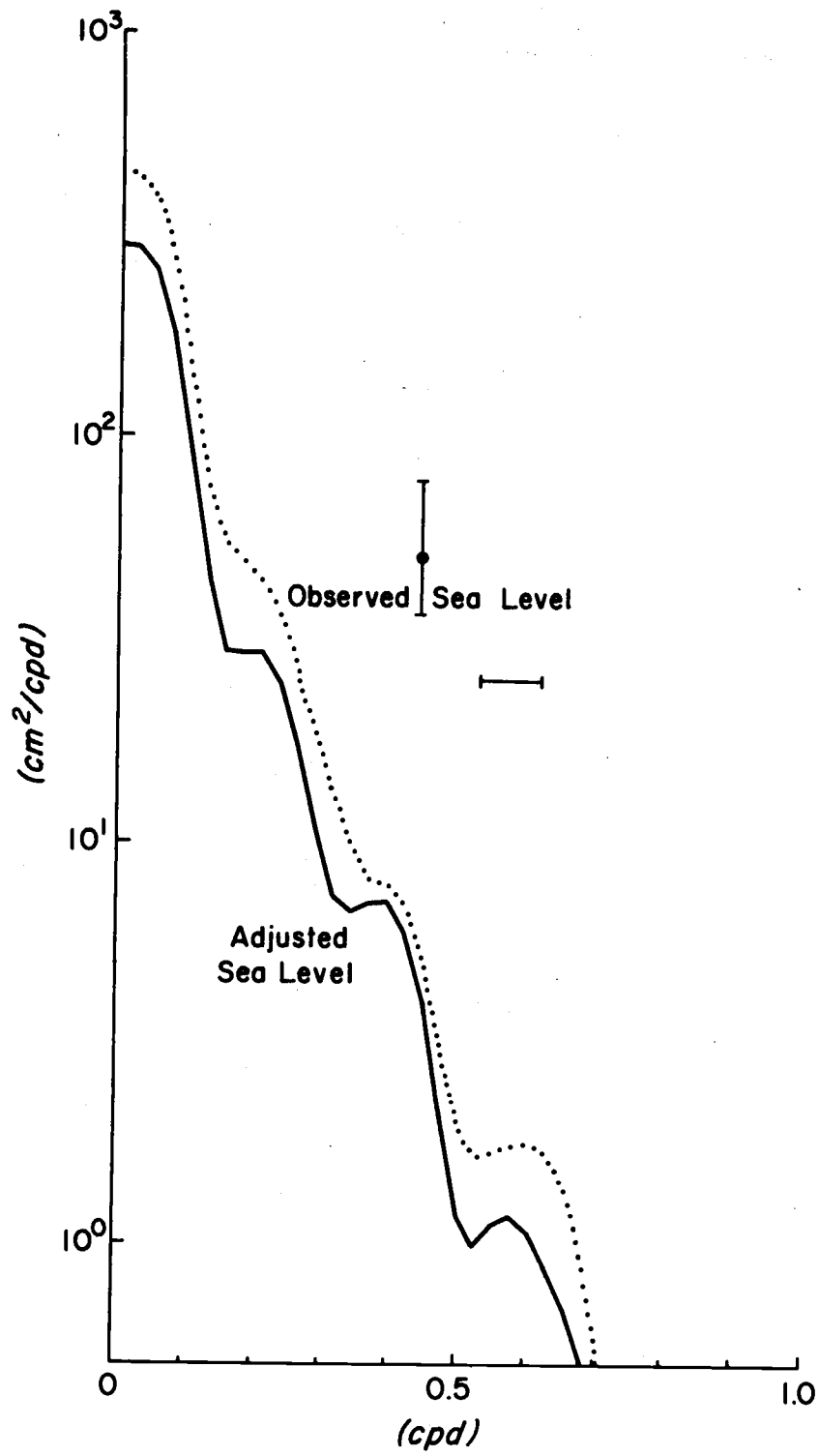
Figure 4-6. Power spectrum of Newport sea level adjusted for atmospheric
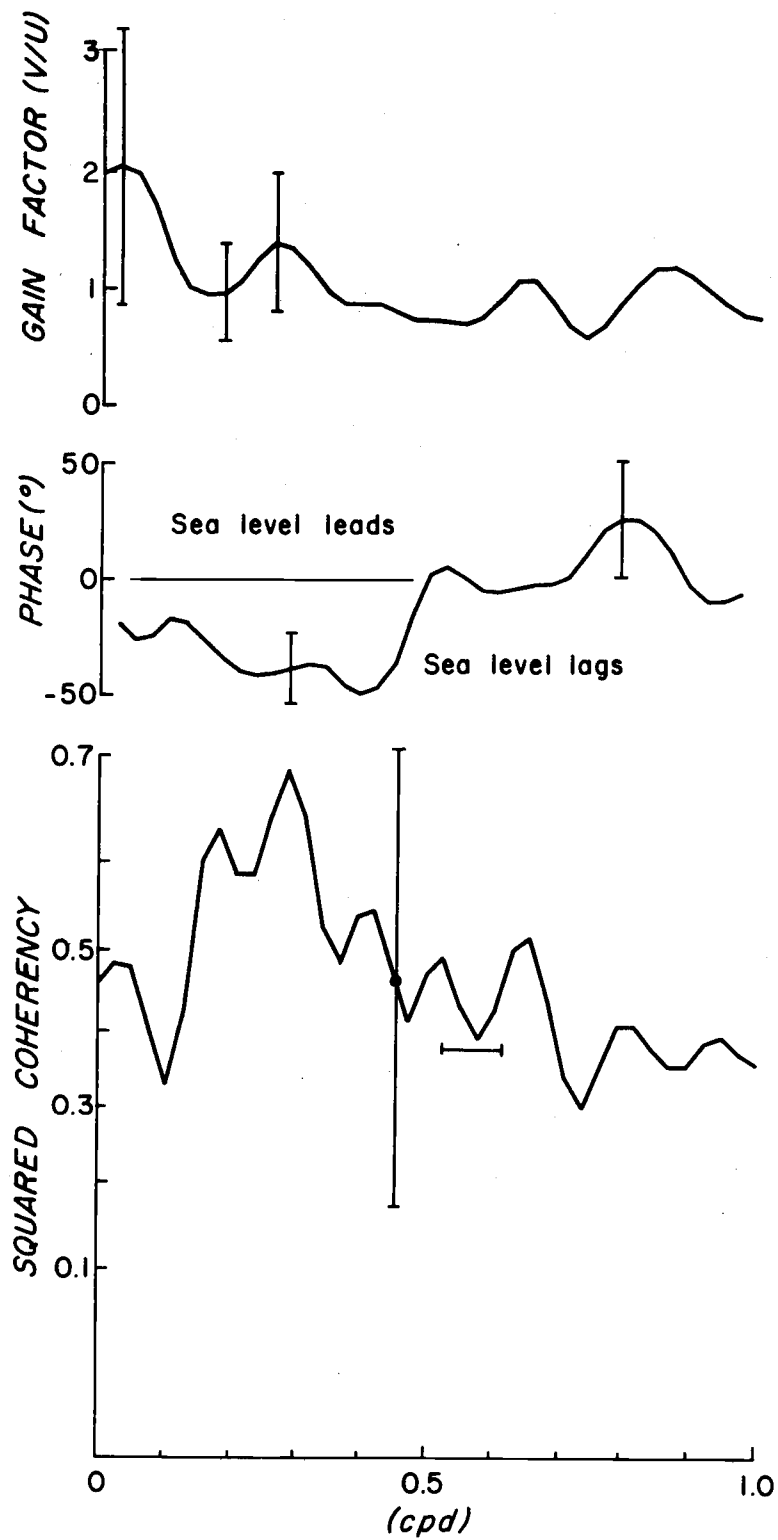pressure effect.

Figure 4-7. Cross spectral indices for sea level vs. atmospheric pressure.
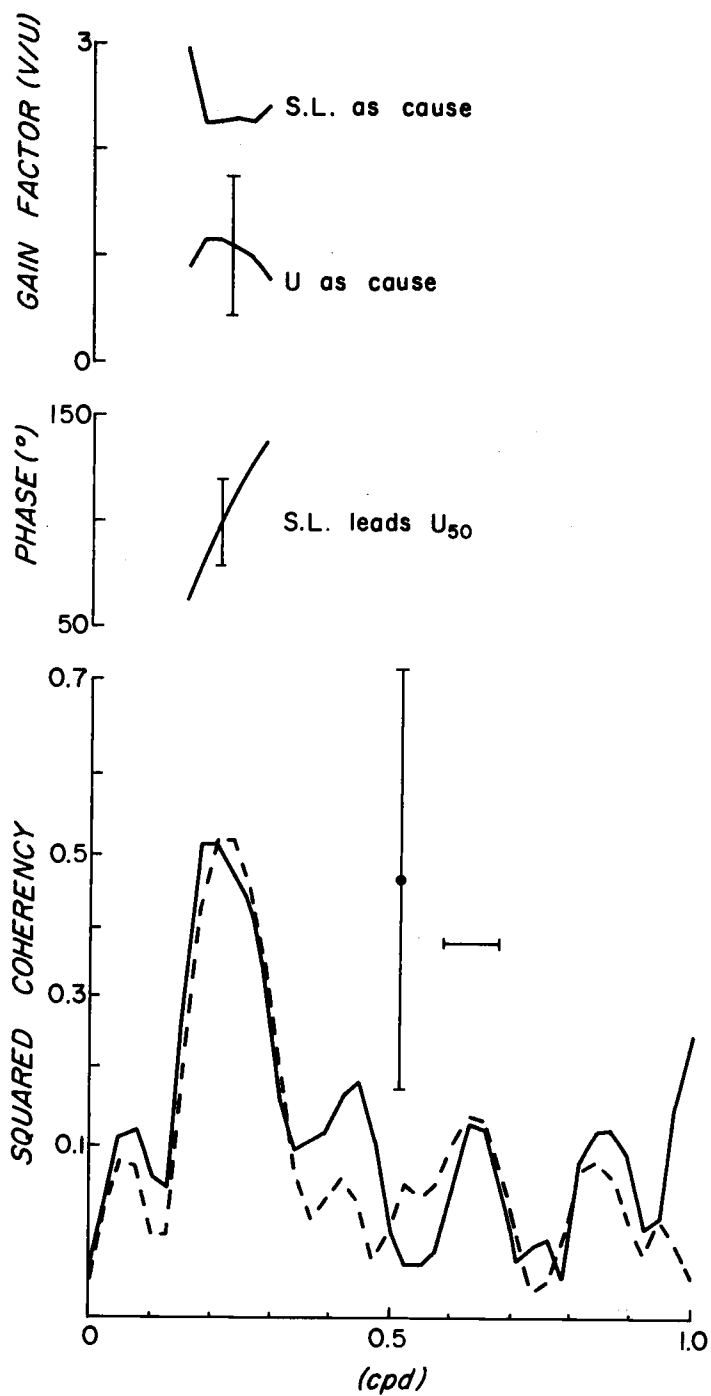
Figure 4-8. Cross spectral indices for onshore (012° system) component of velocity measured at 50 m vs. barometrically adjusted sea level at Newport.

Estimating the relationship between the amplitude of the varia-
tions in the adjusted sea level and the amplitudes of the coherent

variations in the current components is subject, however, to the same

serious difficulties involved in comparing current components. This

is, the sea level slopes and currents within a wave are not simply

related as cause and effect. They are in a dynamic balance similar to

the balance that exists between the individual current components.

Therefore, the desired values have been bracketed by the gain factor

pair as explained above.

Figure 4-9 shows the same indices as Figure 4-8 but for the   v

component vs. the barometrically adjusted sea level. The massive

peak in the coherency spectrum between 0. 2 and 0. 3 cpd and the low

coherency at other frequencies is an interesting feature.

The estimated brackets for the amplitude ratios between the

current components and the adjusted sea level around 0. 22 cpd, as

determined from Figures 4-8 and 4-9, have been included in Table

4-1. The relationship between the longshore component and sea level

compares favorably with the theoretically predicted value.

D.   Analysis of Depth Dependence of Current Variations

It was one of the original intentions of this current sampling

program to detect the presence of long period internal waves. The

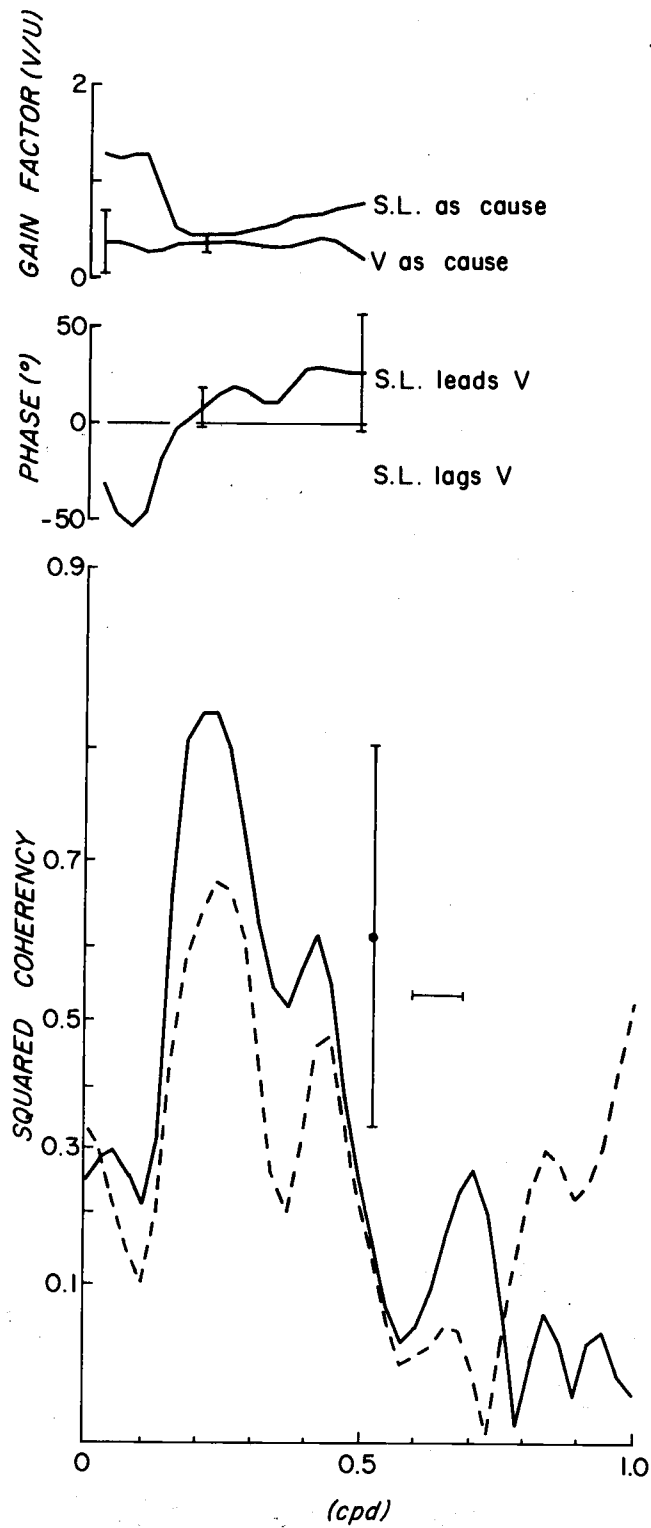recognition of such modes would yield a considerable amount of new

Figure 4-9. Cross spectral indices for longshore (012° system) component of velocity measured at 50 m vs. barometrically adjusted sea level at Newport.

light on the nature of the temporal variations in coastal upwelling.

In order to most effectively detect vertical variations in the horizontal currents, which might be due to internal waves, the current meter array should have been arranged so that at least one current meter was above the main pycnocline and one below. Unfortunately, according to the density profiles shown in Figure 3-4, the pycnocline was usually at or above the top current meter. The top meter, at a depth of 25 meters, was really about as close to the surface as we dared put it. At lesser depths the rapidly reversing currents associated with surface wind waves can "pump" a Savonious rotor and produce erroneously high speed records. The density profiles at DB-7 as shown in Figure 3-4 indicate that for the summer season at least there does not seem to be a distinct region on "top" of the main pycnocline. There is a uniformly sharp increase in density from the surface to a depth of about 20 m. Below about 20 m the density increases gradually with depth.

The traces in Figure 3-3 of the longshore components of velocity at the three depths appear to be quite similar except for a fairly constant displacement. The large variations are reproduced at each depth. This sort of a visual estimate, however, tends to overlook the shears which are present at higher frequencies because the power at those frequencies is much lower. Figure 4-10 shows the power spectra for the u and v components at both 25 and 50 meters
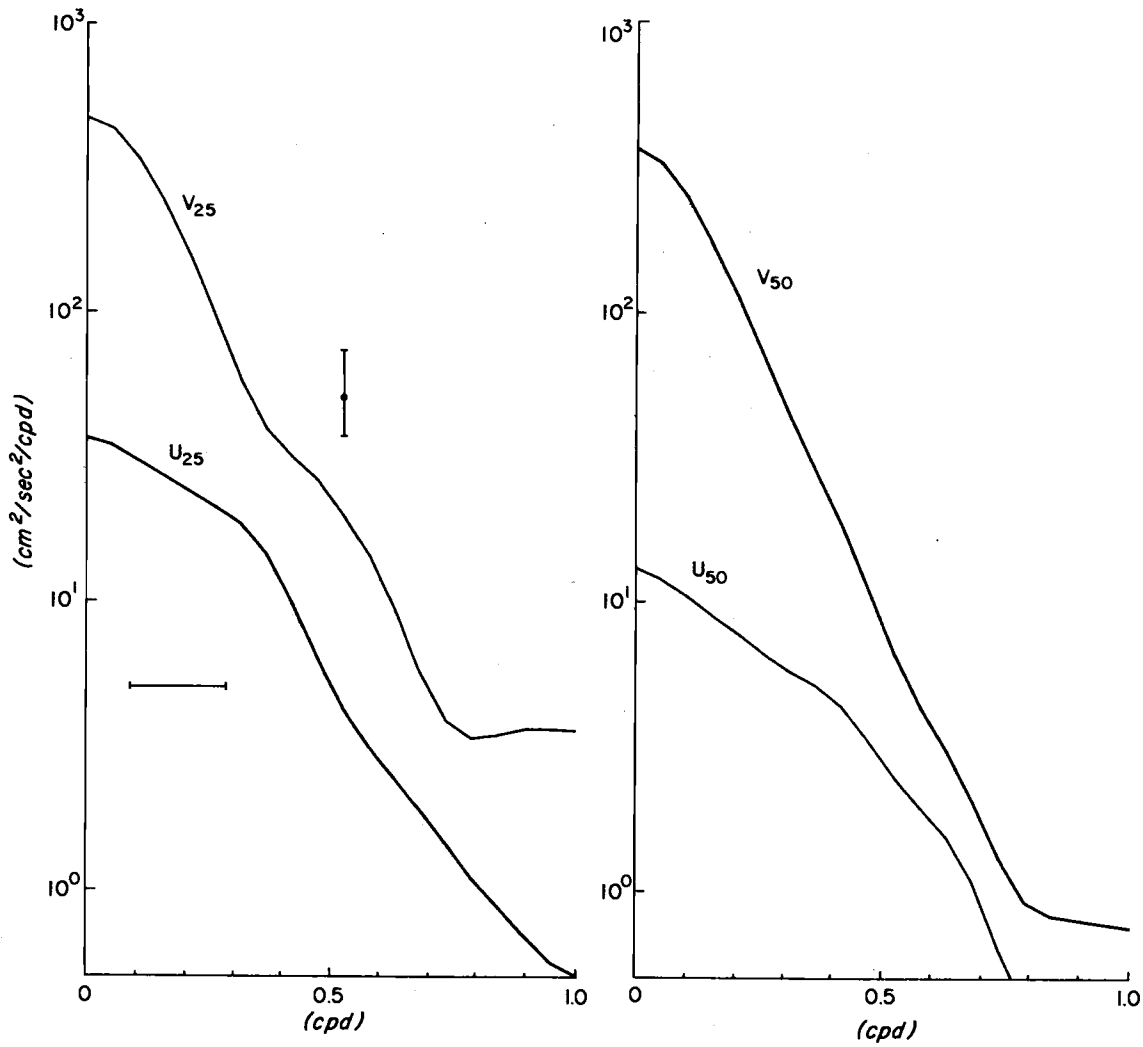
Figure 4-10. Power spectra for u and v components of currents at 25 and 50 meters depth for 57 day period starting 24 June 1968 (020° system).

depth. These spectra, and the spectra in Figure 4-11 were estimated on the basis of simultaneous records 57 days in length and starting at 0000 hours PST 24 June 1968. This is the longest period of time during which at least two current meters at different depths were operating satisfacorily. In order to maintain stability in the spectral estimates the bandwidth has been doubled over that used in the previous spectral work. All components of velocity are here expressed in terms of the topographic coordinate system (020° true).

Figure 4-11 shows the power spectra of the shears (between 25 and 50 meters depth) in the u and v components. The shears were formed as follows:

$$v_s(t) = v_{25}(t) - v_{50}(t)$$

and

$$u_s(t) = u_{25}(t) - u_{50}(t)$$

Figure 4-11 also shows the ratios of the average power densities between 25 and 50 m to the power density of the shear between 25 and 50 m. That is

$$\text{for v component}\quad R_v(\omega) = \frac{P_{v_{50}}(\omega) + P_{v_{25}}(\omega)}{2P_{v_s}(\omega)}$$

$$\text{for u component}\quad R_u(\omega) = \frac{P_{u_{50}}(\omega) + P_{u_{25}}(\omega)}{2P_{v_s}(\omega)}$$
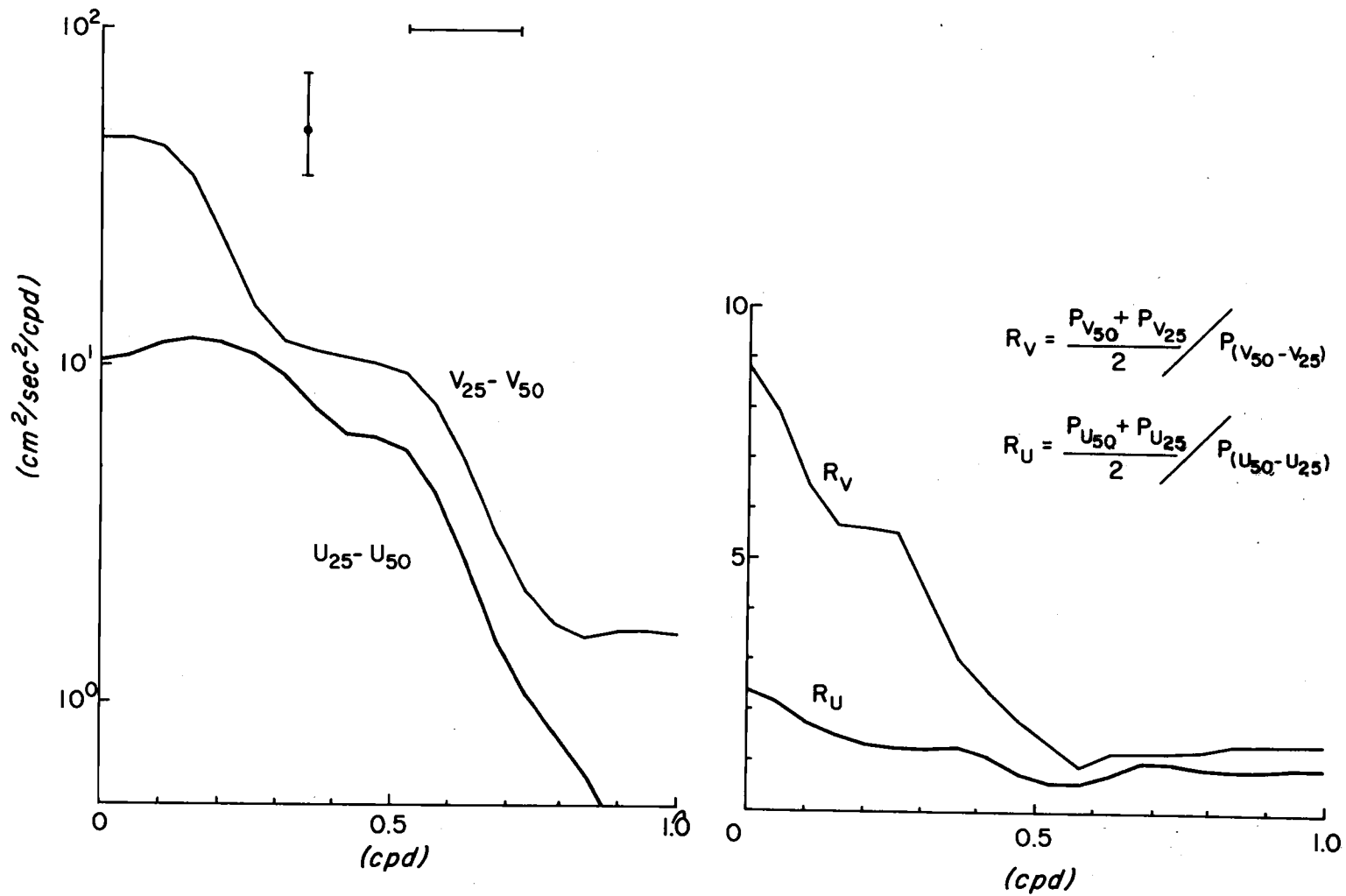
Figure 4-11. Power spectra for u and v shears, and ratios of average powers in the currents to power in the u and v shears.

A high value of the ratio $R(\omega)$ indicates that the motions at that frequency are relatively uniform in the vertical. A low value of the ratio indicates that the currents vary substantially with depth. It is interesting to note in Figure 4-11 that $R_v(\omega)$ is much larger than $R_u(\omega)$ over the frequency range of principal interest (0.0 cpd to 0.3 cpd).

Figure 4-12 shows the squared coherency spectrum and the phase spectrum between the u components measured at 25 and 50 meters and between the v components measured at 25 and 50 meters. All components were taken with respect to the coordinate system aligned with the local bathymetric contours (+v along 020° true and +u along 110° true). The squared coherency spectrum also shows that there exists a stronger association between the longshore components at 25 and 50 m than between the onshore-offshore components at 25 and 50 m.

E. Time Dependence of the Energy Density Around 0.22 cpd

Figure 4-13 is a plot of the u and v current components at a depth of 50 m (012° system) and the barometrically adjusted sea level at Newport. The series have been band passed by a filter with center at 0.22 cpd and half power points at about 0.18 and 0.255 cpd. This is the frequency band in which the shelf wave phenomena seems to be the most intense. The sections displayed extend from 1200 hours

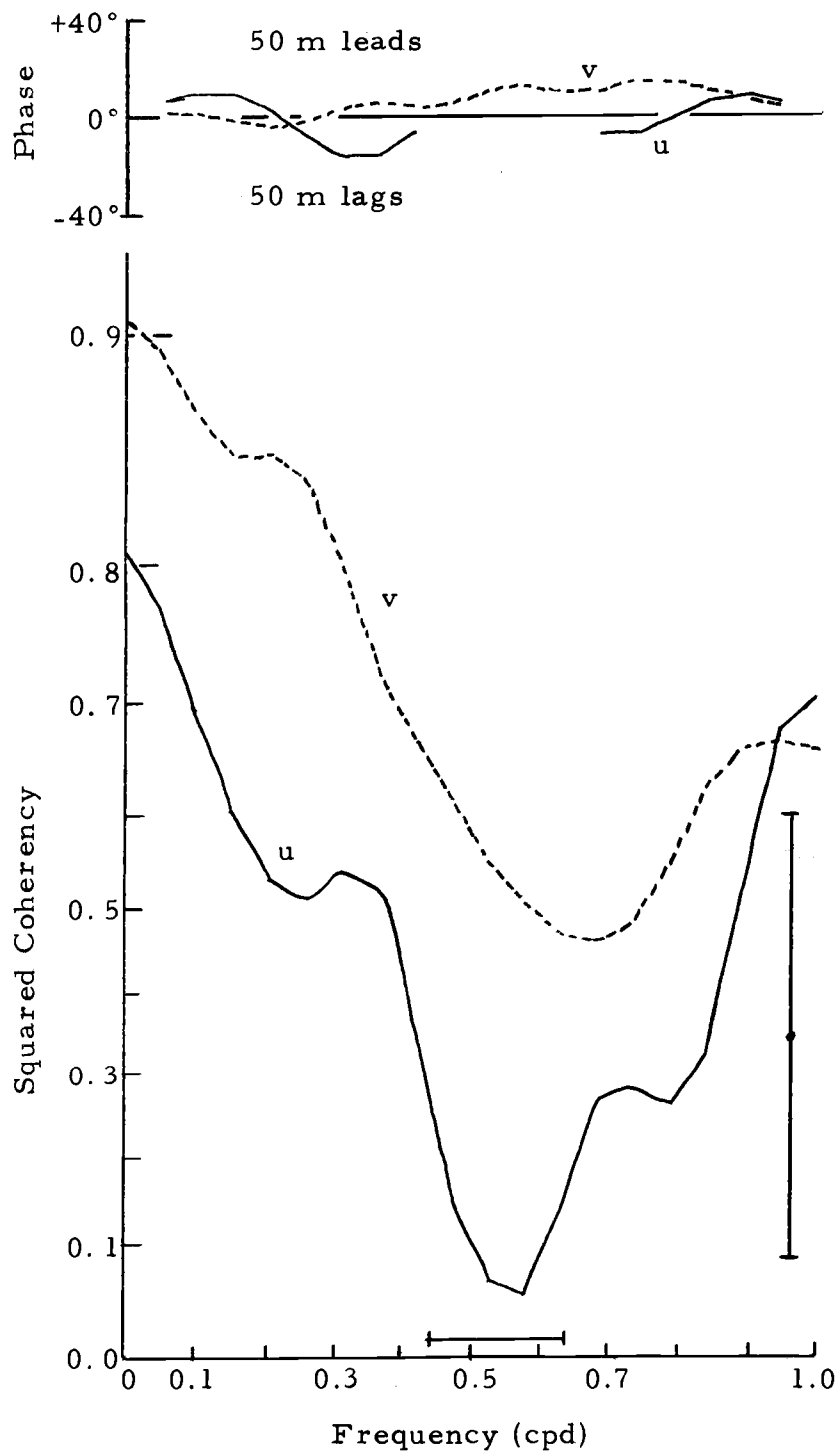Figure 4-12.   Coherency and phase spectra for each velocity com-
              ponent (020° system) between 25 m level and the
              50 m level.
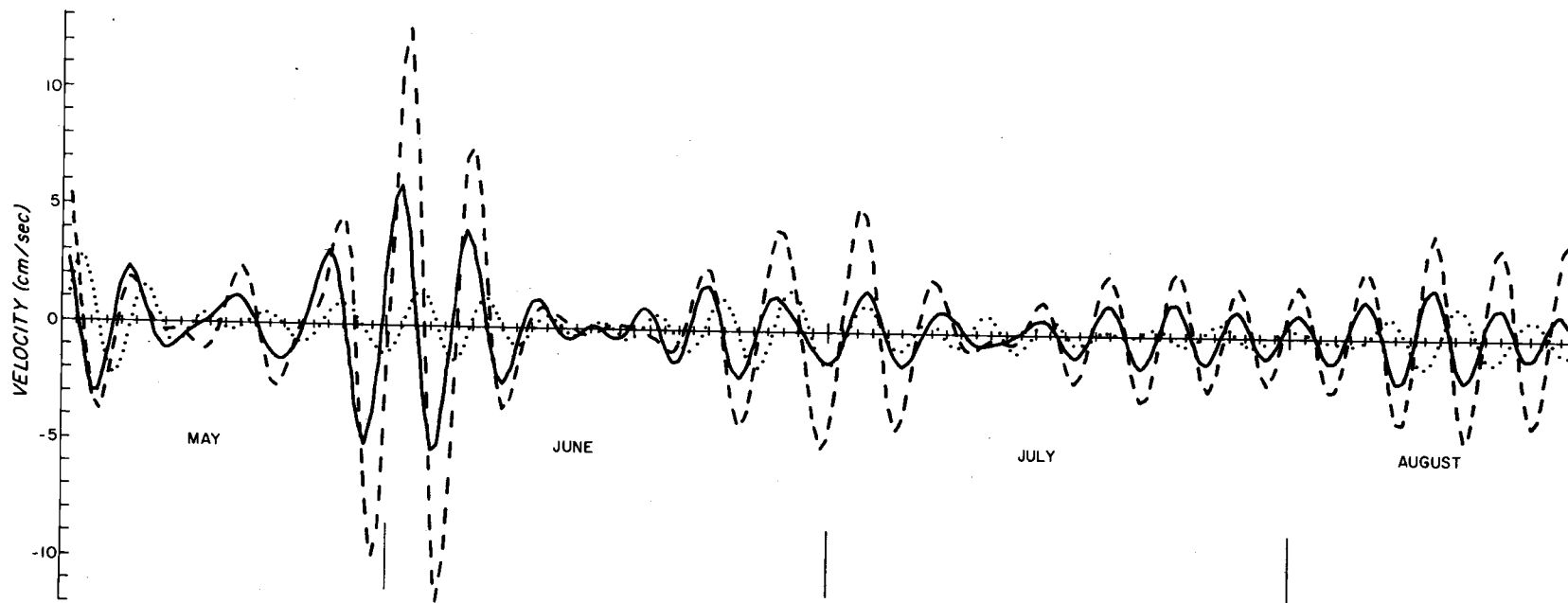
Figure 4-13. Section of u, v (012° system, 50 m depth) and barometrically adjusted sea level records which have been bandpassed for a frequency of 0.22 cpd. On the first day of each month 0000 hours has been indicated by a large vertical bar beneath the traces.

May 5, 1968 until 1200 hours August 19, 1968. This plot demonstrates the time variability in the shelf wave phenomena. The longshore component, v, and adjusted sea level are clearly locked in the phase relationship predicted for shelf waves. The sea level appears to consistently lead v by only a few degrees. During the period of most intense activity, around 1 June, v seems to lead u by about 90° as it should for shelf waves. However, at other times the phase relationship between u and v shifts around. The estimated amplitude ratio $\widehat{R}_{v/u}$ during the 1 June disturbance appears to be about eight. This is considerably higher than the values for $\widehat{R}_{v/u}$ which appear in Table 4-1. It is still not as high as the theoretically predicted value.

V. CONCLUSIONS AND COMMENTS

A. Shelf Waves

In a frequency band extending from about 0.15 cpd to 0.45 cpd, the longshore and onshore components are arranged in time patterns characteristic of continental shelf waves. That is, an offshore flow is followed quite regularly by a longshore flow to the north, an onshore flow and then a longshore flow to the south. This is indicated by the strong coherency between the u and v time series in the principal axis system (Figure 4-5). However, on the basis of the available data, we cannot eliminate the possibility that the currents are directly and locally forced in this regular rotary pattern by regular rotary patterns in the atmospheric pressure field or the wind stress. This line of reasoning has not been pursued, but there are additional indications that shelf waves may be present.

It is not surprising that, as indicated by Figure 4-9, a northward current is accompanied by an elevation in sea level at the coast. What is significant for the band 0.15 cpd to 0.45 cpd, however, is the relative intensity of the current. If these variations are in quasi-geostrophic equilibrium with variations in the slope of the sea surface above the current meters, then the slope is unusually steep. A linear extrapolation of the sea level elevation at the coast based upon this slope would pass through mean sea level somewhere over the

continental slope. This means that the whole system is probably packed in tightly over the shelf. This feature was noted by Collins (1968). As outlined in Table 4-1, the value of the ratio of the amplitude of the sea surface variations to the amplitude of the longshore current variations is quite close to the value predicted (Figure 2-6) for the first mode of a free continental shelf wave. On the basis of this data it is not possible to further determine the relative modal composition of the wave field. A number of current and/or sea level measurements along a line perpendicular to the coast would have been necessary.

B. Baroclinicity

Since the vertical current meter array did not span the main variations in the density field, these records cannot say much about the overall barotropic or baroclinic character of the currents. However, Figure 4-11 together with Figure 4-12 indicate that at frequencies below about 0.3 cpd variations in the longshore flow are substantially more barotropic (uniform in the vertical) than the onshore-offshore flow. This indicates that whatever internal modes may be present place relatively more energy in their onshore-offshore motions and less in their longshore motions than do the barotropic modes. Time variations in the strength of coastal upwelling, an essentially baroclinic phenomena, require compensatory fluctuations in the intensity

of the onshore flows. The contamination of the u component by baroclinic modes is probably responsible for the relatively lower coherency peaks for u vs. v (Figure 4-5) and u vs. sea level (Figure 4-8) and the relatively poor agreement between the barotropic theory and observations for amplitude ratios involving u (Table 4-1).

C. Band Structure

The very large block of energy at frequencies below about 0.15 cpd does not seem to be arranged in similar wavelike patterns. The limitation of the shelf wave phenomena to a relatively narrow band is difficult to understand since, according to the dispersion curves presented in Figure 2-5, the waves can exist at all frequencies between 0 cpd and about 0.7 cpd, the high frequency cutoff for the first mode. It is possible that below about 0.2 cpd variations in the deep ocean and their on-shelf manifestations mask the shelf wave modes. There clearly exists a need for observations of currents and sea level off the shelf which are simultaneous with the on-shelf measurements. One of the fundamental assumptions leading to the shelf wave dispersion characteristics and eigenfunctions was that the energy was inserted, trapped and dissipated almost completely over the continental margin. If the observed motions were being driven by variations in the deep ocean then they might be more like the topographic Rossby

waves observed by Thompson (1969).

No definite conclusions have been reached about the problem of the mechanism of wave generation. The available meteorological observations were not sufficiently complete to warrant the attempt. In connection with the problem of explaining the narrowness of the spectral band in which shelf waves seem to exist, however, one might mention the following interesting coincidence.

Buchwald and Adams (1968) mentioned that since those waves corresponding to the inversion points in the dispersion curves (Figure 2-5) have zero group velocity, they should not be able to transmit their energy away from the generating area. They noted that this mechanism may cause a form of resonance. The result would be a concentration of wave energy around the frequencies and wavenumbers corresponding to the inversion points. Figure 5-1 is a composite figure incorporating Figure 2-5, the shelf wave dispersion curves, and the squared coherency spectrum between v and the barometrically adjusted sea level from Figure 4-9. Note that the frequencies of the three peaks in the squared coherency spectrum correspond rather well with the cut off frequencies for the first three shelf wave modes. This may be just a coincidence. The assignment of the 0.22 cpd peak to the 3rd mode is not consistent with the estimated amplitude ratios between the variations in sea level and v (Table 4-1). The amplitude ratio indicates that the 0.22 cpd peak is a first mode oscillation.
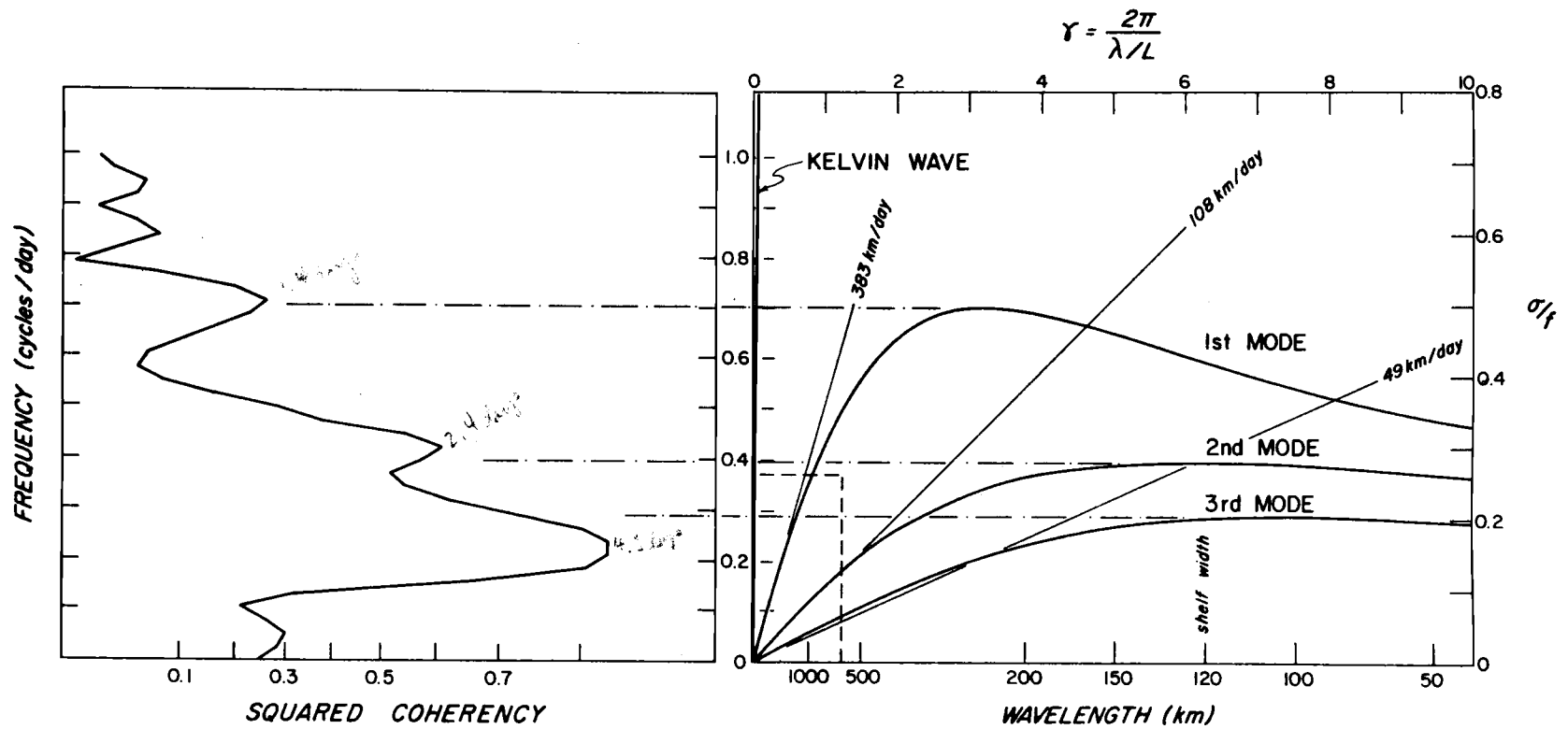
Figure 5-1. Shelf wave dispersion curves from Figure 2-5 together with coherency spectra for v vs. barometrically adjusted sea level from Figure 4-9.

There is another interesting feature, connected with the topography, which might modify the spectral distribution of wave energy at the current meter station. We have already mentioned that although the width of the Oregon continental margin may vary a small amount, the shape of its profile is fairly consistent. A prominent exception is the bank area lying between about 44°37'N and 43°55'N. The current meter station is just to the north of this area. It is possible that the force of a fairly uniform pressure or wind field acting in the coastal region may be spatially modulated by topographic irregularities such as this bank. In other words, topography plus a uniform forcing function may have the same effect as a forcing function containing a longshore bulge equal to the length of the bank. An oscillating bulge in a forcing function is most effective in generating waves whose wave length is twice the length of the bulge. The north-south length of the bank area is about 42' and 78 km. This means that is would generate waves of about 160 km in length.

Figure 5-1 (or Figure 2-5), the predicted dispersion curves, indicate that a wave of length 160 km could exist in the first mode at about 0.66 cpd, in the second mode at 0.38 cpd and in the third mode at 0.25 cpd. The correspondence between these frequencies and the peaks in the longshore velocity-adjusted sea level coherency spectrum is rather good. The first mode waves have negative (southward) group velocities so they should not show up strongly at the current meter

station which is to the north of the bank. The second and third mode waves have very low positive (northward) group velocities. Therefore they should be concentrated in a region just to the north of the bank. This difference might account for the relatively better showing made by waves at the lower frequencies. The main objection to this explanation of the spectral structure is the same objection raised against the resonant interaction explanation just given; i. e., it necessarily associates the lowest frequency peak (around 0.22 cpd) with the third mode. Table 4-1 shows that the relationship between the longshore velocity and the adjusted sea level at 0.22 cpd is strongly indicative of a first mode wave.

BIBLIOGRAPHY

Adams, J. K. and V. T. Buchwald. 1969. The generation of continental shelf waves. Journal of Fluid Mechanics 35(4):815-826.

Barstow, Dennis, William Gilbert and Bruce Wyatt. 1969. Hydrographic data for Oregon waters. Corvallis, Oregon. 84 numb. leaves. (Oregon State University. Dept. of Oceanography. Data report 36 on Office of Naval Research Contract NOOO-14-67-A-0369-0007.)

Bendat, Julius S. and Allan G. Piersol. 1966. Measurement and analysis of random data. New York, John Wiley. 390 p.

Blackman, R. B. and J. W. Tukey. 1958. The measurement of power spectra. New York, Dover. 190 p.

Bottero, J. and R. D. Pillsbury. 1971. Oregon State University. Dept. of Oceanography. Personal communication. Corvallis, Oregon. May, 1971.

Buchwald, V. T. and J. K. Adams. 1968. The propagation of continental shelf waves. Proceedings of the Royal Society A(305): 235-250.

Burt, Wayne V. and Bruce Wyatt. 1964. Drift bottle observations of the Davidson Current off Oregon. In: Studies on oceanography, ed. by K. Yoshida. Seattle, University of Washington. p. 166-180.

Caldwell, D. R. and M. S. Longuet-Higgins. 1971. The experimental generation of double Kelvin waves. Proceedings of the Royal Society. London (In press)

Caldwell, D. R., D. L. Cutchin and M. S. Longuet-Higgins. 1971. Some model experiments on continental shelf waves. (Submitted to the Journal of Marine Research.)

Cartwright, D. E. 1969. Extraordinary tidal currents near St. Kilda. Nature, Vol. 223, August 30, 1969. p. 928-932.

Collins, Curtis Allan. 1968. Description of measurements of current velocity and temperature over the Oregon continental shelf, July 1965-February 1966. Ph. D. thesis. Corvallis, Oregon State University. 154 numb. leaves.

Collins, Curtis Allan and June G. Pattullo. 1970. Ocean currents above the continental shelf off Oregon as measured with a single array of current meters. Journal of Marine Research 28(1): 51-68.

Fisher, Carl William. 1969. A statistical study of winds and sea water temperatures during Oregon coastal upwelling. M.S. thesis. Corvallis, Oregon. Oregon State University. 67 numb. leaves.

Gilbert, William Earl. 1967. A study of seiching in Yaquina Bay, Oregon. M.S. thesis. Corvallis, Oregon State University. 14 numb leaves.

Granger, C.W.J. in association with M. Hatanaka. 1964. Spectral analysis of economic time series. Princeton, Princeton University Press. 299 p.

Hamon, B.V. 1962. The spectrums of mean sea level at Sydney, Coff's Harbour and Lord Howe Island. Journal of Geophysical Research 67(13):5147. (Correction: ibid 68(15):4635.)

Hamon, B.V. 1966. Continental shelf waves and the effects of atmospheric pressure and wind stress on sea level. Journal of Geophysical Research 71(12):2883-2893.

Huyer, Adriana. 1971. A study of the relationship between local winds and currents over the continental shelf off Oregon. M.S. thesis. Corvallis, Oregon State University. 37 numb. leaves.

Jenkins, Gwilym M. and Donald G. Watts. 1968. Spectral analysis and its applications. San Francisco, Holden-Day. 525 p.

Longuet-Higgins, M.S. 1965. Some dynamical aspects of ocean currents. Quarterly Journal of the Royal Meteorological Society 91(390):425-451.

Ma, Heau San. 1970. Sea level response to low frequency atmospheric pressure fluctuations along the northwestern American coast. M.S. thesis. Corvallis, Oregon State University. 29 numb. leaves.

Mooers, Christopher N.K. and R.L. Smith. 1968. Continental shelf waves off Oregon. Journal of Geophysical Research 73(2):549-557.

Mooers, Christopher N. K., L. M. Bogert, R. L. Smith and June G. Pattullo. 1968. A compilation of observations from moored current meters and thermographs (and of complimentary oceanographic and atmospheric data). Corvallis. 98 numb. leaves. (Oregon State University. Dept. of Oceanography. Data report No. 30 on National Science Foundation Grant GA 331, Reference 68-5, June 1968)

Mooers, Christopher N. K. 1968. Cross-stream flows in continuous f-plane frontal models, with application to coastal upwelling fronts. In: Notes on the 1968 Summer Study Program in Geophysical Fluid Dynamics at the Woods Hole Oceanographic Institution, Woods Hole, Mass. Vol. 2. P. 105-142.

Mooers, Christopher N. K. 1970. The interaction of an internal tide with the frontal zone of a coastal upwelling region. Ph. D. thesis. Corvallis, Oregon State University. 480 numb. leaves.

Mysak, Lawrence A. 1967a. On the very low frequency spectrum of the sea level on a continental shelf. Journal of Geophysical Research. 72(12):3043-3047.

Mysak, Lawrence A. 1967b. On the theory of continental shelf waves. Journal of Marine Research 25(3):205-227.

Mysak, Lawrence A. and B. V. Hamon. 1969. Low frequency sea level behavior and continental shelf waves off North Carolina. Journal of Geophysical Research 74(6):1397-1405.

Ochs, Lyle, Jo Ann Baughman and Jeff Ballance. 1970. OS-3 Arand System: documentation and examples. Volume 1. Publication No. CCR-70-4, Oregon State University, Corvallis, Oregon.

Orlanski, Isadoro. 1968. Instability of frontal waves. Journal of Atmospheric Sciences. 25(2):178-200.

Orlanski, Isidoro. 1969. The influence of bottom topography on the stability of jets in a baroclinic fluid. Journal of Atmospheric Sciences 26(6):1216-1232.

Pak, Hasong, George F. Beardsley and Robert L. Smith. 1970. An optical and hydrographic study of a temperature inversion off Oregon during upwelling. Journal of Geophysical Research 75(3):629-639.

Pattullo, June G. and W. B. McAlister. 1962. Evidence for oceanic frontogenesis off Oregon. Science 135(3498):106-107.

Pillsbury, Dale, Robert L. Smith and Ronald C. Tipper. 1969. A reliable low-cost mooring system for oceanographic instrumentation. Limnology and Oceanography 14(2):307-311.

Pillsbury, Dale, Robert L. Smith and June G. Pattullo. 1970. A compilation of observations from moored current meters and thermographs. Volume III: Oregon continental shelf, May-June 1967, and April-September 1968. Corvallis. 102 numb. leaves. (Oregon State University. Dept. of Oceanography. Data report No. 40 on National Science Foundation Grants GA1435 and GA295, Reference 70-3, June 1970)

Pillsbury, Dale. 1972. A description of hydrography, winds and currents during the upwelling season near Newport, Oregon. Ph. D. thesis. Corvallis, Oregon State University. 163 numb. leaves.

Rhines, Peter. 1970. Edge, bottom and Rossby waves in a rotating stratified fluid. Geophysical Fluid Dynamics 1:273-302.

Robinson, A. R. 1964. Continental shelf waves and the response of sea level to weather systems. Journal of Geophysical Research 69(2):367-368.

Smith, Robert L. 1964. An investigation of upwelling along the Oregon Coast. Ph. D. thesis. Corvallis, Oregon State University. 83 numb. leaves.

Thompson, Rory. 1969. Topographic Rossby waves at a site north of the Gulf Stream. (Submitted to Deep Sea Research)

Tick, Leo J. 1966. 1967. Estimation of coherency. In: Spectral analysis of time series, ed. by Bernard Harris. New York, John Wiley. p. 133-152.

APPENDIX

I. LOW PASS NUMERICAL FILTER SPECIFICATIONS

The filtered series $\bar{\eta}(t)$ is formed by taking the following weighted average of the elements of the original series $\eta(t)$.

$$\bar{\eta}(t) = \frac{a_0\eta(t) + \sum_{n=1}^{M-1} a_n(\eta(t-n\Delta t) + \eta(t+n\Delta t))}{a_0 + 2\sum_{n=1}^{M-1} a_n}$$

Δt is the sampling interval for the original series. The weights are given by

$$a_i = \frac{1}{2}\left[1 + \cos\left(\frac{\pi i}{M}\right)\right]\frac{\sin(\pi F i)}{\pi F i}$$

for $i = 0, 1, \ldots, M-1$

This filter is sometimes referred to as a "Cosine-Lanczos" taper. The following table gives the data pertaining to each particular realization of this form as used in this dissertation.

Filter Name	Computations by	Δt for data	M	F (in Nyquist)	Half Power Point (τ in hrs)
40L180	DLC(ARAND)	20 min.	181	0.01946	39
41L360	DLC(ARAND)	10 min.	361	0.00973	39
CL121	Mooers	1 hr.	61	0.0583	39
42L20	DLC(ARAND)	3 hrs.	20	0.1748	39

The filters marked ARAND were produced with the aid of the ARAND (Ochs, Baughman and Ballance, 1970) system subroutine GENER1. The one marked Mooers was taken from Mooers et al. (1968).

The power transfer function for all of these filters, to within about 1%, is given in Figure IA-1.

A. Truncation

A filtered time series usually is shorter than the original time series due to the losses at the beginning and end. These lost portions are each equal in duration to the span of one wing of the filter. Since the filters used here had a very wide span these losses would have been intolerable around the gaps in the current meter records.

In order to eliminate this loss the filters were appropriately shortened as they approached the ends of a time series. The method of shortening was simply to truncate the series of weights and to renormalize. This truncated set of weights of course does not have the sharp response function of the original. The progressive process of degeneration with a decreasing number of weights is shown for 40L180 in Figure IA-2.

B. Low Pass Prefilter

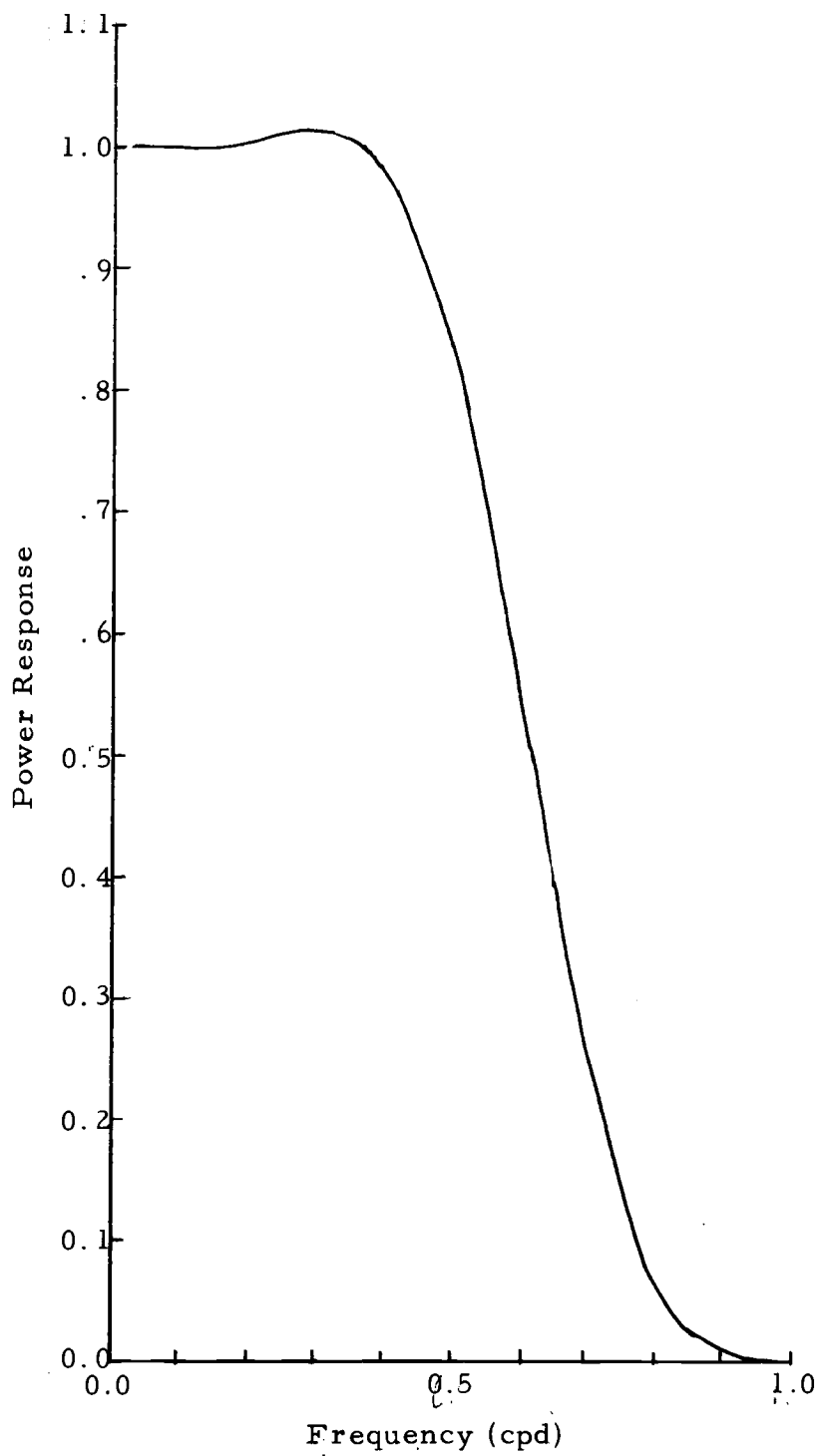The raw Newport sea level data at a sampling interval of
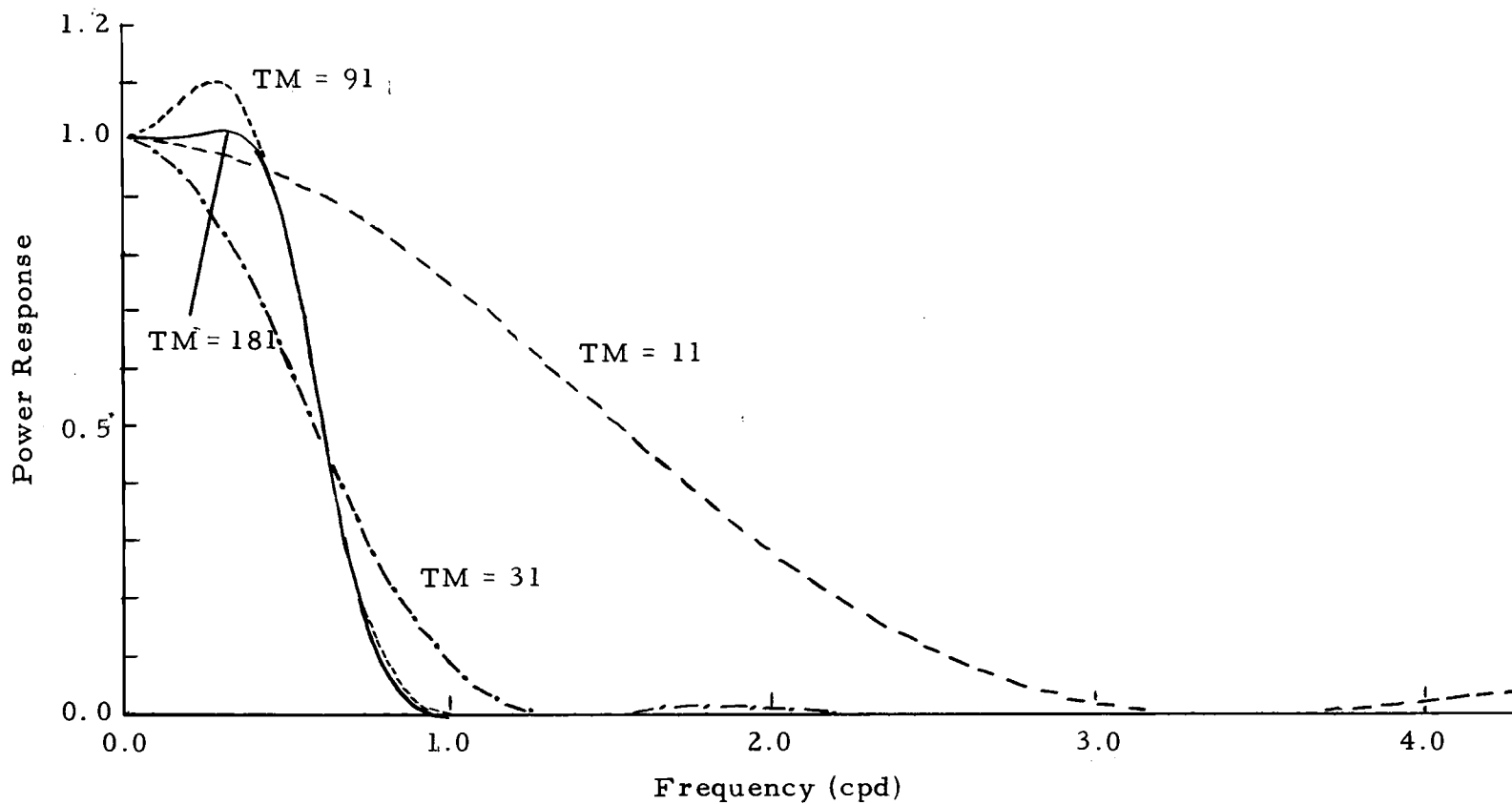
Figure IA-1.   Power response function.

Figure IA-2. Power response function for 40L180 showing degeneration due to progressive truncation. Full filter has 181 unique weights. Weights remaining in truncated filters indicated by "TM."

$\Delta t = 6$ min was prefiltered using the low pass filter 3L40. In this case the smoothed series $\bar{\eta}(t)$ was taken as this weighted average of the points in the original series.

$$\bar{\eta}(t) = \frac{a_0 \eta(t) + \sum_{n=1}^{40} a_n (\eta(t - n\Delta t) + \eta(t + n\Delta t))}{a_0 + 2 \sum_{n=1}^{40} a_n}$$

The weights $a_0, \ldots, a_{40}$ are given by

$$a_n = \frac{2}{40} \left[\frac{1}{2} + \cos(n\Delta\omega) \right]$$

where $\Delta\omega = \frac{\omega_N}{40}$. ω_N is the Nyquist folding frequency (2π radians/12 minutes). The power response function for this filter is approximately

f (cphr)	P(f)
0	1.0
1/8	0.88
1/4	0.009
<1/4	<0.009